a place of mind

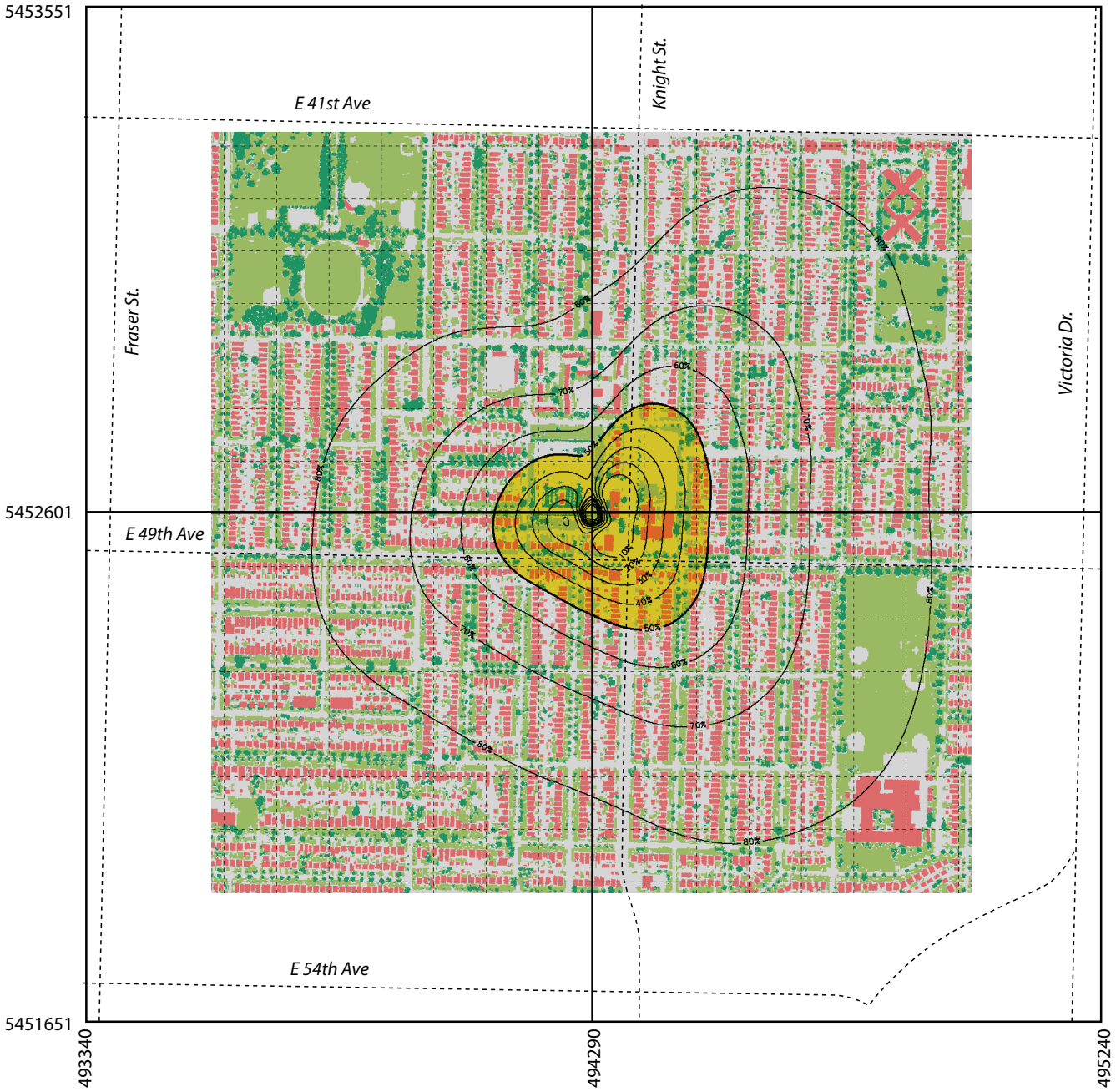

A LiDAR-Based Urban Metabolism Approach to Neighbourhood Scale Energy and Carbon Emissions Modelling

Andreas Christen, Assistant Professor of Geography (Principal Investigator)
Nicholas Coops, Professor of Forestry and Canada Research Chair in Remote Sensing (Co-Investigator)
Ronald Kellett, Professor of Landscape Architecture (Co-Investigator)
Contributing authors: Ben Crawford, Eli Heyman, Inna Olchovski, Rory Tooke, Michael van der Laan
University of British Columbia, 2010

This report by the University of British Columbia was supported by the CanmetEnergy division of Natural Resources Canada with funding from the Program of energy Research and Development.

Canada

Natural Resources Canada

Ressources naturelles Canada

TABLE OF CONTENT

A LIDAR-BASED URBAN METABOLISM APPROACH TO NEIGHBOURHOOD SCALE ENERGY AND CARBON EMISSIONS MODELLING prototypes a remote sensing-based means to neighbourhood-scale energy and carbon modelling. Building on a Vancouver case study neighbourhood for which remote sensing, atmospheric carbon flux, urban form, energy and emissions data have been compiled and aggregated, the project demonstrates a replicable neighbourhood-scale approach that illustrates:

- Holistic, systems-based and context-sensitive approaches to urban energy and carbon emissions modelling.
- Methods of deriving energy- and emissions-related urban form attributes (land use, building type, vegetation, for example) from remote sensing technologies.
- Methods of integrating diverse emission and uptake processes (combustion, respiration, photosynthesis), on a range of scales and resolutions based on spatial and non-spatial data relevant to urban form, energy and emissions modelling.
- Scalable, type-based methods of building energy modeling and scenario-building.
- Benchmark comparisons of modelled estimates with directly measured energy consumption data and two years of directly measured carbon fluxes (emissions) on a research tower above the neighbourhood.

0.0.1 Key Model Results

- **Carbon imports:** Based on project urban metabolism scope and methods, the study area imports approximately 6.69 kg C m^{-2} $year^{-1}$ (or 1.04 t C cap^{-1}) in form of fuels, food and materials and uptakes 0.49 kg C m^{-2} $year^{-1}$ from the atmosphere though photosynthesis of urban vegetation.
- **Carbon exports and sequestration:** Sources within the study area emit 6.22 kg C m^{-2} $year^{-1}$ (0.97 t C cap^{-1}) or 87% of the imports to the atmosphere, and 0.87 kg C m^{-2} $year^{-1}$ (0.14 t C cap^{-1}) or 12% of the imports are exported laterally by waste. 1% of the imported carbon, or 0.09 kg C m^{-2} $year^{-1}$ (0.01 t C cap^{-1}) is sequestered in urban soils and biomass.
- **Relevant emission processes:** Out of all local emissions from the study area to the atmosphere, 2.47 kg C m^{-2} $year^{-1}$ (40%) are originating from buildings, 2.93 kg C m^{-2} $year^{-1}$ (47%) from transportation, 0.49 kg C m^{-2} $year^{-1}$ (8%) from human respiration and 0.33 kg C m^{-2} $year^{-1}$ (5%) from respiration of soils and vegetation. Emissions attributable to fuels, resource and food production, transport or transmission, and waste management outside the study neighborhood were not considered.
- **Fossil fuel emissions:** Out of the local fossil fuel emissions in the study area, 46% originate from the building sector (natural gas), and 54% are attributable to transportation uses (gasoline, diesel). Out of the transportation emissions, 11% (0.31 kg C m^{-2} $year^{-1}$) are attributable to carbon emitted on trips generated within the study area and 89% (2.62 kg C m^{-2} $year^{-1}$) to carbon emitted on trips passing through the study area.

- **Renewable carbon cycling:** Photosynthesis and human, soil and vegetation respiration take up / emit renewable carbon. These processes have potential to offset (take-up) carbon from other sources as well as generate (emit) carbon when carbon pools are disturbed, by urban land use change and (re-)development, for example.
- **Benchmark to direct emission measurements**: Two years of measurements on a carbon flux tower in the centre of the study area allow a comparison of modelled results to directly measured carbon emissions. The modelled and measured emissions agreed very well i.e. 6.71 kg C m^{-2} $year^{-1}$ were measured vs. 7.46 kg C m^{-2} $year^{-1}$ modelled (refers to a subset of the study area weighted by the turbulent source are of the tower). The model is slightly overestimates actual emissions by 0.75 kg C m^{-2} $year^{-1}$ (or 11%) which is mostly attributed to the lack of vehicle speed representation in the transportation model.

0.0.2 Key Findings on Project Methodology

- **Remote sensing:** Remote sensing technologies such as LiDAR and multispectral satellite imagery have been demonstrated to be an effective means to generate, spatialize inputs and extract urban form and land cover data at fine scales (down to 1 m). These urban form attributes and data provide the inputs necessary to energy and emission modelling tasks in the building sector and to quantify vegetation emissions / uptake.
- **Building-type approach:** Type-based modelling methods, data limitations aside, provide an effective means to scale building to neighbourhood energy modelling. These methods also facilitate definition of crucial morphological and performance attributes through which to filter remote sensing data and to scope potential mitigation strategies and scenarios.
- **Comparison of measured with modelled emissions:** Direct carbon flux measurements on urban flux towers are demonstrated to be a method of validation of fine-scale emission inventories / models. Given the prototype nature of the approach and methods, close agreement between tower measurements and model results in this study is a successful and promising outcome.
- **Limitations:** While promising, the urban metabolism approach demonstrated has also been necessarily limited in several ways. Only one metabolic aspect — mass balance of carbon, has been considered and measured. The spatial scale and complexity is modest — a 2km square 'neighbourhood' of moderate land use and urban form diversity. Out of study area carbon emissions generated in the production of food or consumer goods or the extent of local origin trips has not been considered.

0.0.3 Key Findings from Illustrative Scenarios

- **Material emissions reduction targets:** Illustrative scenarios demonstrate that, on a per capita basis, local origin carbon emissions in the Sunset study area could meet British Columbia's 2020 carbon reduction goal (33% below 2007 levels) with full adoption of current best practice

space conditioning and vehicle fuel efficiency standards. However, progress toward greater emissions reductions beyond that goal require greater population and employment density in compact and mixed use, pedestrian- and transit-oriented patterns of urban form. Meeting British Columbia's 2050 carbon reduction goal (80% below 2007 levels) would depend on full adoption of these best practice urban form strategies in combination with significant additional technological improvement in the energy efficiency of buildings, vehicles and infrastructure as well as significant human behaviour change toward less energy intensive lifestyles.

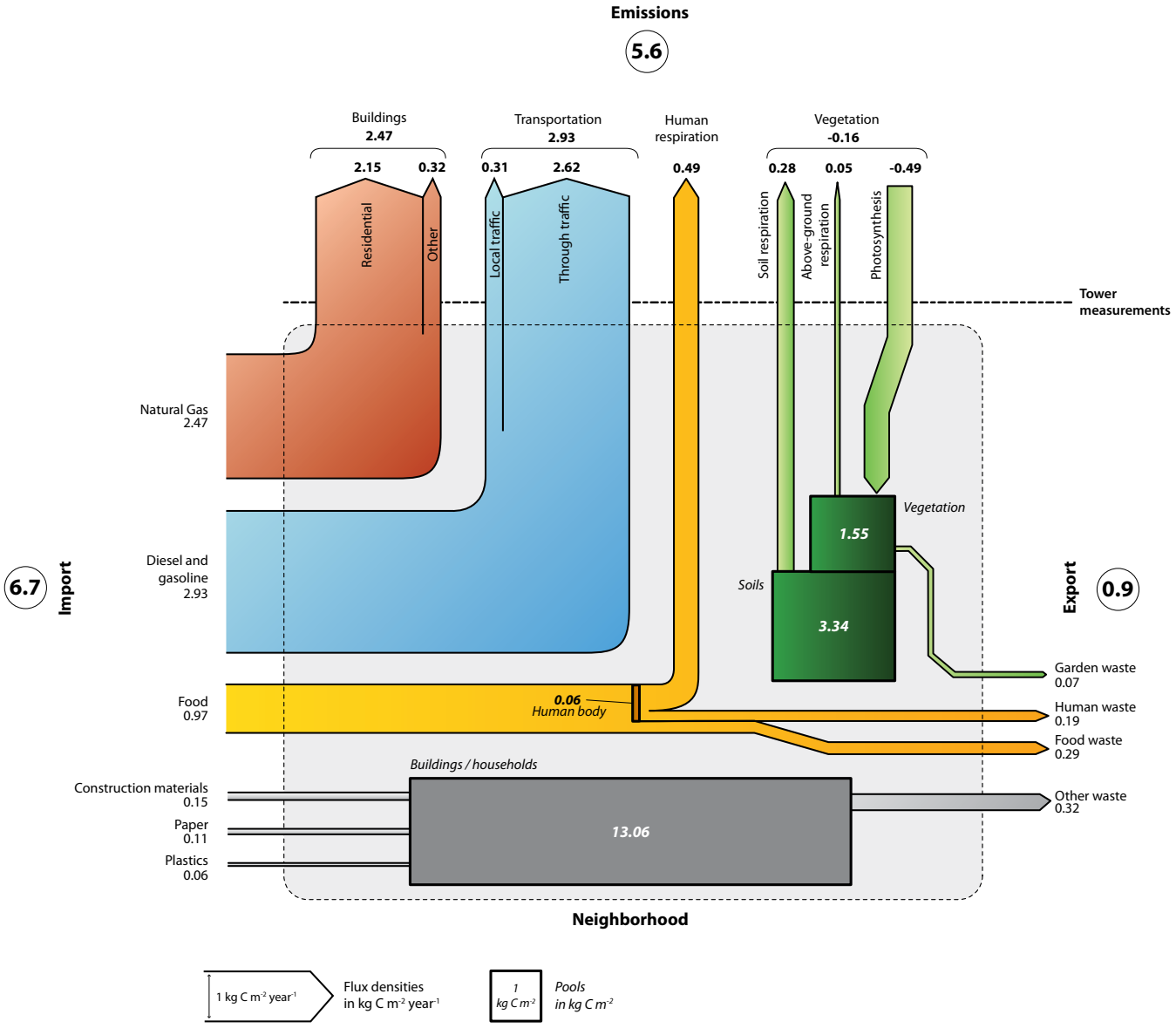

Figure 0.0.1: Integral modelled carbon cycle (fluxes and pools) in the study neighbourhood. Numbers denote carbon fluxes in kg C m^{-2} $year^{-1}$ or carbon pools in kg C m^{-2}. Fluxes leaving the neighbourhood system on top are local carbon emissions into the atmosphere and uptake of atmospheric carbon. Fluxes entering the neighbourhood system on the left hand side of the diagram are lateral imports of carbon, and fluxes leaving the neighbourhood on the right hand side are lateral exports.

1.1 The Context of Neighbourhood-scale Emission Modeling

This section establishes an urban planning and policy context for the study. It outlines the complexity and interdependence of urban emissions sources and their fundamental relationship to many physical attributes of urban form — spatial patterns, intensity, diversity, distribution and proximity of land uses, buildings, streets and mobility functions and their associated energy sources and infrastructure. Systems-based (urban metabolism) understandings of the many relationships and interactions between urban form, energy demand and carbon emissions at neighbourhood- and greater scales are necessary if cities are to improve their energy efficiency and reduce their carbon footprints to meet challenging legislated targets. However, patterns and attributes of urban form are difficult and costly to define and measure using conventional methods and technologies, Advanced remote sensing technologies increase the speed and decrease the cost of the means by which urban form attributes and related data are acquired and organized. Integrated with an urban metabolism- and building typology-based approaches and modelling methods, these technologies offer new opportunities to increase the speed, sensitivity and accuracy of neighbourhood scale energy and carbon emissions modelling. Access to measured neighbourhood scale carbon flux data affords additional opportunity to validate and compare measured and modelled results.

1.1.1 Motivation

Urban areas cover only 2% of the land surface yet account for about 75% of energy consumption and carbon-dioxide (CO_2) emissions. As much as 50% of that consumption and resulting emissions are attributable to urban form attributes such as density, land use mix, settlement pattern, building type and vegetation. Salat (2007, 2008) and Baker (2000, 2003) and Steemers (2003), for example, argue that urban form variation can influence urban building energy demand by factors up to 2.5x and urban energy systems performance by factors up to 2x. Urban form also significantly impacts opportunity for renewable energy strategies and technologies such as solar thermal, photovoltaic electricity, natural ventilation and daylighting. Likewise in transportation, CMHC's Comparing Neighbourhoods for Sustainable Features (2005), California Bill 375 Redesigning Communities to Reduce Greenhouse Gases (2008) and recent urban energy mapping projects (Center for Neighborhood Technology, 2009 for example) demonstrate that urban form attributes significantly influence travel and transportation energy demand by factors up to 3 times.

As many urban form attributes fall within the regulatory domain of local governments, planning policy and regulation in Canadian communities will inevitably depend on urban form-based strategies to meet challenging energy- and emission-reduction targets, targets. British Columbia, for example, has recently completed a community energy and emissions inventory (CEEI) process applicable to all 180+ municipalities in the province. Local governments must now act on knowledge gained from these inventories to integrate CEEI measures with Official Community Plans (OCPs) that link local planning policies, practices and regulations with

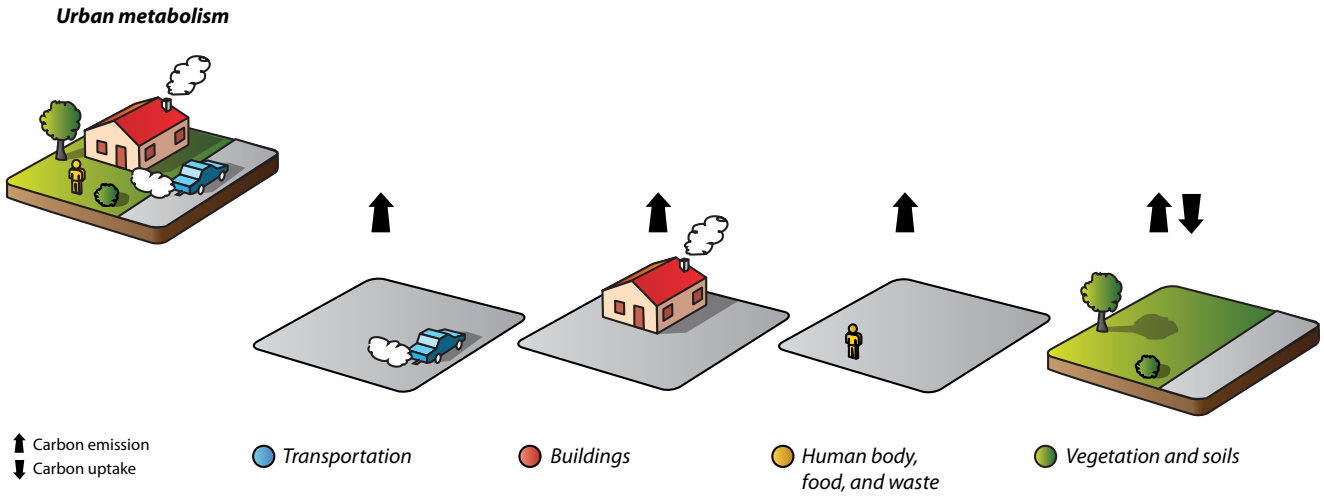

Figure 1.1.1: Simplified components of the urban metabolism controlling CO_2 emissions and uptake. Arrow direction indicates carbon flow —emissions into the atmosphere (up) or uptake by the surface (down). See also Section 1.3.2 for a detailed description of the processes involved.

their energy and emissions implications.

In order to effectively consider and act upon these linkages, communities will need to be able to characterize, model and represent energy and carbon emissions baselines and targets in reference to local land use, density and building policies or regulations. However, communities are currently challenged by the data-, expertise- and resource-intensive tasks of documenting, characterizing and modelling the energy- and emissions-related attributes of urban planning alternatives. A particular challenge has been an affordable, accurate means to characterization and measurement of the surface, volumetric and spatial attributes of urban form elements (land use, street, buildings, open space and vegetation types) and patterns that are the inputs to energy and emissions models. Typically these attributes must be inferred or extrapolated from existing mapped and tabular data, often too coarse and imprecise for effective analysis. Alternatively more appropriate data must be created from labour- and resource-intensive survey measurement and field observation.

This can soon change. Researchers and energy agencies around the world (Sustainable Urban Metabolism for Europe — SUME (2009), Sustainable Urban Planning Decision Support Accounting for Urban Metabolism — BRIDGE (2009), Metabolism of Boston, for example), have begun to represent and model energy in cities as systems and patterns of sources, distribution networks, conversion infrastructure, end uses, waste and related human behaviour as 'whole', linked, dynamic, interdependent systems of natural and anthropogenic processes.

In parallel, recent advances in remote sensing technology have significantly improved the accessibility and accuracy of high resolution, site-specific spatial data that can support an urban metabolism approach to energy- and carbon emissions modelling. Two technologies in particular hold significant promise. Light Detection and Ranging (LiDAR) is an active remote sensing technology that emits and receives laser pulses from which three-dimensional data (see Section

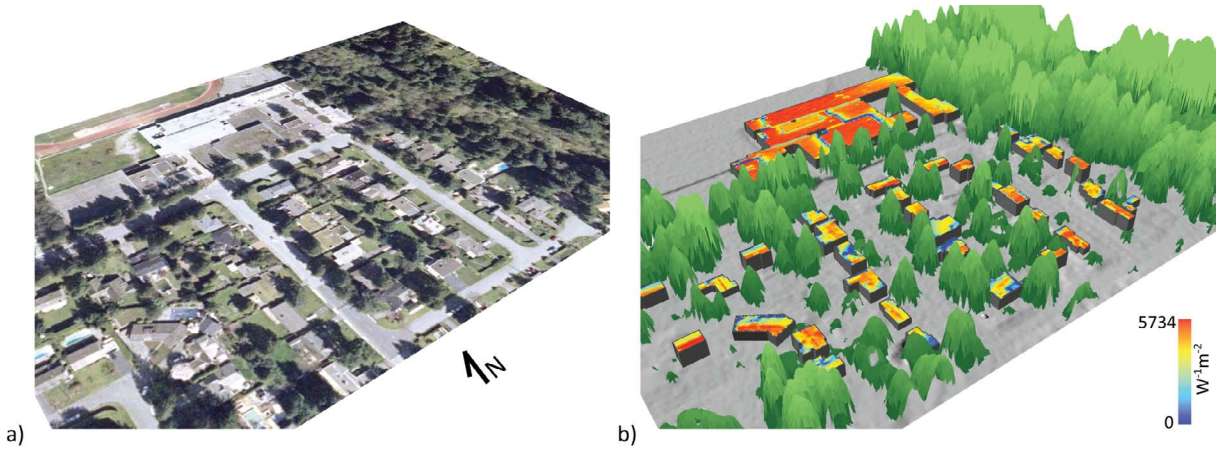

Figure 1.1.2: Example of modelling capacity gained from high spatial resolution remote sensing datasets. (a) A traditional orthophoto and (b) the same area where building and tree heights have been extracted from LiDAR observations and vegetation type characterized from satellite imagery. In this illustration, solar potential is modelled using this spatial data and a solar radiation interception model. Tooke et al. 2009.

2.2) can be quickly and accurately extracted. Integration of LiDAR data with other high-resolution spatial imagery facilitates accurate classification and measurement of complex, energy and emissions significant, urban form and surfaces where in-situ measurements are difficult to acquire.

As the complexity and diversity of urban form and buildings, and their resultant energy performance, present a methodological challenge to neighbourhood scale energy- and emissions modelling, remote sensing expedites and sharpens the processes (Figure 1.1.2) through which inputs to energy and emissions models can be derived or assigned on a parcel or building scale. As building types typically replicate many times at a neighbourhood scale, data can be more accurately scaled up to represent multiple others like them. In this project for example, remote sensing data was used to identify and locate study area building types based on morphological attributes (geometry, area, height, volume, for example). To these age, use, building systems, envelope and other energy performance attributes were assigned and modelled to create energy profiles (see Figure 1.1.3 and Section 2.3)

Finally there is the opportunity presented to validate modelled results against multiple years of measured carbon emissions data collected at a tower at the centre of the study area (see Section 2.7) and utility consumption data in its buildings (see Section 3.7). Effectively integrated and combined, this approach and its methods (urban metabolism + remote sensing + typology-based modelling + calibration against measured data — see Figure 1.1.3) can significantly improve the speed, accuracy and efficacy with which neighborhood scale energy and emissions models can be derived (Section 2) and modelled (Section 3).

DUPLEX, ATTACHED

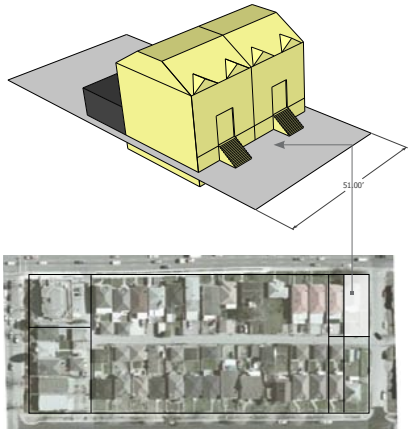

2%
percentage of buildings in the Sunset Neighbourhood classified as SFD between 1965-1990

Source: Google Streets, retrieved on May 17th, 2010

parcel attributes

- 33ft typical parcel width, by 120ft or 100ft deep
- XX% of site is impervious with some open green space as front and backyard planting

morphological attributes

- 205m² average floor area
- typically two storeys high
- 797m³ average building volume

use / occupancy attributes

- privately owned, typically detached garages
- often secondary suites or additional living space are situated above the garage
- average of 3 occupants

envelope attributes

- 180m² skin area
- 28m² aperture (window) area
- 0.16 FWR (aperture-to-wall ratio)

heating system attributes

Electrical or natural gas systems are typically used for space heating. Key values for energy modeling are the proportions of heating type and the efficiency of heating methods.

hot water system attributes

Natural gas systems are typically used for domestic hot water heating. Key values for energy modeling are the system type and the efficiency of heating methods.

construction attributes

Thermal efficiency is typically evaluated by the thermal resistance, or RSI value, of the enclosing surfaces. RSI values for wall, roof and foundation are determined for energy modeling.

BUILDING ENERGY MODELING (BEM)

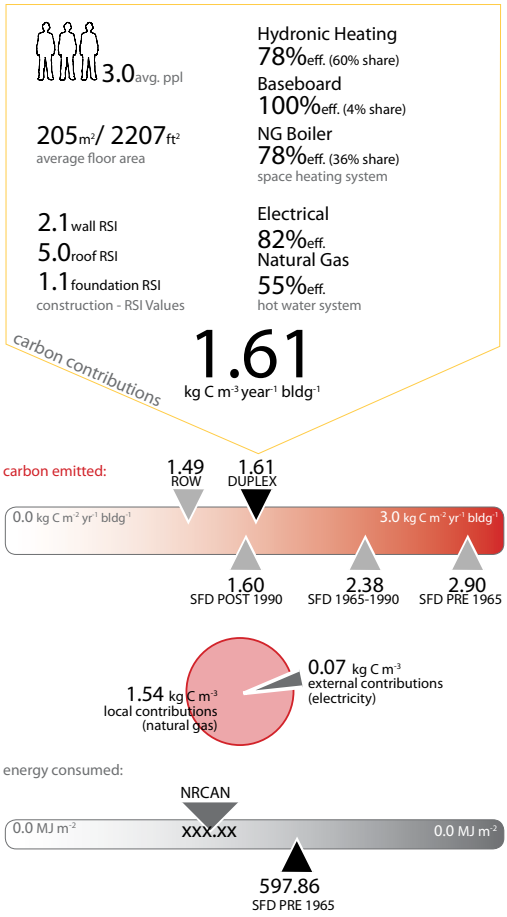

INPUTS - CHARACTERISTICS & PERFORMANCE
Source: elementsdb, LIDAR, field work, GIS, ecoEnergy, BC assessment, BC-Hydro, CMHC, & SHEU

OUTPUTS & BENCHMARKS
Hot2000, & Sunset Tower, and NRCAN

Figure 1.1.3: Example of a building typology approach to energy modelling. Morphological remote sensing identifiers are associated with energy and emissions relevant use, design and construction attributes and modelled to estimate energy demand and carbon emissions benchmarks.

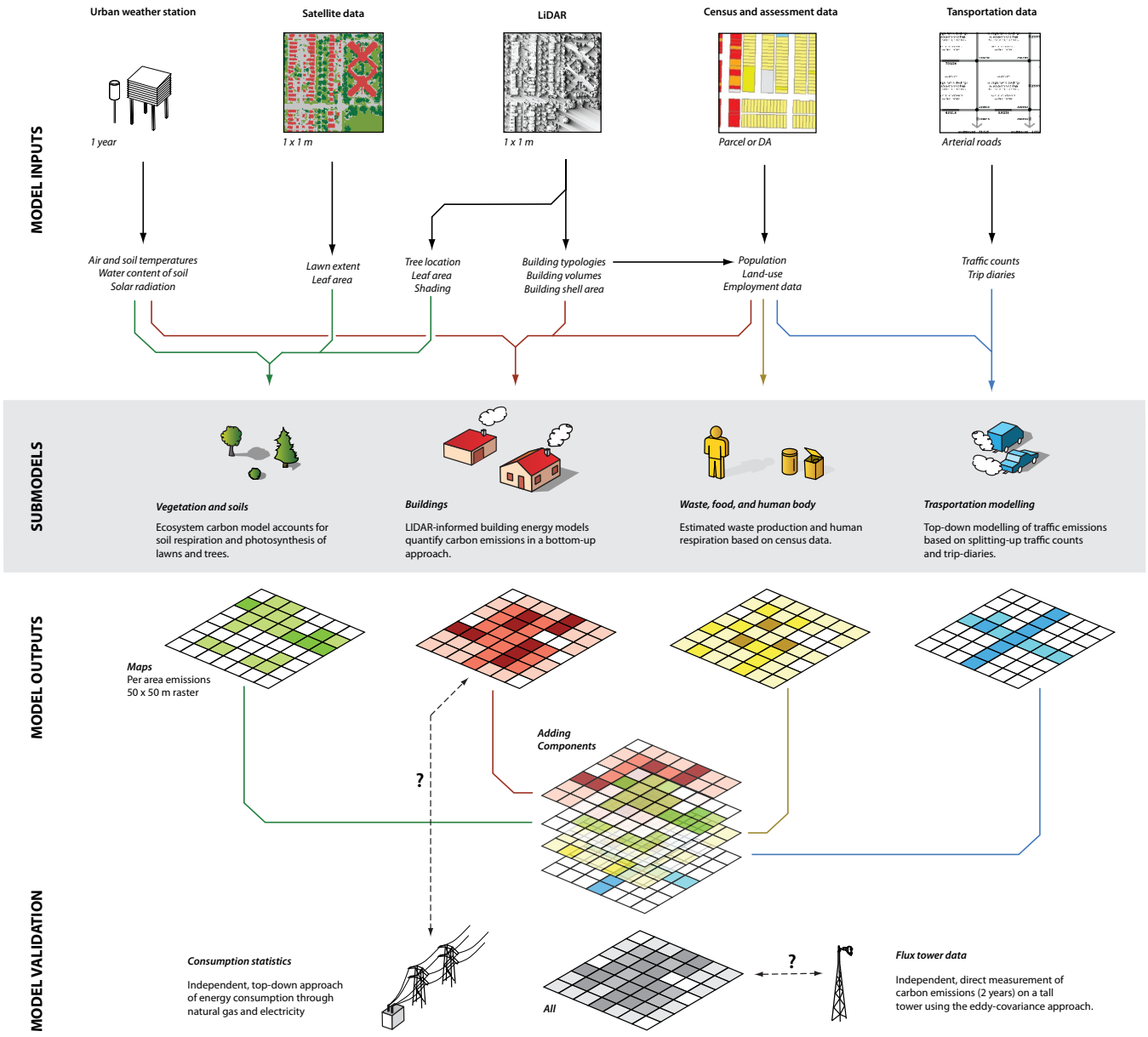

Figure 1.1.4: Diagrammatic representation of project concept and modelling approach. At the centre (grey band) is the project's urban metabolism, systems-based approach in which carbon is attributed to four metabolism components or sub-models — vegetation and soils, buildings, people and transportation. At the top, are the data sources from which sub-model inputs are derived and aggregated. Below are model outputs which are modelled carbon emissions estimates expressed in quantitative (how much) and spatial (where) terms. At the bottom is a model validation step in which energy consumption statistics, modelled outputs and field-measured results are compared.

1.2 Urban Metabolism

This section introduces the concept of an 'urban metabolism approach'. It defines urban ecosystems as dynamic, open systems of material fluxes and material storage on a range of spatial and temporal scales. Further, the challenges of defining system boundaries and comparability between different scales are discussed.

1.2.1 The Metabolism Analogy

In analogy to the metabolism of an organism, the processes accompanying the functioning of a city involving the intake of resources such as power, carbon, water and food and the release (emissions) of heat, greenhouse-gases, pollutants, products and waste can be described as urban metabolism (Wolman, 1965; Kennedy et al., 2007). Figure 1.2.1 shows a schematic urban metabolism with the inputs in form of food, water, raw materials and power, and the outputs such as greenhouse gases, waste and goods. The urban ecosystem is the urbanized area where those materials cycle through and includes various components such as urban vegetation, atmosphere, water, soils, human bodies, goods and buildings.

1.2.2. Sustainability of Urban Ecosystems

While most natural ecosystems are self-maintaining, is clear that no city can function without supply of energy, carbon, water etc. from its hinterland (surroundings). In this way, cities alone are not sustainable as they rely on constant intake of resources from the city's watershed, power grid, economic network, or food-shed. If assessing the environmental sustainability of a given urban system, we should consider all processes associated with a given change as part of the metabolism, including effects that take place beyond the city's limits.

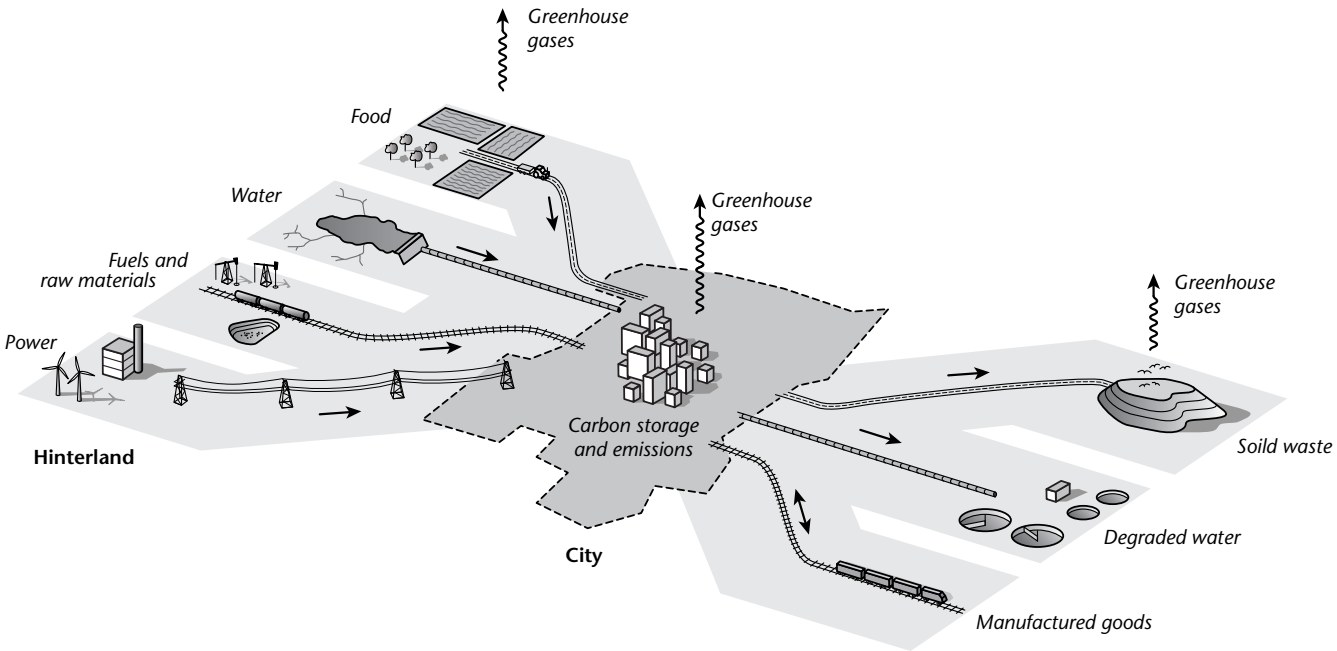

Figure 1.2.1: Schematic of an urban system depicting the urban metabolism with its continuous intake of food, water, raw materials and power, and the conversion into products such as goods, greenhouse gases and waste (modified from Oke et al., 2010).

1.2.3. Scales and System Boundaries

Practically, the complexity of resource and product dependencies in a globalized economy makes the isolation of a single city and its hinterland challenging, if not impossible. Therefore, most studies of material and resource flows, including greenhouse gas emission inventories, are only possible on coarse scales (e.g. Environment Canada, 2009), or omit direct processes outside the system's limits. For example, Figure 1.2.2 illustrates the various scales at which greenhouse gas budgets or inventories are modelled and possible emission reduction actions that are informed by those results.

The finer the scale of interest, the more the system depends on resources and energy supply from outside. Hence buildings, neighbourhoods and cities must be modelled as open systems as most buildings or neighbourhoods do not function without the majority of their energy supplied from outside the system. Although, regions and nations can be independent in some networks (e.g. food), they might still depend on the outside the system (e.g. fossil fuels). The only closed system in some regard is the global scale system, although there is import of solar energy from the sun.

1.2.4. Modelling the Urban Metabolism

The metabolism approach has been applied to whole metropolitan areas at the city-scale (Table 1.2.1) relying mostly on a top-down approach based on consumption, census and economic information available at coarser scales. For example, Table 1.2.1 illustrates that per-capita emissions of carbon dioxide (CO_2) in various cities range broadly and are likely controlled by climate, efficiency of transportation systems, sources of power generation, urban form, and density.

To assess the environmental sustainability of various urban development patterns (land-use mix, urban form), the neighbourhood-scale is more appropriate, as density and land-use change considerably within a city. However, with finer scale (increasing spatial resolution), quantifying consumption and emissions becomes a more challenging undertaking because of reduced data availability at finer scales, and the fact that systems are more open and dynamic (mobility of goods, vehicles and humans within an urban area). Although a neighbourhood (and a city) is by no means self-maintaining, it is possible to model material and energy flows as the result of a dynamic, interrelated system of natural and

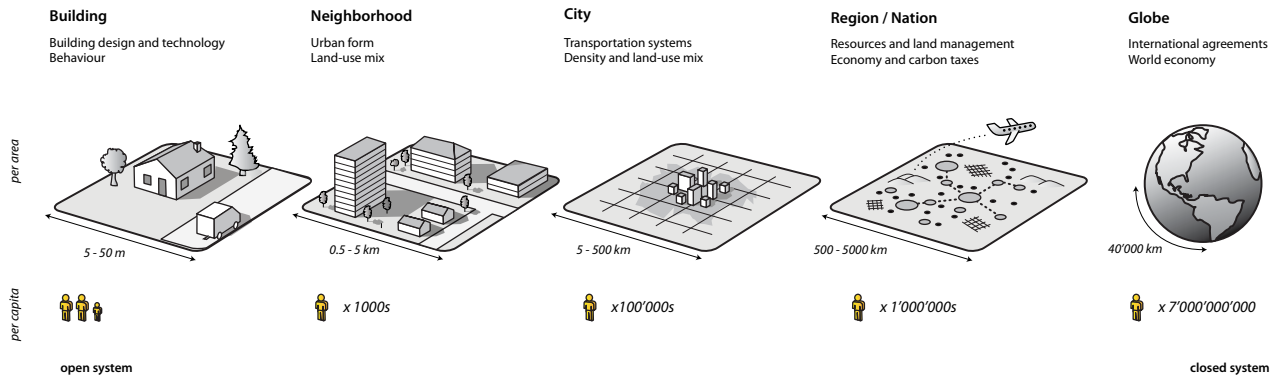

Figure 1.2.2: Scales of urban and regional greenhouse-gas inventories and scale-dependent decisions (technological, behavioural and policy) that could reduce emissions.

Table 1.2.1: Per capita carbon emissions (in form of CO_2) in various metropolitan areas or cities (modified from Pataki et al., 2006).

City	Latitude (°)	Per Capita Carbon Emissions (t CO_2 cap^{-1} $year^{-1}$)	Source
Tokyo, Japan	36^{0}N	4.3	Hanya & Ambe (1976)
Hong-Kong, China	22^{0}N	4.8	Warren-Rhodes & Koenig (2001)
Vancouver, Canada	49^{0}N	5.1	BC Ministry of Environment (2009)
London, UK	52^{0}M	5.5	Chartered Institute of Wastes Management (2002)
Brussels, Belgium	50^{0}N	5.9	Duvigneaud & Denayeyer-De smet (1977)
Sydney, Australia	34^{0}N	9.1	Newman (1999)
Toronto, Ontario	43^{0}N	14.0	Sahely et al. (2003)

anthropogenic processes at the neighbourhood scale using a combination of bottom-up (upscaling) and top-down (downscaling) approaches. For example, Codoban and Kennedy (2008) analyzed the urban metabolism of four representative urban neighbourhoods in the Greater Toronto area to assess the sustainability of urban development strategies.

At the finest scale, we can model the metabolism of a single building. This scale again is well suited for modelling, and for many applications, detailed information on a particular building is known. At the building scale, mostly urban form, technology and behaviour of the occupants control the energy and materials input and waste output, including greenhouse gas emissions.

There are many materials or forms of energy that could potentially be tracked using the urban metabolism approach, including food, water, etc. The current study focuses on the metabolism of carbon at the neighbourhood scale.

1.3 The Urban Carbon Cycle

This section is applying the urban metabolism approach to carbon budgeting within urban systems. It discusses the concept of lateral and vertical carbon fluxes, carbon pools and associated conversion processes involved in the urban carbon cycle.

1.3.1 The Carbon Budget

An urban carbon cycle can be defined for any scale of urban ecosystem (city, neighbourhood, building). For a given system with its spatial boundaries, carbon can be conceptually tracked through quantifying inputs and outputs (e.g. emissions into the atmosphere), as well as storage changes within the systems (Figure 1.3.1). The magnitude of carbon fluxes or pools can be informed by either direct measurements at system boundaries, top-down, or bottom-up modelling. As the total carbon is conserved, we can write for any system:

(Carbon inputs) = (Carbon outputs) - (Storage changes in carbon pools)

This essentially is a material flow analysis for carbon and means that we quantify all internal storage changes (pools), inputs and outputs (fluxes) for the system. Inputs and outputs can happen at different boundaries, and we conceptually separate lateral fluxes from vertical fluxes (Figure 1.3.1).

1.3.2 Lateral Carbon Fluxes

Lateral fluxes refer to the mass of carbon imported (or exported) per time into (or out of) a system at the lateral (side) boundaries. Lateral fluxes can be expressed in kg C $year^{-1}$ or normalized by the systems ground area (in kg C m^{-2} $year^{-1}$). Lateral fluxes are in most cases anthropogenic processes and import carbon as fossil fuel (gasoline, diesel, natural gas), food, construction material, etc. into the urban ecosystem, and export carbon in form of goods, solid or liquid waste through supply and management channels (Churkina, 2008). Lateral fluxes typically transport carbon in form of carbohydrates, not carbon dioxide.

1.3.3. Vertical Fluxes

Vertical fluxes are essentially emissions of carbon dioxide into the atmosphere although the term also incorporates carbon-dioxide uptake by urban vegetation (photosynthesis). Vertical fluxes are fluxes at the system's upper boundary (land-atmosphere interface) and result from chemical processes in the system, namely combustion, respiration, and photosynthesis:

Combustion – Combustion is the controlled burning (oxidation) of fossil fuels in engines and heating systems. The process of combustion is resulting in a release of carbon dioxide while gaining energy in form of electricity, heat, or mechanical energy. To date, the dominant fossil fuels used in an urban ecosystem are natural gas, gasoline and diesel, historically also wood and coal were important. Mass flux densities of fossil-fuel combustion can be conceptually separated into emissions from vehicles, emissions from buildings due to space heating and emission from industrial processes. Those emissions follow diurnal, weekday and seasonal human activity cycles (traffic, heating requirements).

Respiration – is the oxidation of carbohydrates by living organisms associated with the release of energy. The process of respiration is resulting in a release of carbon dioxide while gaining energy for the metabolism to maintain living functions. We distinguish between autotrophic respiration (trees, humans) and heterotrophic respiration (microbes) in soils and waste. Respiration rates are depending on the activity of the organism involved, which can be in the case of plants and microbes be controlled by temperature and water availability.

Photosynthesis – is the biological process of carbohydrate formation by fixation of atmospheric carbon dioxide by plants. This happens in the chlorophyll-containing tissues of leaves, needles and other plant parts under input of sunlight (photosynthetic active radiation in the range 400 – 700 nm). Urban vegetation (trees, lawns, gardens etc.) can be expected to show slightly higher rates of photosynthesis due to (i) decreased water stress due to additional water availability by irrigation, (ii) generally warmer and more conservative temperatures in urban ecosystems (urban heat island) that extend the vegetation period and reduce frost damage, and (iii) fertilization by elevated atmospheric nitrogen deposition and elevated carbon dioxide concentration in cities (Trusilova and Churkina, 2008). On the other hand, air pollution can also lead to significant physiological stress and damage and reduce photosynthetic rates in areas where in particular ozone concentrations are high.

Similar to lateral fluxes, vertical fluxes (and hence emissions) are also expressed in kg C $year^{-1}$ or normalized by the system's ground area (in kg C m^{-2} $year^{-1}$). Other studies have reported emissions in kg CO_2 $year^{-1}$, but as vertical fluxes are the result of the chemical transformation processes between carbohydrates and carbon dioxide it is more useful to conserve carbon, not carbon dioxide when providing budget equations.

1.3.4 Carbon Pools

The term carbon pool refers to locally stored deposits of organic carbon in the urban ecosystem. Carbon pools are vegetation, soils, buildings, furniture, and human bodies. For example, if urban trees sequester carbon through photosynthesis, this carbon is stored locally in the urban ecosystem in tree biomass and soil. As tree biomass and soil pools grow over time, the accumulation of carbon in those pools has to be protected to sustainably offset emissions. Carbon pools can be expressed in kg C or normalized by the ground area (in kg C m^{-2})

The assessment of carbon pools is important to quantify potential and limits of carbon sequestration and estimate emissions following urban land-cover and form changes (i.e. development, redevelopment, removal of soil, increase in vegetation). Emission reduction strategies and policies must not only focus on changes in steady-state vertical and lateral fluxes but also incorporate disruptions to carbon pools.
Some carbon pools are closely coupled to the vertical or lateral fluxes and their magnitude ebbs and flows according to the inputs and outputs. For example, carbon in biomass and soils changes on daily and seasonal cycles following input by photosynthesis and output by respiration. Other

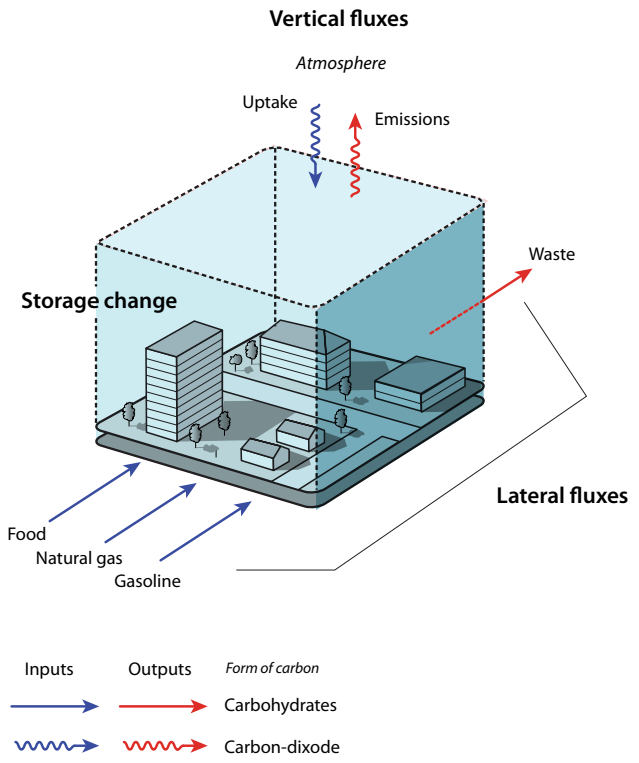

Figure 1.3.1: Conceptual representation of internal storage changes, lateral and vertical carbon fluxes for a neighbourhood-scale urban ecosystem.

carbon pools in an urban ecosystem are essentially immobile (e.g. buildings) and their carbon is rarely released to the atmosphere (e.g. in the unlikely event of a building fire, or on longer time-scales after demolition). The turnover rate of carbon in a given carbon pool is a measure of its activity.

1.3.5 Components of the Urban Carbon Cycle

In this study, vertical fluxes (i.e. emissions) are conceptually separated into four components that are illustrated in Figure 1.3.2

Buildings and Industry – This component includes stationary combustion sources transforming mostly fossil fuel carbon (natural gas, oil, coal) or renewable carbon (wood fires) into carbon dioxide for space heating or cooling, and industrial processes. The detailed methods to estimate building-related emissions in this study are described in Section 2.3.

Transportation – Mobile combustion sources transform fossil fuels (gasoline, diesel) or potentially renewable carbon (biofuels) into carbon dioxide. The challenge with estimating the magnitude of this component is accounting for the relatively extreme variation in space and time, and attributing emissions to a selected urban activity (see also section 1.3.6). The detailed methods to estimate transportation-related emissions in this study are described in Section 2.4.

Human body, food and waste – This component includes both stationary and mobile processes of respiration as a result of the human metabolism and heterotrophic (microbial) decomposition of waste. Although the carbon cycled through this component is entirely renewable (the human food chain starts with plants that sequester atmospheric carbon), there are external emissions associated with food production, and potentially accompanying methane emissions resulting from urban waste management that still cause disruptions to the global climate system.

Urban vegetation and soils – This component can act as sink or source through photosynthesis and respiration. As it entirely involves renewable carbon it is not accounted for in most studies. However, the ability of urban vegetation to sequester fossil fuel carbon in urban biomass and soils make this

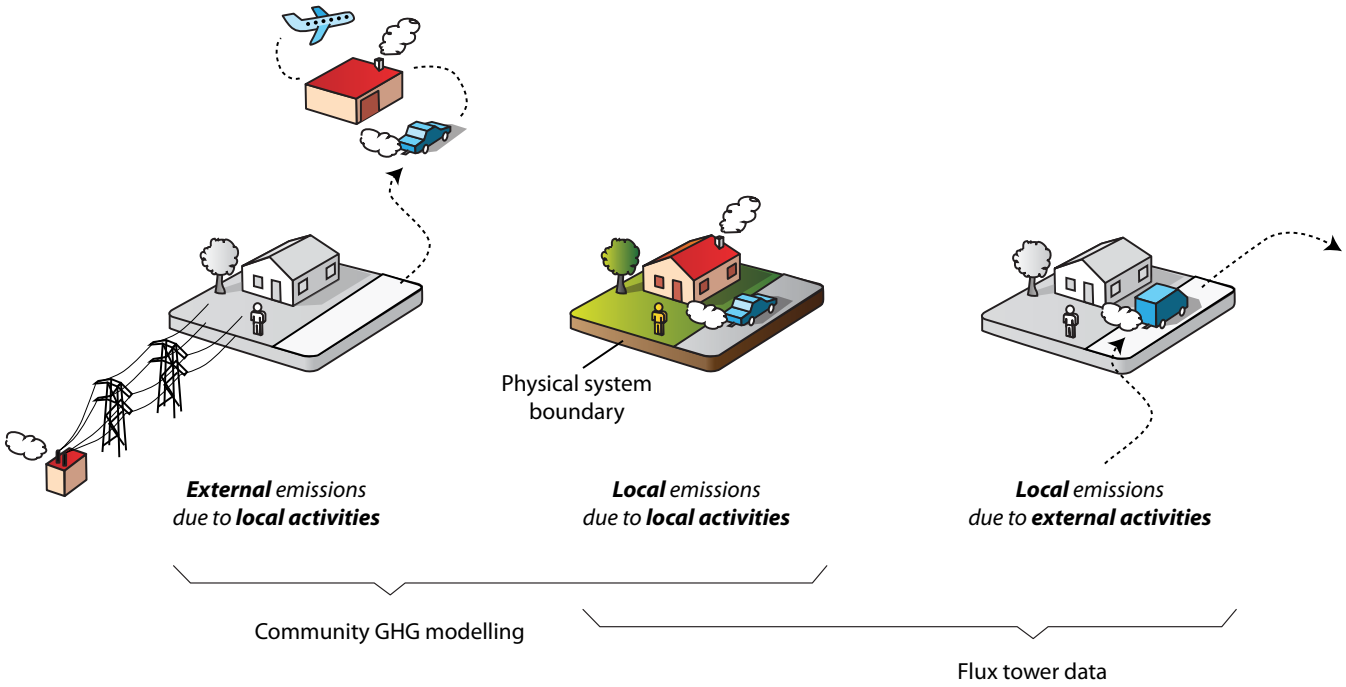

Figure 1.3.2: The concept of local and external emissions for a given urban ecosystem.

component relevant in urban metabolism studies. Fluxes are highly variable in time and space and largely influenced by the management of urban vegetation. The detailed methods to estimate uptake and emissions from vegetation in this study are described in Section 2.5.

1.3.6 Local and External Emissions

Some of the components discussed in section 3.1.5 are mobile (cars, trucks, humans), others use energy in form of electricity, materials or food that result in carbon emissions outside the system boundary. Figure 1.3.3 underlines the spatial differences between emissions that can be locally detected within the urban system (e.g. using a flux-tower, Section 2.6) and the desired deliverables for community-scale carbon modelling that include emissions due to activities in a specific sector that might happen outside the system:

- Local emissions due to local activities – refers to the release (or uptake) of carbon dioxide within the neighbourhood (system boundaries) due to combustion, respiration or photosynthesis.
- External emissions due to local activities - refers to the release of carbon dioxide outside the neighbourhood (system boundaries) due to combustion or respiration associated with activities within the neighbourhood.
- Local emissions due to external activities - refers to the release of carbon dioxide within the neighbourhood (system boundaries) due to combustion and respiration from objects or humans travelling through the neighbourhood, but not associated with activities in the neighbourhood (e.g. through-traffic).

Table 1.3.1 lists for each component (buildings, transportation, human body, vegetation and soils) – emission processes in each of the three above cases.

Table 1.3.1: Examples of external and local carbon dioxide emissions in neighbourhoods.

	External Emissions due to Local Activities	Local Emissions due to Local Activities	Local Emissions due to External Activities
Buildings	Power generation emissions associated with power consumption within the neighbourhood	Natural gas combustion of buildings within the neighbourhood	(none)
Transportation	Trips out of the neighbourhood to work, school, recreation, etc.	Trips within community	Through-traffic
Human Body	Human respiration outside the neighbourhood by residents	Human respiration	Human respiration of people travelling through
Vegetation and Soils	Garden waste disposal outside system	Photosynthesis and respiration of plants within the neighbourhood	(none)

References:

Baker, N., Steemers, K. (2000). *Energy and environment in architecture: a technical design*. New York: E&FN Spon.

BC Ministry of Environment (2009). *Community Energy & Greenhouse Gas Emissions Inventory: 2007.* Government of British Columbia.

Bory, B., & Shremmer, C. (2009). *SUME — Sustainable Urban Metabolism for Europe*. Retreived on June 20, 2010 from http://www.corp.at/corp_relaunch/papers_txt_suche/CORP2009_143.pdf

BRIDGE (2010). *Sustainable Urban Planning Decision Support Accounting for Urban Metabolism*. Retreived on June 20, 2010 from http://www.bridge-fp7.eu/

Canada Mortgage and Housing Corporation (2005). *Comparing Neighbourhoods for Sustainable Features.* Retreived on June 20, 2010, from http://www.cmhc-schl.gc.ca/en/co/buho/sune/index.cfm

Centre for Neighborhood Technology Energy (2009). *Chicago Regional Energy Snapshot*. Retreived on June 20, 2010, from http://www.cntenergy.org/media/Chicago-Regional-Energy-Snapshot.pdf

Chartered Institute of Wastes Management (2002). *A Resource Flow and Ecological Footprint Analysis of Greater London.* Best Foot Forward, London.

Churkina G. (2008). *Modeling the carbon cycle of urban systems*. Ecol Model, *216*(2), 107-113.

Codoban, X., & Kennedy C. (2008). Metabolism of neighbourhoods. *Journal of Urban Planning D-Asce*, 134(1), 21-31.

Duvigneaud P., & Denayeyer-De Smet S (1977). Traveaux de la Section Belge du Programme Biologique International, Bruxelles. In L'Ecosystéme Urbs. In *L'Ecosystéme Urbain Bruxellois* (eds Duvigneaud P, Kestemont P), pp. 581–597.

Environment Canada (2009). *National Inventory Report 1990 – 2007: Greenhouse Gas Sources and Sinks in Canada*. Greenhouse Gas Division of Environment Canada.

Hanya T., & Ambe Y. (1976). A study on the metabolism of cities. In *Science for a Better Environment* (ed. HESC Science Council of Japan), pp. 228–233. Kyoto.

Kennedy C., Cuddihy, J., & Engel-Yan J. (2007). The Changing Metabolism of Cities. J*ournal of Industrial Ecology, 11*(2), 43-59.

Kaufmann, Robert and Boston University (2009), *Collaborative Research on the Metabolism of Boston: Clean Energy and Environmental Sustainability Initiative*. Retreived on June 20, 2010 from http://www.bu.edu/energy/research/projects/metabolism-of-boston

Ministry of the Environment, Province of British Columbia (2009). *Community Energy and Emissions Inventory Reports*. Retreieved on June 20, 2010 from http://www.env.gov.bc.ca/cas/mitigation/ceei/index.html

Newman, P. W. G. (1999). Sustainability and cities: extending the metabolism model. *Landscape and Urban Planning, 44*, 219–226.

Office of the Governor, State of California (2008). *Senate Bill 375: Redesigning Communities to Reduce Greenhouse Gases*. Retreived on June 20, 2010 from http://gov.ca.gov/fact-sheet/10707

Oke, T. R., Mills G., Voogt J., & Christen A. (2010, in prep.). *Urban Climates*. Cambridge University Press.

Pataki, D., Alig, R., Fung, A., Golubiewski, N., Kennedy, C., McPherson, E., Nowak, D., Pouyat, R., & Lankao, P. (2006). Urban ecosystems and the North American carbon cycle. *Global Change Biology, 12*(11) 2092-2102.

Sahely, H. R., Dudding, S., Kennedy, C. A. (2003). Estimating the urban metabolism of Canadian cities: greater Toronto Area case study. *Canadian Journal of Civil Engineering, 30*, 468–483.

Salat, S. (2007). Energy and Bioclimatic Efficiency of Urban Morphologies: Towards a Comparative Analysis of Asian and European Cities. *In Proceedings of the International Conference on Sustainable Building Asia* (pp. 161-166). Seoul: Fraunhofer IRB. Retreived on June 20, 2010 from http://www.irbdirekt.de/daten/iconda/CIB8015.pdf.

Salat, S. (2008). Density - Energy Consumption - Urban Texture. *URBA 2000*. Retreived on June 20, 2010 from http://www.urba2000.com/club-ecomobilite-DUD/IMG/pdf/SALAT.pdf.

Salat, S., & Morterol, A. (2008). Factor 20: A Multiplying Method for Dividing by 20 the Carbon and Energy Footprint of Cities: The Urban Morphology Factor. *Chamber of French Commerce and Industry in China*. Retreived on June 20, 2010 from www.ccifc.org/index.php/fre/content/download/1470/19204/file/Factor%2020,%20the%20Urban%20Morphology%20Factor%20-%20Serge%20Salat%20(21%20May%202008).pdf.

Steemers, K. (2003). Energy and the city: density, buildings and transport. *Energy and Buildings, 35*(1), 3-14.

Trusilova, K. & Churkina, G. (2008). The response of the terrestrial biosphere to urbanization: land cover conversion, climate, and urban pollution. *Biogeosciences, 5*(6), 1505-1515.

Warren-Rhodes, K., & Koenig, A. (2001). Escalating trends in the urban metabolism of Hong Kong: 1971–1997. *Ambio, 30*, 429–438.

Wolman, A. (1965). The metabolism of cities. *Scientific American*, 179-190.

2.1 The 'Sunset' Neighbohrood in Vancouver

This section introduces the case study site and its principal population, land use, buildings and transportation related attributes.

2.1.1 The Sunset Neighbourhood Case Study

Sunset neighbourhood in south central Vancouver — an area bounded by E. 41st Avenue and the Fraser River to the north and south and Ontario Street and Knight Street to the west and east — is one of the city's most ethnically diverse neighbourhoods. The majority of the population live primarily in single-family residential areas (typically RS-1S, a single family zone in which any dwelling may add a rental suite). The area's commercial and higher density residential nodes and corridors are located primarily along arterial streets such as Fraser and Knight (N-S) and 41st, 49th, 57th and SE Marine Drive (E-W). Within Sunset, this project's study area is an approximately 2 km square area (red area in figure 2.1.1) at the western edge of the neighbourhood. At the centre of this study is a carbon flux instrumented tower (see Section 2.7).

2.1.2 Study Area Attributes

Most buildings are residential and lower density (approximately 12 dwelling units hectare^{-1}). Within the study area are 4155 detached dwellings. Approximately 55% have secondary suites.
At an average of 3.7 persons, the residential dwellings support a population of 23168 persons. Approximately 37% of dwellings were built before 1965, 38% between 1965 and 1990, and 25% post 1990. The majority of single family homes are heated from natural gas.

In addition, there are a smaller number of non-residential — commercial, mixed use, light industrial and institutional building types that accommodate

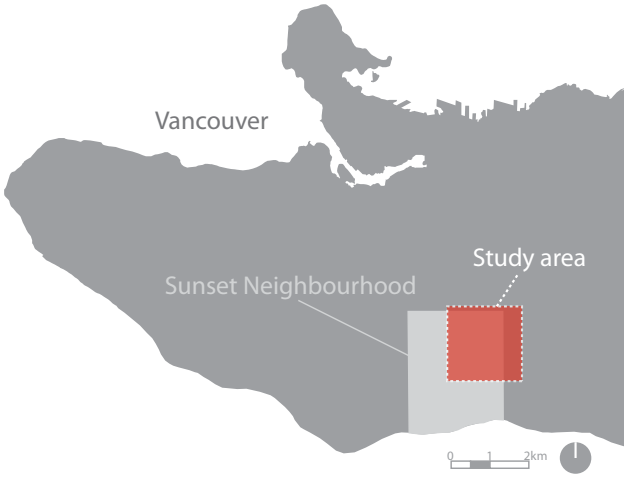

Figure 2.1.1: Location of study area (Sunset neighbourhood highlighted in light grey). Approximate outline of study area in red.

Figure 2.1.2: Illustrative photos of principal dwelling types within study area. Clockwise from upper left: pre-1965 single family bungalow; 1965 – 1990 single family with secondary suite option; duplex; rowhouse; apartment; and, mixed use. Images generated using Google Maps and Streetview (http://maps.google.com/).

Figure 2.1.3: Illustrative photos of principal commercial and other non-residential types within study area. Clockwise from upper left: smaller scale retail and restaurants; local grocery; mixed use, office, light industry, school. Images generated using Google Maps and Streetview (http://maps.google.com/).

The street network in the study area is an atypical pattern of one very high volume north-south arterial street (Knight Street), one high volume east-west arterial street (East 41st Avenue), four more moderate volume arterials (Fraser and Victoria north-south, and East 49th and East 54th / 57th east-west) and many low volume local streets between. Knight Street, the central north south corridor in the study area serves a significant regional transportation as a commuting corridor and major truck route to major employment areas (Surrey and Richmond for example) on the south side of the Fraser River with connections to the U.S. border truck crossing. Arterial trip loads and with them transportation related energy demand and carbon emissions throughout the study area are much higher than would be anticipated of a neighbourhood of this type.

Figure 2.1.4: Figure-ground plan of study area from Figure 2.1.1. The Sunset study area highlighted is centred around a carbon flux tower at the intersection of Knight and East 49th Avenue.

Figure 2.1.5: Illustrative photos of arterial streets within study area. Left to right by row from upper left: north-south arterials are Fraser Street, Knight Street, Victoria Drive; middle left: east-west arterials are East 41st Avenue, East 49th Avenue and East 57th Avenue; and lower left: local streets are Fleming Streets, East 47th Avenue and Elgin Street. Images generated using Google Maps and Streetview (http://maps.google.com/).

2.2 Remote Sensing Data Inputs for Emission Modelling

This section describes the remote sensing techniques applied to extract buildings and vegetation characteristics over the Sunset study site. LiDAR data provides a raw three-dimensional surface from which individual objects (buildings and trees) can be extracted using geometric algorithms. Those features with limited three-dimensional structure, such as ground vegetation, are not discernable using LiDAR data; therefore additional analysis of satellite imagery is used to extract lawns, bushes, gardens, and ornamental plants as 'ground vegetation'. Individual trees in the study area were also extracted using manual aerial photo interpretation integrated with height information from the LiDAR data. The features derived from the remote sensing products are used to inform further analysis on the contribution of buildings (Section 2.3) and vegetation (Section 2.5) to neighbourhood-level carbon and energy fluxes.

2.2.1 LiDAR in the Urban Environment

Remote sensing devices offer a wide range of opportunities to automatically derive land cover features across varying terrain. Current remote sensing campaigns in urban areas utilize numerous technologies from conventional photographic image acquisition to more sophisticated devices that measure the three-dimensional form of the urban surface. Data captured by remote sensing devices has the capacity to reveal a wide-range of processes active in an urban setting, and analysis of this data can provide planners and decision-makers with critical information for the management of urban ecosystems.

Remote sensing technologies are divided into two categories of sensors: 1) passive sensors, that use light reflected off a surface to produce an image; and 2) active sensors, that generate and receive their own source of energy to produce data. Both of these technologies play an important role in the analysis of land cover in urban environments. Traditionally, passive sensors have been used almost exclusively for urban planning purposes in the form of aerial- and ortho- photographs. However, recent advances in active remote sensing devices can provide topographic information at a scale appropriate for urban analysis. Light detection and ranging (LiDAR) devices represent the leading technology in active remote sensing.

Functioning on the principle of echo-returns, LiDAR provides an accurate calculation of the distance to objects by emitting a pulse of laser energy and recording the time it takes that same pulse to return to the device. While the direction of the laser path is stationary, LiDAR devices are often attached to a vehicle to enable the acquisition of ranging data across geographic space. In the case of urban analysis, the LiDAR device is typically mounted to a fixed-wing or helicopter platform. Recording the exact location and orientation of the platform at the time that each laser pulse is emitted enables an accurate extraction of elevation-above-sea-level for features intercepting the laser pulse. Current LiDAR devices emit more than 100,000 laser pulses per second and have the ability to record multiple returns for a single pulse. Secondary returns can be used to provide additional height measures for those objects that do not reflect the entire signal on first contact with the pulse (e.g. trees).

2.2.2 Extraction of Building Typologies and Characteristics

LiDAR data was provided through the Environmental Prediction in Canadian Cities (EPiCC) project with funding from the Canadian Foundation for Climate and Atmospheric Sciences (CFCAS) and was acquired in March 2007 using a TRSI Mark II discrete-return sensor attached to a fixed-wing platform with an average point density of 0.7m^2. To precisely estimate the height of objects using LiDAR technology requires an accurate representation of the ground surface as the height of objects intercepting the laser beam are calculated relative to the ground topography. Returns pre-classified as ground were used to generate a digital elevation model (DEM) with a 1 m pixel size using the natural neighbour interpolation algorithm (Sambridge et al., 1995; Sibson, 1981). This DEM was then subtracted from the non-ground returns transforming the elevation data into height above ground surface. Furthermore, a maximum height surface model was developed using the highest LiDAR return heights (above ground surface) and the natural neighbour algorithm to form a continuous 1m surface. A 3-by-3-pixel median filter kernel was then applied to the image and subtracted from the original gridded layers to smooth holes and spikes in the raster images resulting from lack of data, edge effect, water absorption and birds. Pixels with a difference of 50m were selected as erroneous and replaced using Delaunay triangulation.

The procedure used to extract building and tree features from the LiDAR data follows the techniques of Goodwin et al. (2009). The first step to quantify the structure of trees and buildings in urban environments involved isolating the LiDAR returns that interact with vegetation. To do this, the LiDAR last return layer was examined. Since the solid form of building rooftops typically reflects the entire laser pulse, few building returns tend to be represented in the last return layer, while gaps in the three-dimensional structure of trees allows the laser pulse to produce a second signal return lower in the canopy. Nonetheless, some urban features, such as building edges and powerlines, also generate second pulse returns; therefore a spatial filtering step was applied. A 9 by 9 pixel moving kernel was used to iteratively assess the number of pixels containing second returns from a series of projected vectors between 1 and 180°. When the number of cells intercepting a given vector was greater than 4 they were classified as linear features (generally representing building edges) and subsequently removed. Finally, a second filter was applied to indentify clusters of trees by establishing a threshold where 80% of the total pixels within the kernel were identified as tree pixels. These clusters were then grown by reassigning pixels with non-tree pixels in the moving window as the tree class. The resulting layer is a binary image of LiDAR pixels representing the planimetric extent of trees. The extracted tree layer is used to mask the original first return LiDAR grid producing a height layer of non-tree features. An area threshold of 40m^2 and a height threshold of 3m were applied to each remaining object to select buildings from the LiDAR dataset. The output result from this technique provides a classification layer that describes the spatial extent and number of 1) tree crowns or clusters of tree crowns and 2) buildings (Figure 2.2.1).

After all buildings were extracted from the LiDAR data, a set of post-processing steps were required to: remove secondary buildings including garages and sheds, smooth building edges, and associate buildings to relevant land parcels. The secondary building removal technique used a polygonal layer of all buildings with three Boolean operations to determine the non-dwelling/non-commercial edifices on each lot. The operations included the removal of structures: less than 50m^2 in area, less than 75m^2 and intersecting a 4m buffer of an alleyway, and not intersecting a 25m buffer of a street. After the secondary build features were removed, a polygon simplification algorithm was applied (Bayer, 2009) to smooth the pixilation artifacts from the raster building extraction technique (Figure 2.2.2). The last step in deriving the buildings involved separating buildings according to parcel data. The LiDAR extraction technique cannot separate adjoining buildings (e.g. ground-level commercial structures), therefore post-processing is required to divide building polygons based on cadastral land parcel data provided by the City of Vancouver. Goodwin et al. (2009) undertook a comparison of building areas derived from LiDAR and compared them to areas as interpreted from aerial photography. The comparison demonstrated the approach is accurate (r^2= 0.73, $p<0.001$) however some buildings had significant errors due to adjacent buildings not being discriminated (i.e. commission errors). When these outliers were removed the r^2 value increased to 0.96. Commission errors (i.e. buildings that were not identified) were also evident within some residential areas with the overall percentage difference between estimates equal to 35% (n = 98), which reduced to 16% (n = 83) following the removal of commission errors. This suggests that building area estimates are comparable to aerial photography when LiDAR can separate individual buildings from the surrounding features (Goodwin et al., 2009).

After successful extraction of building polygons using the previously mentioned techniques, a suite of building morphological features were extracted to inform typologies for existing energy consumption models. A number of metrics related to roof slope morphology, roof shape morphology, volume, area, and surface area were calculated and multivariate statistics were used to determine the metrics that represented distinct attributes for further analysis. Result of a factor analysis (Table 2.2.1) indicate the appropriate division of categories into roof-orientation, roof-slope and building volumetric categories, from which percent North- and East-facing roof, percent of roof slope under 20 degrees, and volume are the preferred variables to represent the determined categories.

2.2.3 Extraction of Urban Vegetation\ Characteristics

In the previous subsection the extraction of trees was introduced as a preliminary step in the procedure for deriving buildings, and this layer provided the necessary information for the accurate representation of trees across the study area. However, lawns, bushes, gardens, and ornamental ground vegetation also represent a substantial portion of surface cover in urban areas required for estimating carbon sequestration and soil respiration (section 2.5). While the geometrically distinct characteristics of trees facilitates the extraction of these features using LiDAR data, lawns and soils are

Table 2.2.1: Factor analysis of building morphological features

Variable	Orientation Factor	Volumetric Factor	Slope Factor
North-facing roof (%)	-0.89	0.14	0.05
South-facing roof (%)	-0.88	0.18	0.04
East-facing roof (%)	0.84	-0.25	0.01
West-facing roof (%)	0.79	-0.45	0.01
Volume (m^3)	-0.26	-0.78	0.43
Surface area (m^2)	-0.36	-0.74	0.43
Slope under 20^0 (%)	-0.37	-0.45	-0.73
Slope 20^0 to 30^0 (%)	0.27	0.39	0.57
Slope over 30^0 (%)	0.27	0.33	0.39
Proportion of Total Variance Explained	0.27	0.18	0.14

inseparable on the basis of geometry alone. As a result, supplementary remote sensing datasets were used to provide the spectral properties necessary to accurately derive ground vegetation estimates.

In this project, satellite imagery was also used. A Quickbird image was acquired over the study area on June 28th 2008. The image was calibrated to radiance values using the provided metadata and then orthorectified using the rational polynomial coefficients (RPCs) provided from DigitalGlobe and a 25m DEM of the area. To further ensure accurate alignment with the LiDAR data a secondary geographic registration was performed using a 2004 orthophotograph and the panchromatic Quickbird band producing a RMS error of 0.66m.
The procedure involved in extracting the ground vegetation (predominantly lawns) involved integration of both the Quickbird multispectral data and the LiDAR first returns layer. The LiDAR layer provided the necessary information to distinguish ground from non-ground features. In this step only those areas where first return values (normalized using the digital elevation model of bare ground) less than 1m were used for analysis. After determining ground, a normalized difference vegetation index (NDVI) was produced from the red and near-infrared bands of the Quickbird image with a threshold of 0.2 to help discern vegetated from non-vegetated surfaces. The combined result provides a layer of ground vegetation for the study area (Figure 2.2.1) (Tooke at al. 2009).
The derivation of individual trees and relevant attributes (e.g. height, crown diameter) in an urban setting is not currently possible using existing technology and extraction algorithms. Although studies have successfully derived these metrics for homogeneous forest stands, the heterogeneous composition of urban areas and the variety of tree species and shapes found in the city prohibit the extension of forestry-based techniques to urban analysis. Therefore, to extract individual trees across the study area for this project, manual aerial photo interpretation was performed on 10cm orthoimagery collected in 2008. Crown diameter was estimated directly from the imagery, while

Figure 2.2.1: Results of the extraction techniques to derive primary buildings, trees, and ground vegetation using LiDAR data and Quickbird satellite imagery.

Figure 2.2.2: A city block in study area that displays a) resulting building polygons from the LiDAR extraction technique, and b) resulting building polygons after post-processing to simplify polygon shapes, remove secondary structures, and separate buildings by land parcel boundaries.

heights were derived from the LiDAR. To mitigate interpreter error and to ensure the top of the tree crown was extracted, the LiDAR height layer was filtered for maximum values within a 5-by-5-cell kernel and the interpreted stem locations were used to extract the underlying height value. These crown diameter and height metrics were derived for a 400m buffer around the tower and values were extrapolated outwards to the rest of the study area.

2.3 A Building Typology Approach to Carbon Emission Modelling

At present the relationship between building morphology, energy use and carbon emissions is not well defined. This has been in large part due to the difficulty in accurately characterizing urban form, which is both time consuming and labour intensive. Cities however, are assemblages of development patterns, which are in turn made up of replicated parts such as building types. These types often share similar characteristics, for instance morphological and performance attributes. A typology approach, which includes these differences, can better inform policy decisions by describing the important factors influencing carbon emissions within a development pattern. This section describes a building typology approach informed by LiDAR data to estimate building carbon emissions at the Sunset neighbourhood.

2.3.1 Carbon Emissions Associated with Building Energy Use

Building construction, morphology and urban density all influence building energy demand, and ultimately the amount of carbon emissions released into the atmosphere. The demand for energy is a result of space heating, domestic hot water (DHW), lighting, space cooling, and auxiliary equipment loads. In Vancouver, a large part of residential energy use is dedicated to space heating, of which the majority is powered by natural gas. The combustion of natural gas produces C as a by-product and for every GJ of energy produced from natural gas approximately 13.9 kg of C is released into the atmosphere (BC GHG Assessment Guide, 2008). Electricity, another significant source of building energy, typically provides power for building lighting, auxiliary equipment and space cooling or may entirely replace natural gas as the primary source of energy. Although emissions in BC resulting from electricity production are significantly less than natural gas due to the large proportion of hydroelectric power, electricity produced from diesel and natural-gas-fired power plants drive-up the emissions factor to 1.67 kg C GJ^{-1} (BC GHG Assessment Guide, 2008). Although onsite renewable energy production may offset carbon emissions, the existence of such equipment was not observed during field visits and thus excluded from the current modelling framework.

2.3.2 A Building Typology Approach to Carbon Emissions Modelling

Past research that estimates the spatial and temporal pattern of building energy use has typically followed one of two routes: top-down approaches that use aggregate data to scale down and bottom-up approaches that focus on individual buildings and scale-up to larger areas (Heiple and Sailor, 2008). A bottom-up typology approach was used to document, classify and estimate the portion of tower measured carbon emissions attributable to buildings. However, local data was supplemented by inventory estimates when neighbourhood data was not available. The typology approach describes the Sunset neighbourhood through a series of prototypes that are characteristic of the existing building stock, which assumes a correlation between building use, physical form and energy performance. Through fieldwork and a synthesis of precedent energy modelling studies (e.g. CanmetENERGY urban archetypes)

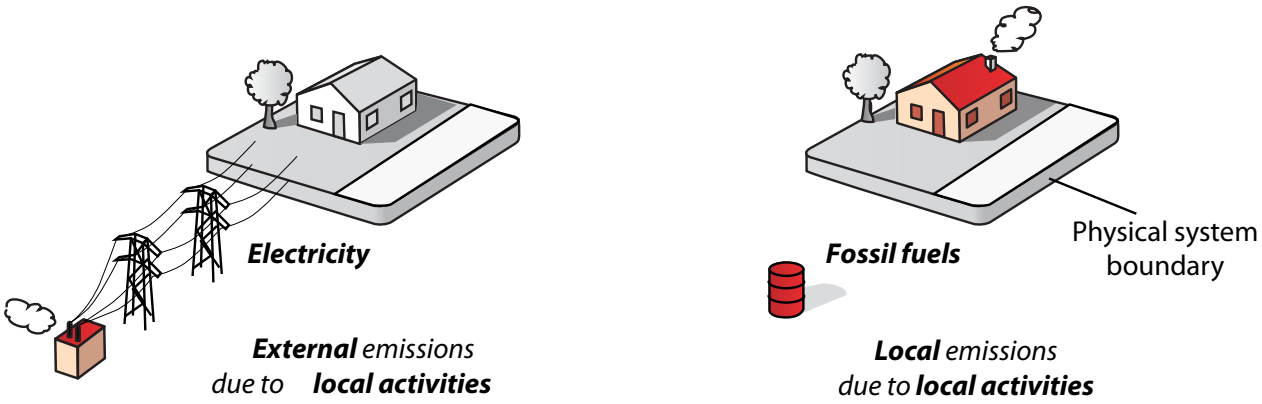

Figure 2.3.1: Conceptual representation of building carbon emissions from local and external sources.

two overarching building categories emerged for the Sunset neighbourhood (residential and 'other,' non-residential) along with thirteen sub-types. For each sub-type the important morphological and performance measures were collected to inform the carbon emissions intensities modelled (kg C m^{-3} $year^{-1}$).

Why a building typology method? A typology method is a systematic approach to synthesize and visualize otherwise complex variations in the urban ecosystem. The study site included 4558 buildings and the challenge was to compose a representative sample that described the diversity of building types and their variation in energy use. The resulting types represent replicable and replaceable instances, meaning types representative of the Sunset neighbourhood allow for a quick overview of the energy performance of various building types. This can ultimately lead to the assessment of alternative development scenarios, and the benchmarking of carbon emissions in a neighbourhood.

What is the structure of the building typology? The typology concept focuses on building attributes relevant to energy consumption; these include (a) morphological attributes of buildings, such as heated volume, and window, wall and roof areas (b) energy performance attributes such as heating system types and RSI values (thermal resistance). These attributes, along with building use were identified as key energy performance indicators and formed the basis of the building typology categorization (Figure 2.3.2).

What types were used in the Sunset neighbourhood? The development of each typology involved the synthesis of several data sets in a geographical information system (GIS). First cadastral data available from the City of Vancouver was synthesized with BC Assessment data. During this process each building parcel was associated with a property identifier (PID). This was used to join land use and sub-type data to each residential and 'other' parcel. Further information was documented for residential parcels, which included finished floor area, vintage and heating system. A spatial join was then applied in GIS between the parcel data and each building extracted from LiDAR

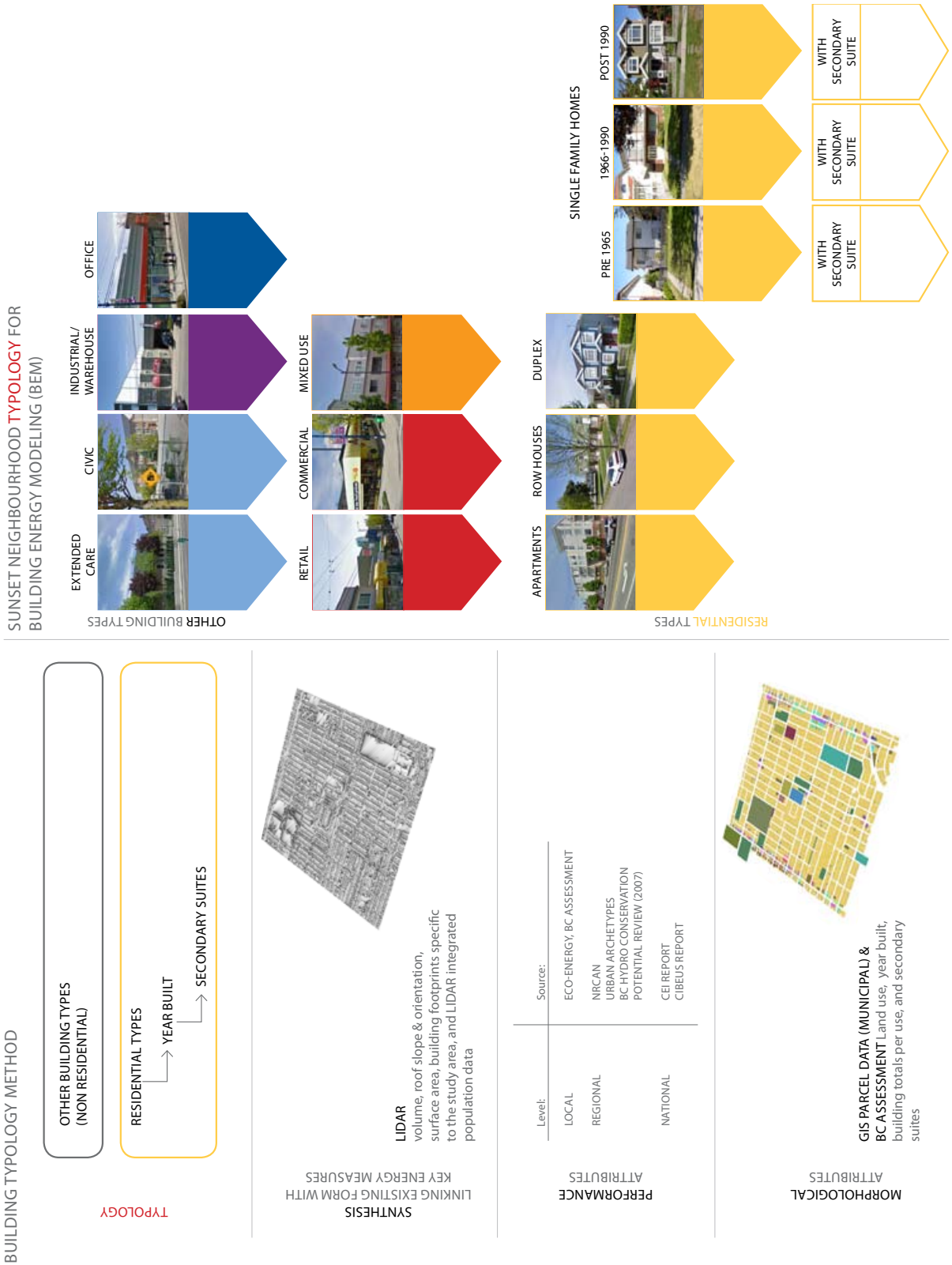

Figure 2.3.2: A Schematic representation of the typology used in the Sunset neighbourhood. Building sub-types were classified in three steps that described use, form and construction vintage.

data, which included the associated morphological attributes (see section 2.2).
Step 1: Building Use - Building land use was the first step in the categorization; this included residential and 'other' (non-residential) types. 'Other' building types included extended care, warehouse, civic, office, retail, commercial and mixed use. Of the 4558 buildings sampled in the Sunset neighbourhood, 95% were residential, a significant percentage necessitating a more rigorous categorization.

Step 2: Building Form - The second categorization further divided the residential buildings stock based on form (stacked, detached and attached), resulting in four additional categories: apartments, row houses, duplexes and single family detached. Of the total number of residential buildings in the study area 97% are single family dwellings (SFD).

Step 3: Building Vintage - The third categorization to further divide the SFD was based on year of construction, this resulted in three additional categories: SFD built before 1965, SFD built between 1965-1990, and SFD built post 1990. These categories were selected based on energy performance differences and house characteristics, such as building volume, window areas and roof slope (see section 2.3.5). Additionally, a significant proportion of these SFD have secondary suites (data provided by BC Assessment) and thus each sub-type was assigned a derivative. These derivatives were modelled with larger occupancies (see section 2.3.4) and adjusted morphological and system attributes accordingly. Occupancy of building types other than residential were assigned default values provided by OEE Screening tool. Although this is a modelling limitation, accurate estimates of employment in the area were not available through assessment data.

2.3.3 Building Energy Modelling

Building volumes provide an estimate of the space to be heated. This information alone however, is not sufficient to assign an energy demand and thus the integration of typology attributes was key in quantifying building carbon emissions. To estimate emissions both data sets were integrated into two building energy models (BEM), one dedicated to ground oriented residential sub-types and another program for 'other' building types. The energy consumption of ground oriented residential typologies was simulated using the HOT2000 energy analysis program and for all other typologies the OEE Screening tool was used. HOT2000 applies a bin-based method to calculate energy use and has been widely used in North America. The model has undergone extensive validation (Haltrecht and Fraser, 1997) and is primarily used in performance evaluation programs by researchers, utilities and governmental agencies. Through campaigns such as the ecoENERGY retrofit program, accurate libraries of construction details have been collected and input into HOT2000, these now represent a range of Canadian archetypes. In order to provide the HOT2000 wizard with additional locally relevant inputs for Sunset neighbourhood several steps were taken to extract the morphological and performance attributes needed. First, building volume for each typology was derived from LiDAR

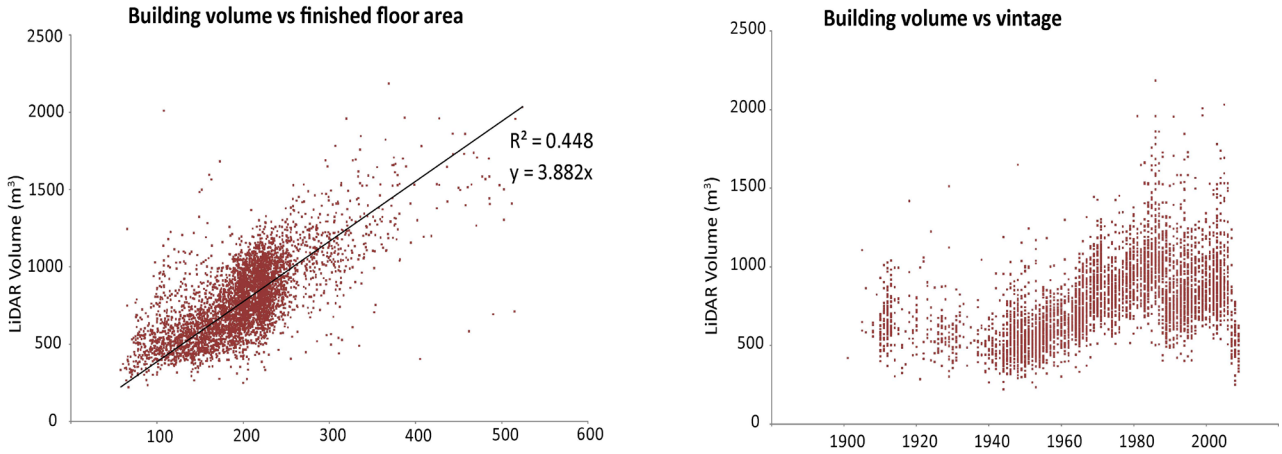

Figure 2.3.3: (a) LiDAR derived building volume plotted against the finished floor area of ground-oriented residential and (b) Building volume plotted against construction year for ground-oriented residential.

data and associated with a heated floor area (Figure 2.3.3). Then, a representative model was created in a 3D modelling software. The morphological characteristics from this model, where matched to the sub-type characteristics from the LiDAR data. Further details, such as window, wall and roof areas where imported alongside the heated floor area into each HOT2000 BEM. The associated energy performance indicators of the BEM, such as insulation values and air exchange rates were taken directly from the ecoENERGY retrofit data of local homes where available. Unfortunately, out of the 4500 homes in the neighbourhood only 10 ecoENERGY retrofit files were available. Although few records were aquired and the current procedure to obtain these files was arduous, the ecoENERGY data source provides a tremendous resource for local energy and emissions mapping. Where no local data was available municipal and provincial estimates were used in place. All emissions factors followed the BC Greenhouse Gas Emissions Assessment Guide, 2008.

In order to capture the variability in energy use of each typology throughout the neighbourhood a sensitivity analysis was performed. In this evaluation building orientation, space heating and DHW systems were changed in the BEM. A total of eight simulations were run for each typology and the final energy use and emissions were weighted according to the primary and secondary heating system (share provided through BC-Assessment data). The calculation of each sub-types emissions was estimated:

$$C_{ST} = C_I \bullet V_b / A_b$$

Where C_{ST} = the sub-type carbon flux. C_I is the carbon intensity modelled in the BEM. V_b is the building volume and A_b is the building footprint.

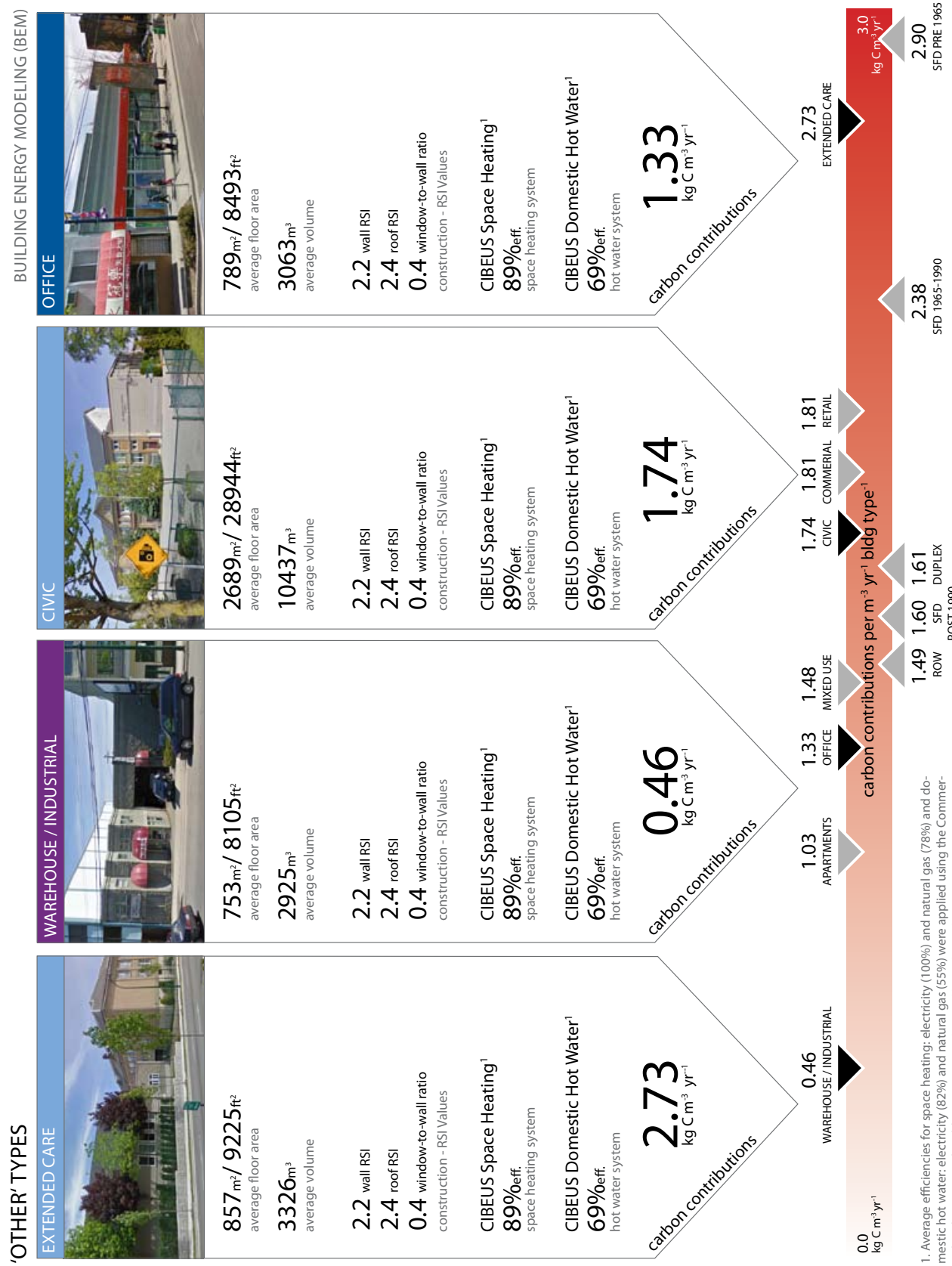

Figure 2.3.4: Building typology with appropriate Building Energy Modeling (BEM) attributes and corresponding carbon contributions in m^{-3} $year^{-1}$ $building\ type^{-1}$

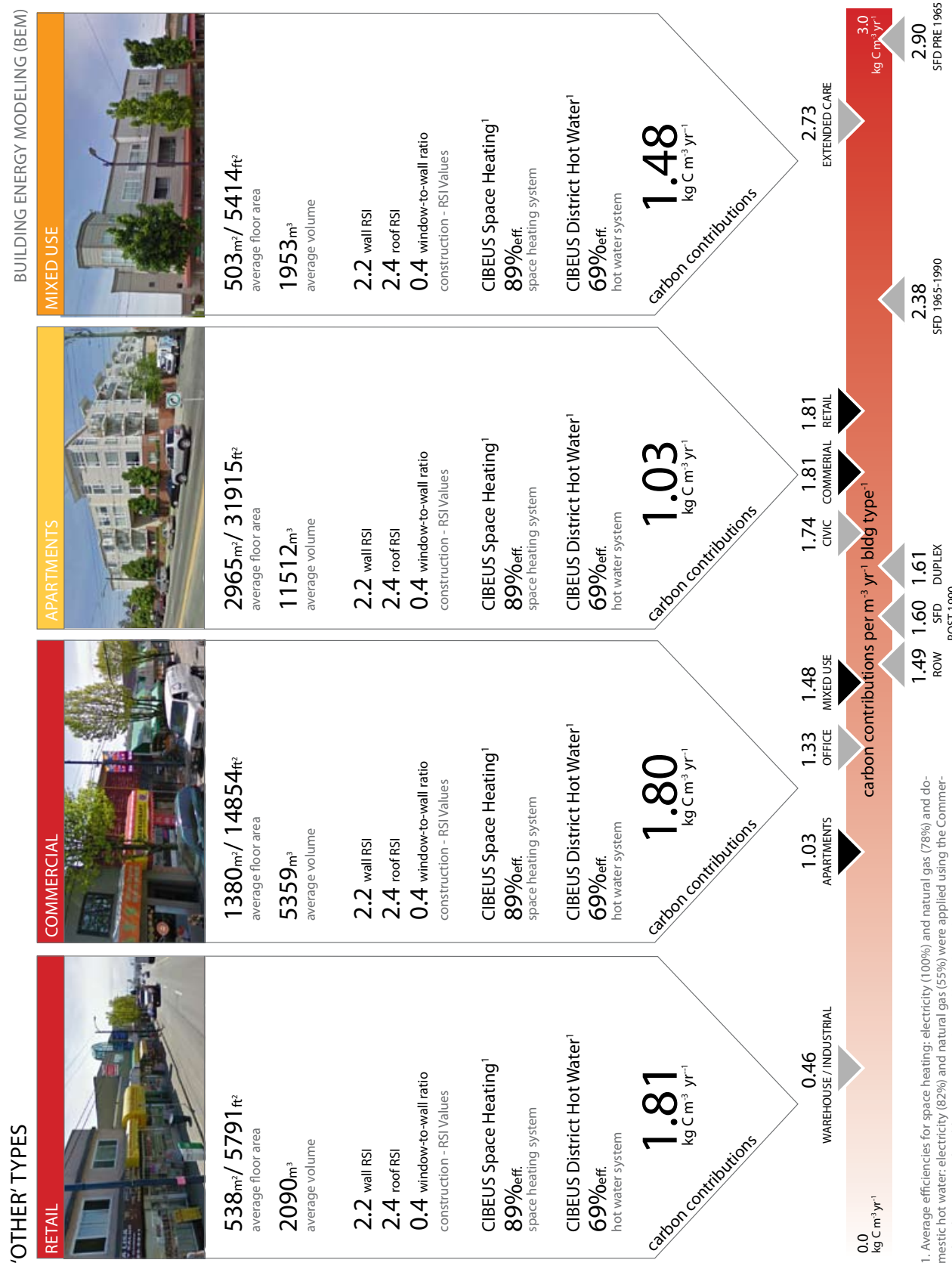

Figure 2.3.4: Continued from previous page

Figure 2.3.4: Continued from previous page

RESIDENTIAL, ROW & DUPLEX

ROW

3.0 avg. ppl

205 m² / 2207 ft²
average floor area

2.1 wall RSI
5.0 roof RSI
1.1 foundation RSI
construction - RSI Value
0.24 FWR
window-to-wall ratio

Hydronic Heating 78% eff. (60% share)
Baseboard 100% eff. (4% share)
NG Boiler 78% eff. (36% share)
space heating system

Natural Gas 55% eff. (4% share)
Electrical 82% eff. (96% share)
hot water system

1.49
kg C m^{-3} yr^{-1}

carbon contributions

DUPLEX

3.0 avg. ppl

205 m² / 2207 ft²
average floor area

2.1 wall RSI
5.0 roof RSI
1.1 foundation RSI
construction - RSI Value
0.16 FWR
window-to-wall ratio

Hydronic Heating 78% eff. (60% share)
Baseboard 100% eff. (4% share)
NG Boiler 78% eff. (36% share)
space heating system

Natural Gas 55% eff. (4% share)
Electrical 82% eff. (96% share)
hot water system

1.61
kg C m^{-3} yr^{-1}

carbon contributions

LOCAL AND EXTERNAL CONTRIBUTIONS

ROW

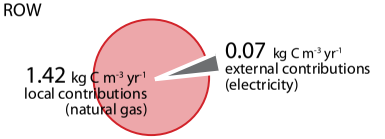

DUPLEX

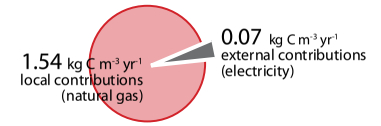

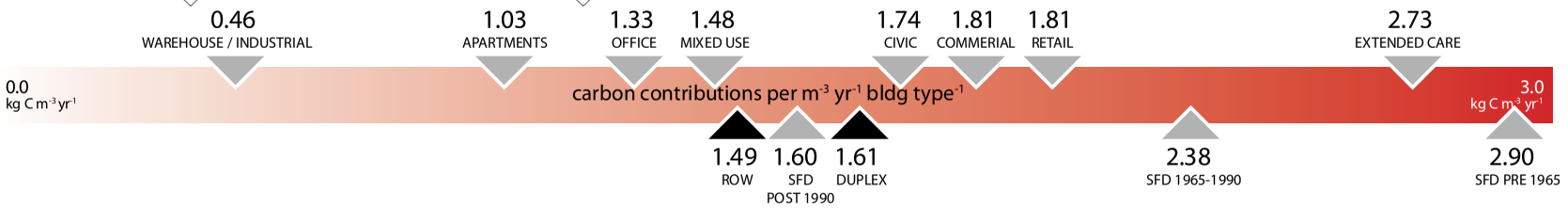

OUTPUTS & BENCHMARKS HOT2000 & Sunset Tower, and NRCAN

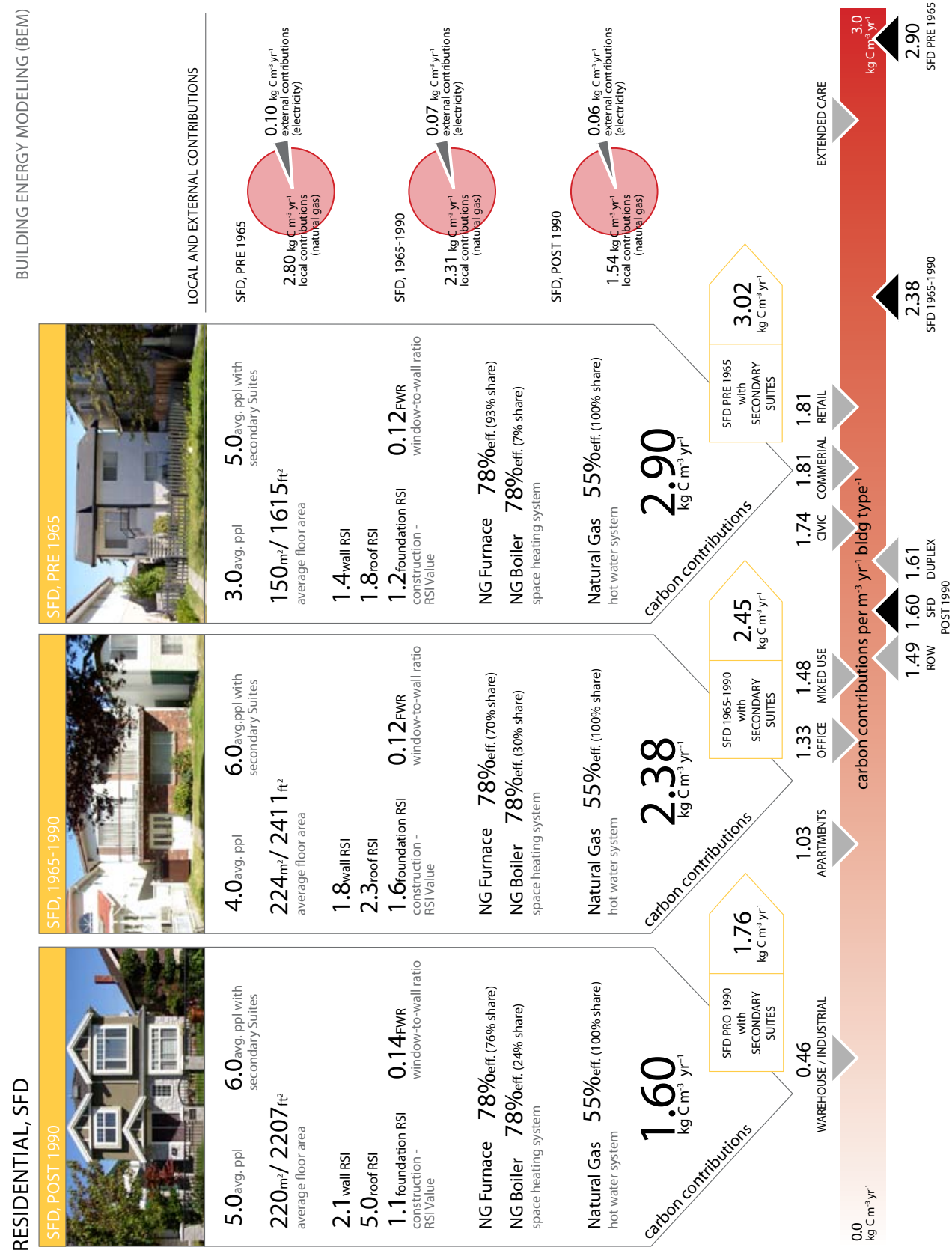

Figure 2.3.4: Continued from previous page

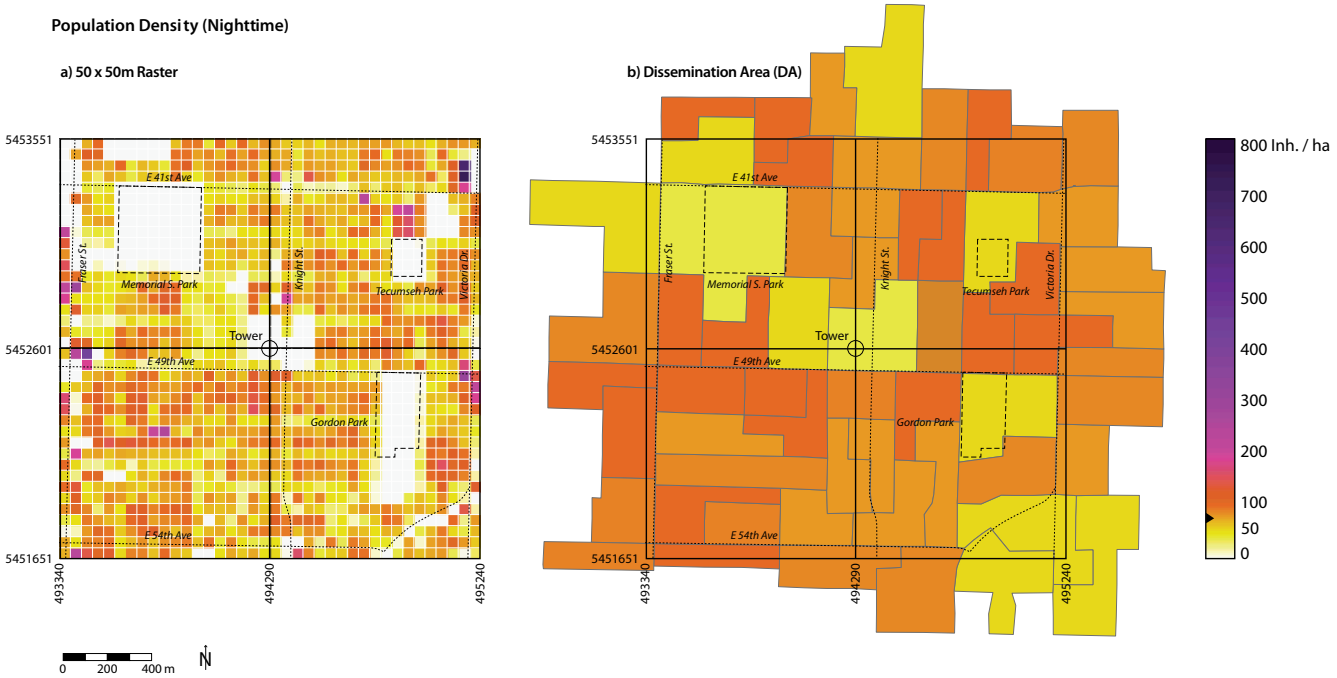

Figure 2.3.5: Population density (inhabitants ha^{-1}) shown by (a) 50 x 50m raster that combines Statistics Canada Dissemination Area (DA) census data, BC Assessment data and LiDAR volume data, and (b) DA-level Statistics Canada population data.

2.3.4. LiDAR volume-based building occupancy distribution

By distributing nighttime population accurately to buildings, the sources of human respiration can be estimated spatially (see section 3.3.1) and the energy load for different building types can be assigned. The source for population values is Statistics Canada's 2006 census, but this only allows for population information down to the dissemination areas (DA) that cover multiple city blocks and do not necessarily overlap with the boundaries of the study area. In this report, the spatial resolution has been downscaled to 50 x 50 m grid elements using building volumes derived from LiDAR and land assessment data as proxy data for the distribution.

Step 1: Firstly, Census data was used to separate population based on dwelling type. The number of inhabitants living in apartment dwellings vs. ground-oriented dwellings was calculated separately for each DA - as this information is not directly provided by the census data (only the approx. number of dwellings by type and the total population are provided). This was done by plotting P_{total}/D_{total} vs. D_{apt}/D_{total} for each DA separately, where P_{total} is the total population of the DA, D_{total} is the total number of dwellings in the given DA and D_{apt} is the total number of apartment dwellings in a DA (provided by Statistics Canada). A linear regression through D_{apt}/D_{total} vs. P_{total}/D_{total} with data from all DAs allowed for an allocation of the average number of people living in each apartment dwelling vs. average number of people living in ground-oriented dwellings for the entire study area.Although the

actual number of inhabitants living in an apartment dwelling vs. the average number of inhabitants living in a ground-oriented dwelling could vary from one DA to another, the ratio between the two was assumed to remain constant across the study area. This means that within each DA the total number of people living in each of the two dwelling types can be calculated from the total population, number of apartment dwellings and the number of ground-oriented dwellings, all of which are provided by Statistics Canada.

Step 2: This information was then associated with building typology data in GIS (see section 2.3.2) which contained the needed building volume and land use to spatialize population.

Step 3: In order to account for partial DAs near the site area border a subset of the DAs were selected. This subset included those (i) completely within the study area (i.e. LiDAR data available) and (ii) contained at least one apartment building according to the BC Assessment data. For complete DAs with apartments, the total number of inhabitants per dwelling type (step 1) and the corresponding total volume per building type (step 2) were extracted. The resulting numbers were summed for all complete DAs.

Step 4: Using the totals for all complete DAs from step 3, a series of global (study area-wide) parameters were calculated in order to establish the average volume occupied by a person (m^3 Inh^{-1}) living in either an apartment or ground-oriented dwelling. This was done by dividing the total volume of each building type by the total number of inhabitants in the corresponding dwelling type (both from step 3).These values were then used to create attribution factors that allowed for a 'volume adjustment' in order to make the volume occupied by a person in a ground-oriented dwelling the same as that of someone in an apartment. This adjustment allows for the population of buildings to be based on an 'adjusted volume' regardless of their type.

Step 5: The LiDAR volume of each individual building in the study area, including those excluded in step 4, was multiplied ('adjusted') by the attribution factor based on the building's type. As a result, all non-residential buildings were assigned a volume of zero, while the volume of apartments was increased by a factor of 1.30 and the volume of all ground oriented dwellings decreased by a factor of 0.70. The adjusted volumes for each building type were totaled for each DA, complete or incomplete.

Step 6: The adjusted volume of each residential building was divided by the total adjusted volume of all buildings in the particular DA. This corresponds to the modeled fractional population of the building in the DA.

Step 7: For all buildings in each complete DA, the fractional population was multiplied by the census total population of the entire DA to obtain a value for the population of the building. For buildings in incomplete DAs, the adjusted volume of the building was divided by the global volume/inhabitant value to obtain an estimate.

2.3.5. Density Effects and Up-Scaling to the Neighbourhood

Once all sub-type's energy and carbon intensities had been documented the results were made spatial in GIS. This distribution followed one of two methodologies explored, which were based on the hypothetical amount of information available. The first, with which the current results are presented (see section 3.1), followed a scenario where detailed building information was available. The second scenario explored the possibility of using LiDAR to automatically classify the buildings stock.

Scenario 1: GIS informed mapping

In this step the GIS synthesized data set is used to inform the spatial pattern of carbon emissions. The defined sub-types carbon intensity (kg m^{-3} $year^{-1}$) is mapped to the associated buildings and total emissions is derived using the LiDAR volume.

Scenario 2: LiDAR informed mapping

In this step a reduced level of information is assumed and an automatic classification of buildings attempted. Using fieldwork data collected for approximately 200 homes, three SFD typologies were defined (SFD outlined earlier). The morphological characteristics of these homes were used as a training data set for the entire neighbourhood. This data was input into a decision tree regression and showed promising results where 73% of the homes were properly classified using volume as an indicator.

Lastly, it is important to note that although morphological characteristics and energy performance attributes are important indicators of carbon emissions other impacts from surrounding buildings and vegetation additionally impact energy demand. Although general relationships were established for shading impacts in the BEM, these neighbouring effects have not been fully accounted for in the current methodology.

2.3.6 Carbon Storage in Buildings

Organic carbon is stored in buildings in substantial amounts. This carbon is incorporated in the building's structure, but also in furniture and books (Churkina, 2009).

Carbon stored in furniture

The carbon stored in furniture and books was estimated:

$$C_{bf,n} = P \bullet f_c \bullet m_f$$

Where P is population density, m_f is the average estimate of the mass of furniture and books per capita (300 kg Inh^{-1}), f_c is the fraction of carbon matter per dry mass in wood and construction materials (0.5 kg C kg^{-1}). $C_{bf,n}$ is the neighbourhood-wide pool of carbon stored in furniture and books in kg C per m^2 urban area.

Carbon stored in building structure

The storage in residential buildings structure materials (framing, flooring, roofing, and walls) was estimated:

$$C_{bs,n} = \rho_{bw} \bullet f_c \bullet \lambda_R$$

ρ_{bw} is the wood mass per unit of floor area which was estimated ρ_{bw} = 97 kg m^{-2} in a standard US

residential home (based on Keoleian, 2000). f_c is the fraction of carbon matter per dry mass in wood (0.5 kg C kg^{-1}). $C_{bs,n}$ is the neighbourhood-wide pool of carbon stored in building structures in kg C per m^2 urban area. λ_R is the ratio of total floor area of residential buildings A_R to total ground area of the neighbourhood A_G:

$$\lambda_R = A_R / A_G$$

A_F was available for residential ground-oriented buildings through BC assessment. For apartments and non-residential buildings it was calculated from LiDAR volume V_b based on a regression against residential ground-oriented buildings:

$$A_R = c_r \bullet V_b$$

where c_r = 0.2441 m^2 / m^3 was determined empirically by comparing V_b and A_R for all ground oriented buildings.

Commercial buildings were accounted for separately following the above approach, but based on Chrukina (2009) it was assumed that they contain only 10% of the carbon stored in residential buildings.

2.4 Transportation Modelling

This section describes the approach and methods used to derive carbon emissions from the transportation urban metabolism component.

2.4.1 Calculating Carbon Emissions from Transportation

The challenge to the transportation component of the urban metabolism was to estimate the proportion of tower measured carbon emissions attributable to fossil fuels burned in vehicle trips to, from and through the case study area. That challenge was complicated by the absence of consistent, sufficiently detailed and appropriately scaled neighbourhood scale travel and transportation data upon which to compile an annual travel snapshot of how many trips, of what type (to from or through) and length, by how many vehicles, of what type, using how much of which fuels — and converting answers to those questions to carbon units. Each question had to be approached separately and incrementally.

How many trips? Traffic monitoring through the City of Vancouver is done on a piecemeal, intermittent basis. From time to time, automatic directional traffic counting devices are placed for 24 hour or greater periods on arterials and major roadways. Less frequently, manual counts of traffic movements (right turn, left turn, through etc.) are taken at significant intersections at peak traffic periods — usually a few hours in a few days. Even less frequently, manual counts of movements by vehicle type or class are taken at the most significant intersections — usually 12 hours of a single day. All of these are posted to VanMap — the City of Vancouver's web-based spatial data set.
Within the project study area were 13 directional traffic count sites with one or more sets of recent (since 2005) 24-hour weekday traffic counts, 9 intersection traffic movement counts with a few hours of peak travel data and 1 vehicle class traffic intersection movement count with 12 hours of data. Data gathered at these points were used to estimate a weekday traffic profile for the study area. In this profile all vehicle trips (including local origin or destination trips) were assumed to enter or exit the study area along one of the arterials for which data was available. To simplify the method, only trips exiting the study area were considered. Count sites with more than one data set after 2005 were averaged (see Table 2.4.1).

To convert average weekday trips to annual total trips, each weekday number was prorated by a multiplier of 346.75 (weekday to annual) based on the measured distribution of traffic by day elsewhere in Vancouver (personal conversation City of Vancouver transportation staff). This factor is based on an average daily traffic distribution as follows: Monday = .95, Tuesday, Wednesday, Thursday = 1.0, Friday = 1.05, Saturday = 0.9 and Sunday = 0.75.

To, from or through? No neighbourhood scale mode split data are available. However, according to the last available regional trip diary survey (Ministry of Transportation and Greater Vancouver Transportation Authority, 2004) average trip rates and mode splits in the City of Vancouver segment of the Metro region are 3 trips per capita, .605 of which are by automobile. These rates were used

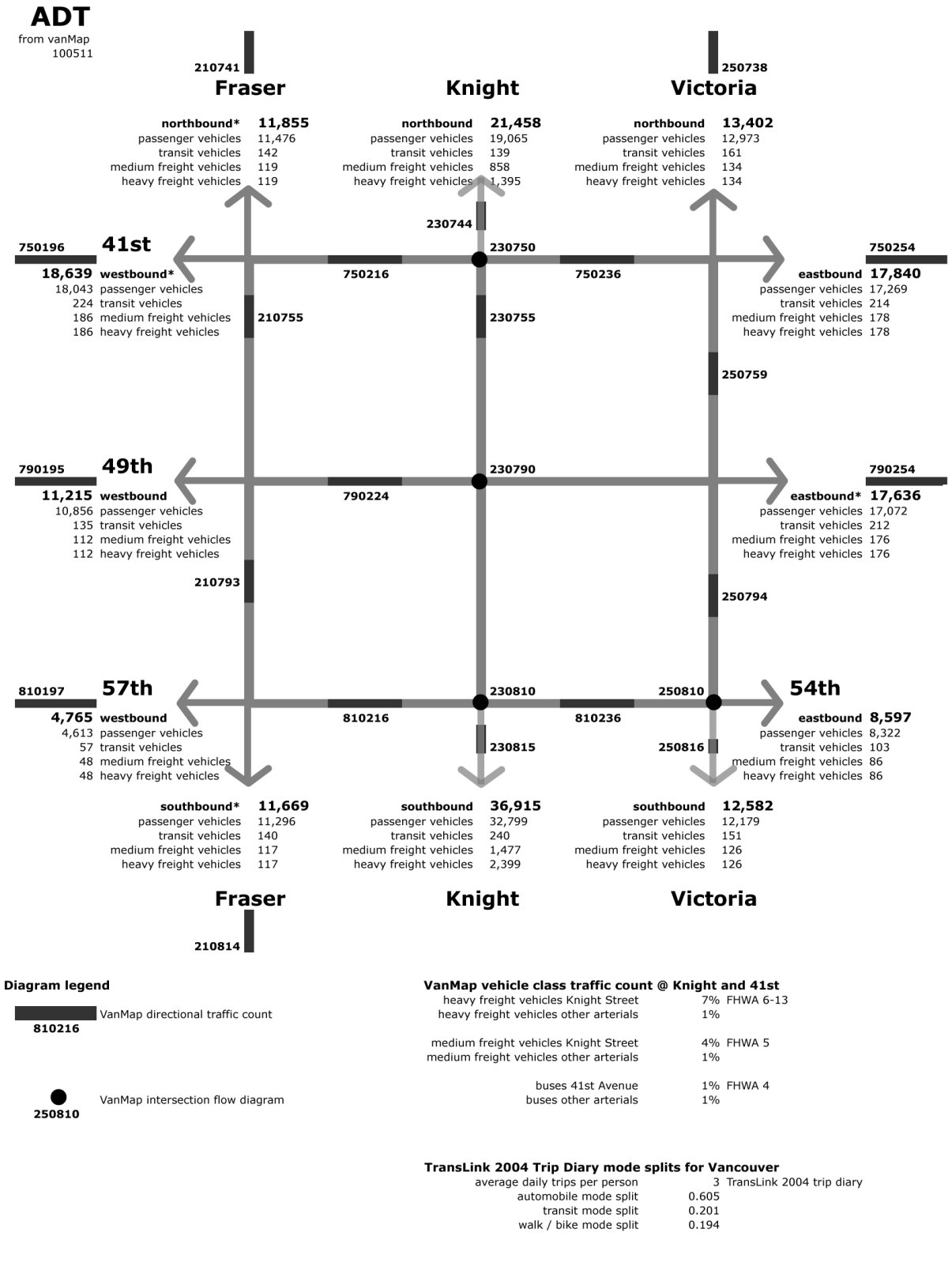

Figure 2.4.1: Simplified plan diagram of average weekday arterial traffic by vehicle class. Numbered line segments are directional traffic count sites. Numbered dots are intersection traffic movement 12-hour manual count sites. A 12-hour manual traffic count at the Knight Street and East 41st Avenue intersection (noted as 230750) provided vehicle class data. Source: City of Vancouver.

Table 2.4.1: Traffic count data by acquisition location (see Figure 2.4.1). Source: City of Vancouver.

OUTBOUND ADT

from vanMap 100504

* anomalous data point omitted

		OUTBOUND						
		NORTH	WEST	SOUTH	EAST	12 / 24 hr	date	
N	**FRASER / 41ST**	**11,855**		**11,854**				
—	210741_05	12,305		12,441		24	18-19 July 2005	Mo-Tu
—	210741_06	11,648		11,127		24	21-22 August 2006	Mo-Tu
—	210755_05	12,085		12,192		24	18-19 July 2005	Mo-Tu
—	210755_06	11,382		11,655		24	21-22 August 2006	Mo-Tu
W	**41ST / FRASER**		**18,639**		**16,943**			
—	750196_05		16,574		15,813	24	29-30 August 2005	Mo-Tu
—	750196_06				16,529	24	29-30 August 2006	Mo-Tu
—	750216_05		20,704		18,487	24	29-30 August 2005	Mo-Tu
W	**49TH / FRASER**		**11,215**		**11,371**			
—	790195_05		10,722				26-27 July 2005	Tu-We
—	790224_05		11,707		11,371	24	26-27 July 2005	Tu-We
W	**57TH / FRASER**		**4,765**		**5,609**			
—	810197_06		4,164		4,410	24	17-18 May 2006	We-Th
—	810216_06		5,365		6,807	24	19-21 June 2006	Mo-We
S	**FRASER / 57TH**	**11,669**		**11,681**				
—	250793_06	11,669		11,681		24	21-22 August 2006	Mo-Tu
—	210814_06						28-29 August 2006	Mo-Tu
N	**KNIGHT / 41ST**	**22,496**		**21,821**				
—	230744_05	20,652		19,786		24	21-22 July 2005	Th-Fr
	230744_07	21,458		20,953		24	15-16 February 2007	Th-Fr
•	230750							
—	230755_07	25,378		24,723		24	15-16 February 2007	Th-Fr
S	**KNIGHT / 57TH**							
•	230810	**30,501**		**36,915**				
—	230815_06	30,501		36,915		24	27-29 June 2006	Tu-Th
S	**57TH / KNIGHT**		**12,302**		**8,000**			
—	810216_06		*		6,807	24	19-21 June 2006	Mo-We
—	810236_05		12,161		8,411	24	6-8 December 2005	Tu-Th
—	810236_06		12,443		8,783	24	17-18 May 2006	We-Th
N	**VICTORIA / 41ST**	**12,493**		**13,511**				
—	250738_05	10,013		13,295		24	30-31 August 2005	Tu-We
—	250738_07	13,830		13,476		24	4-5 April 2007	We-Th
—	250759_05	12,728		13,464		24	30-31 August 2005	Tu-We
—	250759_07	13,402		13,807		24	7-8 May 2007	Mo-Tu
E	**41ST / VICTORIA**		**18,407**		**17,840**			
—	750236_05		18,598		18,248	24	23-24 August 2006	We-Th
—	750254_05		18,358		18,047	24	25-26 August 2005	Th-Fr
—	750254_06		18,264		17,224	24	23-24 August 2006	We-Th
E	**49TH / VICTORIA**		**18,311**		**17,636**			
—	790254_05		18,358		18,047	24	25-26 August 2005	Th-Fr
—	790254_06		18,264		17,224	24	23-24 August 2006	We-Th
E	**54TH / VICTORIA**		**12,302**		**8,597**			
—	810236_05		12,161		8,411	24	6-7 December 2005	Tu-We
—	810236_06		12,443		8,783	24	17-18 May 2006	We-Th
S	**VICTORIA / 54TH**	**11,787**		**12,582**				
—	250794_05	11510		12,365		24	30-31 August 2005	Tu-We

to estimate the local portion of annual trips as follows: Study area population = 23,135 x 3 trips per capita x .605 by automobile = 41,990 weekday trips. Prorated against total non-freight vehicle trips estimated above, the local trip share was estimated at 24% and through trips at 76% of total trips throughout the study area.

By what kinds of vehicles? The carbon emissions intensity from transportation sources depends in significant part on vehicle type and its associated fuel and fuel efficiency — average gasoline fueled passenger vehicles emitting approximately one third the carbon of a diesel fueled truck and trailer per kilometer. Trips by vehicle were estimated using a four type classification (Figure 2.4.3 and Table 2.4.2) of light vehicles and transit vehicles primarily moving people to jobs and services, medium freight vehicles primarily moving goods and materials to out-of-study area local destinations, and heavy freight vehicles primarily moving goods and materials to more distant destinations.
How many of which types of vehicles on which study area streets was more challenging. As one intersection traffic count by vehicle class was available (at Knight Street and East 41st Avenue at the northern centre of the study area) that distribution was used to estimate vehicle classes on arterials as follows. At this location, Knight Street, being a principal truck freight route in the region, accommodates a greater share of medium and heavy freight vehicles than did East 41st Avenue as follows:
Based on these proportions, freight and transit traffic was allocated to Knight Street as calculated. All other arterials were assumed similar to East 41st Avenue.
By what trip length? All local origin and destination trips were considered to be an average of 1 km — approximately the distance from the centre of the study area to an arterial exit point. All through trips were considered to be an average of 2 km — approximately the distance from entry to exit along a study area arterial. Using these average trip lengths, total annual kilometers travelled, by vehicle class, was estimated within the study area.
How much of which fuel? Average fuel efficiencies (NRCan, 2007) were used to estimate the amount of fuel combusted for each trip and vehicle type. Light vehicles were estimated to average 11.5 litres of gasoline / 100 km. Medium freight vehicles were estimated to average 26.5 litres of gasoline / 100 km. Heavy freight vehicles and buses were estimated to average 39 litres of diesel fuel / 100 km. Total annual fuel consumed in the study area was estimated for each vehicle class / fuel type.

How much carbon? Total annual fuel consumed in the study area was converted to tCO2e using the conversion factors of 241 gCO_2e / liter for gasoline and 276 gCO_2e / liter for diesel fuel (NRCan, 2007). CO_2e was converted to gC using a factor of 0.273 (Ministry of Community Services, 2008). The resulting values were proportionally attributed to each arterial corridor and local streets based on km travelled (Table 2.4.2) and vehicle class (Table 2.4.3)

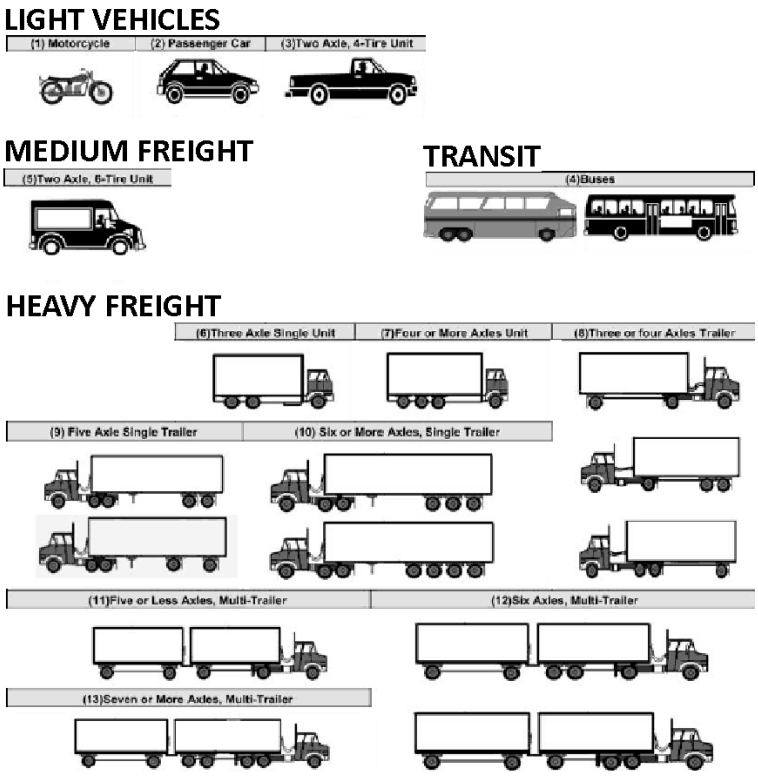

Figure 2.4.3: Project vehicle classes referenced to US Federal Highways Administration vehicle classes

Table 2.4.2: Estimated proportion of vehicle types by class at Knight Street and East 41st Avenue over 12 hours. Source: 'All vehicles' average from City of Vancouver Thursday-Friday traffic counts 21, 22 July 2005 and 15-16 February 2007. Share by vehicle type from City of Vancouver manual vehicle class count at Knight Street and East 41st Avenue (date).

Vehicle Type	Knight Street	East 41st Avenue
All Vehicles (both directions)	29,958	25,159
Medium Freight	1,091	268
	3.5%	1%
Heavy Freight	2,081	137
	7%	0.5%
Transit	202	342
	0.6%	1.3%

Table 2.4.3: Vehicle type classification by size, fuel type, fuel efficiency and carbon intensity.

Vehicle Type	Fuel	Fuel Efficiency L/100km	gC / km	FHWA Class
Light Passenger	Gasoline	11.5	75.6	FHWA 1-3 Two axle, four tire vehicles passenger cars, motorcycles
Medium Freight	Gasoline	26.5	174.3	FHWA 5 Single frame, two axle, dual rear wheel (delivery type)
Heavy Freight	Diesel	39.3	296.0	FHWA 6-13 Multiple axles truck, truck and trailer, truck and multiple trailers
Transit	Diesel	39.3	296.0	FHWA 4 Two or more axle, six or more tire busses

2.5 Accounting for Carbon Cycling in the Human Body, Food and Waste

This section discusses the methods used in this study to estimate carbon storage and fluxes related to carbon cycling though the human metabolism and related food and waste products.

2.5.1. Carbon Flows Associated with the Human Metabolism

Figure 2.5.1 illustrates simplified carbon fluxes associated with the human metabolism and food consumption. In contrast to natural ecosystems, where food is grown within the system, it is clear that in an urban ecosystem with anthropogenic food distribution systems, the majority of food - and hence carbon - is imported from outside the system. With the current urban land-use patterns the human food-web is spatially disconnected from the local urban vegetation component, and urban agriculture and gardening play negligible roles in the carbon cycle at the neighbourhood scale.

Part of the carbon contained in food products that is imported to the neighbourhood is lost in the preparation and/or storage of meals. This carbon is then laterally exported (garbage and liquid waste water). In this study we only account for food losses in distribution and residential households in the neighbourhood, not in agriculture or industrial processing.

The human body ingests the remaining carbon to gain energy and temporarily stores that carbon. Part of the carbon contained in food products is respired (oxidized) in the process of human respiration. Another part is lost though human waste (urine and faeces) and therefore laterally exported out of the neighbourhood through sewer systems.

In this study, for simplicity reasons, greenhouse gas emissions outside the neighbourhood system due to production and transport of food, or carbon emissions related to waste processing are excluded. They might play important roles on a community scale, in particular when incorporating methane emissions. We also note that carbon cycled through this component is renewable carbon, as it originated from plants photosynthesizing atmospheric carbon-dioxide at the bottom of the human food-chain.

2.5.2. Carbon storage in the human body

The neighbourhood-wide carbon pool in the human body was calculated based on Churkina et al. (2009):

$$C_{h,n} = P \bullet m_h \bullet f_d \bullet f_c$$

Where P is population density (in Inh. m^{-2}), m_h is the average mass of the human body (60 kg, including water), f_d is the fraction of dry mass per total body mass (0.3), f_c is the fraction of carbon matter per dry mass in the human body (0.5 kg C kg^{-1}). Although humans are highly mobile, for attributing the values to the spatial domain, the nighttime residential population from the Statistics Canada 2006 census was used. The resulting $C_{h,n}$ is the neighbourhood-wide pool of carbon stored in the human body in kg C per m^{-2}. The m^{-2} refers to the urban plan area in the study area.

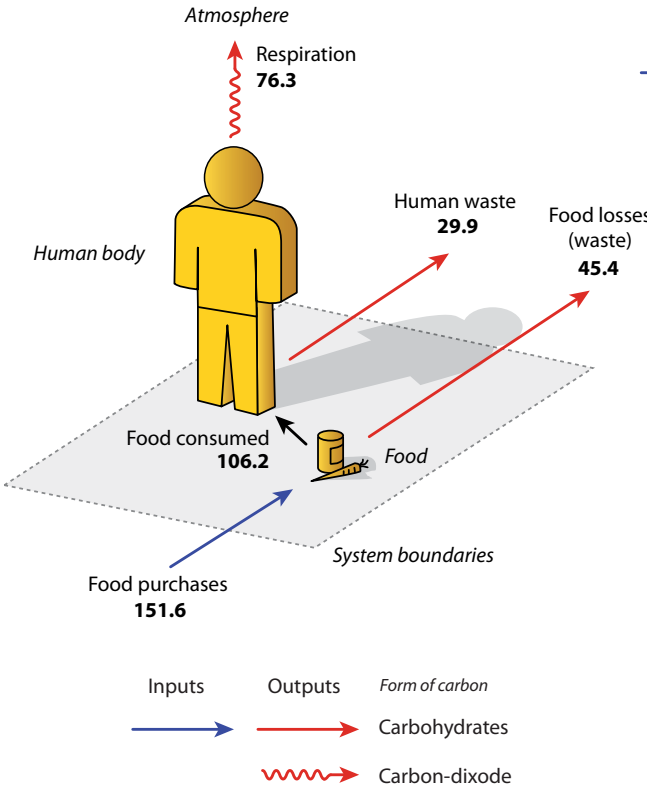

Figure 2.5.1: Conceptual representation of the carbon fluxes and storages involving the human body. Numbers refer to per capita estimates in kg C cap^{-1} year^{-1} as described in this section.

2.5.3 Respiration by the Human Body

The injection of carbon-dioxide by human respiration into the atmosphere was calculated by

$$E_{h,n} = P \bullet f_r$$

P is population density (in Inh. m^{-2}). f_r is the annual respiration of a human body in kg C year^{-1} and set to 76.3 kg C year^{-1} cap^{-1} according to Moriwaki and Kanda (2004). They estimated the respiration of carbon dioxide per person of 8.87 mg CO_2 s^{-1} based on medical literature. Global-scale estimates are about 0.57 Gt C year^{-1}, which translates to 93.4 kg C year^{-1} cap^{-1} on the global average (Prairie and Duarte, 2006). The resulting $E_{h,n}$ is the neighbourhood-wide carbon flux (emission) released by human respiration in kg C m^{-2} year^{-1}.

2.5.4. Carbon Fluxes due Food Imports and Food Waste

The flux of carbon through food into the neighbourhood was estimated based on nation-wide food consumption statistics (Statistics Canada, 2004). Statistics used include per capita consumptions on a mass basis for selected various food groups (Table 2.5.1). For each food category, "mass of food consumed" and "mass of food lost" was converted to dry matter content using a category-specific dry matter content f_{dr}. Dry matter was converted to carbon mass $C_{(cat)}$ using an average carbon content of f_c = 0.5 kg C kg^{-1} dry matter:

$$C_{(cat)} = m_{(cat)} \bullet f_{dr\,(cat)} \bullet f_{c\,(cat)}$$

Summing the different categories, results in a total per capita carbon consumption of 106 kg C cap^{-1} year^{-1} and food losses of 45.4 kg C cap^{-1} year^{-1} (Table 2.5.1). It is interesting to note that the major portion of carbon lost is carried by the liquid waste flow (not solid garbage) which can be explained by the high dry matter content of cooking water, disposed through kitchen sinks (Codoban and Kennedy, 2008).

The numbers were multiplied by the nighttime (residential) population density P (in Inh. m^{-2}) to retrieve per-area flux densities of food imported and food lost in kg C cap^{-1} year^{-1}:

$$F_f = C \bullet P$$

Table 2.5.1: Consumption statistics and carbon content of various food products (modified from Codoban and Kennedy (2008), using data from Statistics Canada (2004) and Baccini and Brunner (1991))

Food Category	Dry Matter Context f_{dr}	Mass of Food Entering System $m_{(cat)}$	Mass of Food Consumed $m_{(cat,c)}$	Mass of Food Losses $m_{(cat,l)}$	Mass of Carbon Consumed $C_{(cat,c)}$	Mass of Carbon Lost $C_{(cat,l)}$
	%	kg C cap^{-1} year^{-1}	kg C cap^{-1} year^{-1}	kg C cap^{-1} year^{-1}	kg C cap^{-1} year^{-1}	kg C cap^{-1} year^{-1}
Cereal Products	88	88.6	65.3	23.3	28.7	10.3
Fruits	15	81.2	50.5	30.7	3.8	2.3
Vegetables	15	183.4	112.0	71.4	8.4	5.4
Pulses	90	7.7	6.8	0.9	3.1	0.4
Red Meat	35	64.0	28.3	35.7	5.0	6.2
Poultry	30	35.3	13.2	22.1	2.0	3.3
Fish	20	9.5	6.7	2.8	0.7	0.3
Milk	12	91.3	67.5	23.8	4.1	1.4
Cheese	60	12.1	8.9	3.2	2.7	1.0
Other Dairy	36	24.1	5.1	19.0	0.9	3.4
Eggs	25	9.2	7.5	1.7	0.9	0.2
Sugars & Syrups	95	40.8	30.5	10.3	14.5	4.9
Oils & Fats	99	30.7	22.0	8.7	10.9	4.3
Tree Nuts	80	1.5	1.3	0.2	0.5	0.1
Alcoholic Beverages	10	102.2	99.5	2.7	5.0	0.1
Nonalcoholic Beverages	10	339.4	302.7	36.7	15.1	1.8
Total per Capita		**1121**	**828**	**293**	**106.2**	**45.4**

2.5.5 Carbon Fluxes due to Human Waste

The carbon exported from the system in form of human waste was determined as the difference of the carbon consumed (106.2 kg C cap^{-1} year^{-1}, section 2.5.4) minus the carbon respired (76.3 kg C cap^{-1} year^{-1}, section 2.5.3). This is justified because the adult human body does not accumulate biomass. The carbon flux due to human waste out of the system was calculated 29.9 kg C cap^{-1} year^{-1}. This number comes close to estimated dry matter losses in the literature, which are given with 52 kg year^{-1} cap^{-1} (Baccini and Brunner, 1991). This corresponds to 31 kg C year^{-1} cap^{-1}, when applying f_c = 0.5. To convert this value to a per-area estimate, similar to 2.5.4, the value was multiplied by the nighttime (residential) population density P (in Inh. m^{-2}).

2.6 Vegetation and Soils - A Terrestrial Ecology Approach to Urban Carbon Cycling

This section describes methods used to quantify carbon storage, carbon emissions and carbon uptake by urban vegetation and soils. Results are found in Section 3.4.

2.6.1 Carbon Storage in Soils

Although organic matter is often present in the soil to a depth of 1 or 1.5 m, most is in a surface layer of from 1 to 20 cm (Buringh, 1984). Carbon storage in soils in the study area was estimated based on lab analysis of soil organic matter mass fraction m_o (in kg kg^{-1}). A total of 20 soil cores were taken in 2008 on four lawn lots in the neighbourhood (Christen et al., 2010). For each lot, soil organic content was measured separately in the lab for 0-3, 3-6, 6-10, 10-15 and 15-20 cm depth layers. Those cores excluded tree root material (which is accounted for under 'vegetation biomass'). For each layer, this was converted to an organic matter density in the soil f_o using measured average soil bulk-density (ρ_s = 0.94 Mg m^{-3}), and the ρ_o was then converted to the carbon density ρ_c (kg m^{-3}) assuming that f_b = 58% of the mass of organic matter content is carbon (van Bemmelen factor):

$$\rho_c = m_o \bullet \rho_s \bullet f_b$$

An exponential function was fitted through the four depth layers of ρ_c. This function ρ_c was integrated over the profile (down to 1 m depth) to retrieve total organic carbon in the soil. We assumed that topsoil that contains organic carbon is only found below pervious surfaces (i.e. has been removed under buildings and streets). So C_s is multiplied by the plan area fraction of pervious surfaces λ_b to estimate the neighbourhood-wide carbon pool $C_{s,n}$

$$C_{s,n} = C_s \bullet \lambda_p$$

2.6.2 Carbon Storage in Vegetation

The carbon storage in vegetation was estimated separately for tree biomass (above-ground and below ground, leaf biomass, needle biomass) and lawn biomass.

Carbon storage in trees:

Carbon stored in trees and specific parts was calculated based on literature urban-specific allometric relationships (Nowak, 1996). Bushes (< 2m) are not considered in this study.

Leaf area index, leaf biomass, and tree woody biomass were calculated for all trees on public and private land in a circle of 400m around the carbon flux tower. In this circle, all trees were manually digitized based on air photos, and their height was extracted from the LiDAR dataset (Table 2.6.1). For a subset of this dataset, also tree crown diameter was measured, and to partition total biomass into above-ground and below-ground biomass (roots), a root-to-shoot ratio of 0.26 was applied (Cairns et al., 1997). To upscale from the 400m to the entire study area, LiDAR derived tree volume was used.

To calculate lateral carbon export from the neighbourhood through biomass removal we assumed a typical life-span of urban trees of T_l = 75 years. The annual exported of carbon in tree woody biomass by tree removal / death was estimated as

Table 2.6.1: Tree characteristics in a circle of 400 m around Sunset tower.

	Density (stems/ha)	Average Tree Height (m)	Average Total Biomass (kg)
All Trees (n=95)	19.20	9.04	1662
Coniferous (n=23)	4.44	11.13	2620
Broadleaf (n=742)	14.76	8.41	1374

$1/T_l$ of the total carbon pool. We further assume that two-thirds of all leaves of deciduous trees are removed out of the study area in the fall season.

Carbon storage in lawns:

The estimation of the carbon stored in above-ground biomass of residential lawns was based on destructive samples of the grass cover in four different lots in the neighbourhood. Dry matter mass of those samples was measured in the lab and on average the dry-matter density of the grass canopy was ρ_{vl} = 1.05 kg m^{-2} (0.65 – 1.61 kg m^{-2}, included mosses). To convert to carbon density, a generic factor of the carbon fraction in biomass of f_o = 0.5 (kg C kg^{-1}) was applied. This value was multiplied by the plan area fraction of lawns in the neighbourhood:

$$C_{vl,n} = \rho_{vl} \bullet f_o \bullet \lambda_{vl}$$

2.6.3 Respiration by Urban Soils, Lawns and Trees

Respiration from soils and lawns ($R_{soil+lawn}$) was modelled based on approx 280 closed-chamber measurements with an opaque chamber on residential lawn in the neighbourhood. $R_{soil+lawn}$ was then modelled over the year based on year-long observations of soil volumetric water content and soil temperatures of four residential lawns in the study area (Figure 2.6.1). Details of the measurement and modelling procedure can be found in Liss et al. (2009).

Respiration from above-ground biomass (R_{tree}) was modelled based on measurements from a portable photosynthesis measurement system (Li-6400, Licor Inc., Lincoln, Nebraska, USA). A total of 12 urban trees and shrubs in the study area were sampled including Sugar Maple, Purple Leaf Flowering Plum, Dwarf and Rosebay rhododendron, Cherrylaurel, American Chestnut, Oregon Ash, European Beech, American Elder and Silver Maple. The photosynthesis measurement system was programmed to determine dark respiration of leaves as a function of air temperature. Average dark respiration at 25ºC was determined 1.03 µmol s^{-1} m^{-2} leaf area. Above-ground respiration was scaled using modelled leaf area index (see Section 3.4, seasonally changing) in the neighbourhood. Using year-round air temperature measurement, data was

integrated in 5-min steps over the complete year 2009. Details of the measurement equipment can be found in Liss et al. (2010).

2.6.4 Carbon Uptake by Photosynthesis

Photosynthesis by residential lawns (P_{lawn}) was modelled based on closed-chamber measurements with a clear chamber and co-located photosynthetically active radiation (PAR) measurements (Figure 2.6.2). Using a LiDAR-derived DEM, for each hour of the year 2009, PAR irradiance of was distributed on a 1 x 1 raster for all lawn surfaces (including shading by trees and buildings) based on measured short-wave irradiance on tower top. P_{lawn} was then modelled based on modelled PAR irradiance (Ogren and Evans, 1993) taking into account soil volumetric water content in the study area. Details of the modelling procedure can be found in Christen et al. (2009).

Photosynthesis by trees (P_{trees}) was modelled based on measured light-response curves from 12 representative trees in the neighbourhood (same as listed in Section 2.6.3), and in combination with a multi-layer radiation transmission model run at 1 m^3 resolution in the study area over the year 2009. Similarly to the lawn photosynthesis mode, the tree photosynthesis model was driven by measured short-wave irradiance from the carbon flux tower.

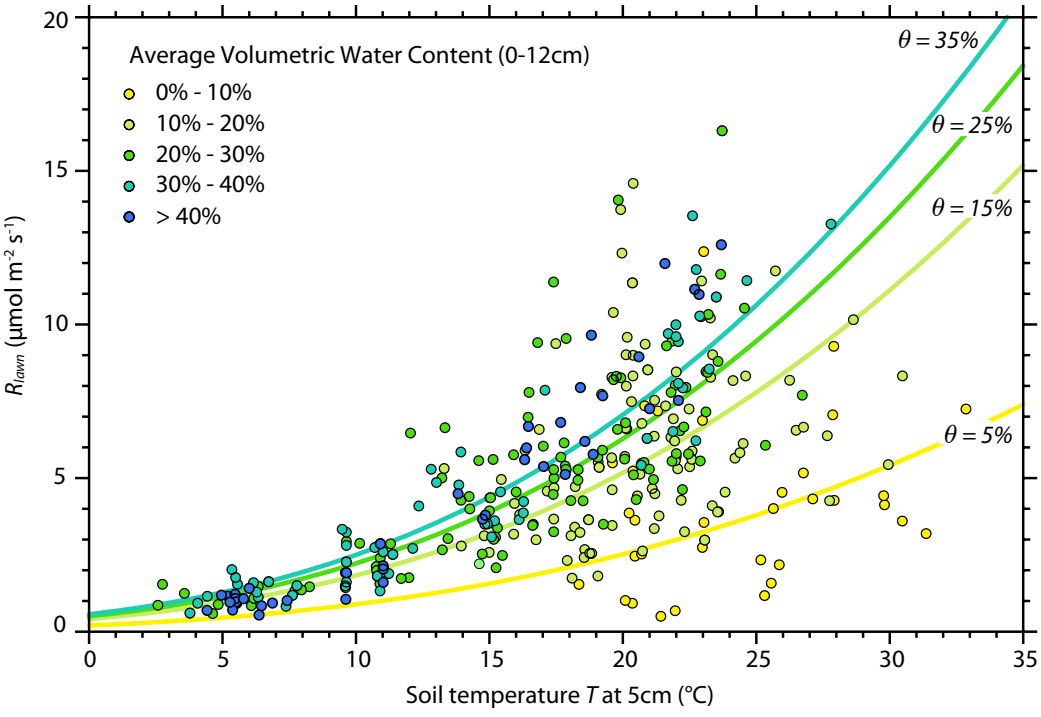

Figure 2.6.1 Measured (dots) and modelled (lines) lawn respiration as a function of soil temperature and soil volumetric water content (from Christen et al. 2009).

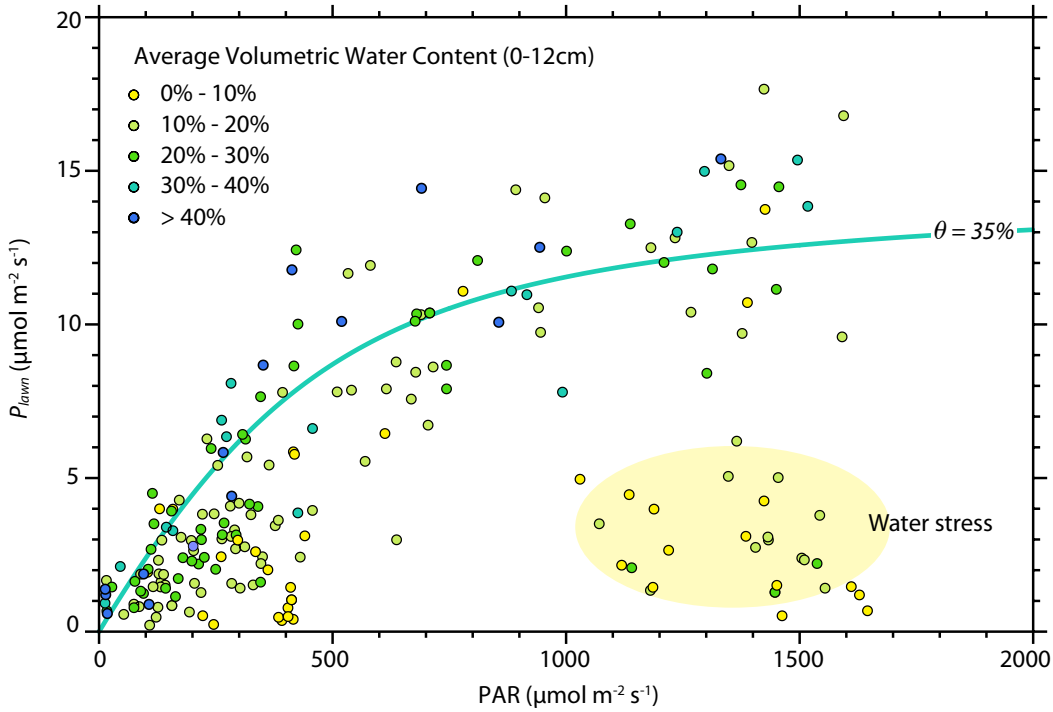

Figure 2.6.2: Measured (dots) and modelled (line, for water content at 35%) lawn photosynthesis as a function of photosynthetically active radiation (PAR) and soil volumetric water content (from Christen et al. 2009).

2.7 The Use of Direct Carbon Flux Measurements for Model Validation

This section describes the direct and continuous measurement of carbon emissions over a two-year period in the study area. The methodology of tower-based carbon flux measurements, including infrastructure and data post-processing procedures, are described. The results from these tower-based measurements will be compared to modelled emissions in Section 3.6.

2.7.1 The Eddy Covariance Method

Eddy covariance (EC) is a method to continuously and directly measure surface-atmosphere exchanges of energy and trace gases. EC can be used to quantify the exchange (vertical flux, see section 1.3.3) of greenhouse gases including CO_2. EC is currently used at several hundred research sites worldwide to continuously monitor CO_2 fluxes between various natural and managed ecosystems and the atmosphere, including farm land, grasslands, tundra, and forests (e.g. Baldocchi, 2008). The EC approach allows for a quantification of emissions as it measures the net mass of CO_2 exchanged per unit area of surface over a given time (a flux density in g C m^{-2} s^{-1}). There are significant theoretical and practical limitations to the method, which can be overcome by properly choosing a measurement location and technology.

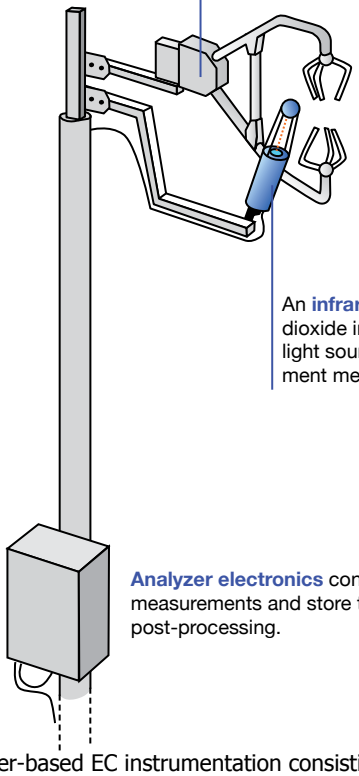

Figure 2.7.1: Tower-based EC instrumentation consisting of an ultrasonic anemometer and a fast trace-gas analyzer. This set-up was operated at the carbon flux tower in the study area as part of the CFCAS network 'Environmental Prediction in Canadian Cities' from May 2008 to April 2010 (see Section 2.7.3).

The EC method fundamentally rests on principles of mass conservation and directly measures atmospheric turbulence and trace gas concentration fluctuations in the atmosphere above the surface of interest. Measurements are done at frequencies between 20 and 5 Hz to fully capture the highly dynamic state of the turbulent atmosphere (Tropea et al, 2007). These rapid measurements are coupled with simultaneous, co-located CO_2 concentration measurements, which allows for in situ quantification of the transport of CO_2 by turbulent eddies between the surface and atmosphere. The specific instrumentation required for EC is a fast anemometer to measure vertical wind velocities coupled with a fast gas analyzer to measure CO_2 concentration fluctuations (Figure 2.7.1).

To make representative readings, EC systems need to be installed on towers significantly above the surface of interest. Typically, a measurement height of 2-3 times the tallest surface objects is sufficient to ensure that mixing and air flow is representative. Ideally, towers are slender and/or latticed to minimize flow disturbances, yet rigid enough to minimize tower swaying and instrument movement. The ideal measurement surface is extensive and flat with homogeneous surface cover to maintain representative measurements for a range of conditions and avoid a major restrictive situation - advection. Advection is a horizontal flux of CO_2 into the measurement volume transported by flow from an upwind surface with different CO_2 characteristics. With proper tower citing and instrument choices, however, advection can be avoided and EC measurements at a single point above a surface are representative of the CO_2 exchange for an entire ecosystem.

EC instrumentation is also sensitive to inclement weather. Rain, snow, or dew on the sensing elements of the instruments can compromise wind velocity and trace gas concentration measurements. Typically, data from rainy or snowy periods is withheld from analysis.

2.7.2. Carbon Flux Measurements in Urban Areas

In urban areas, the extreme spatial variability of urban cover and form make representative citing of EC instruments difficult (Grimmond et al. 2002). The limitations set by logistical and experimental difficulties encountered in urban environments are much higher even than they are for ecosystems with a more uniform structure and form. Nevertheless, in recent years, numerous EC sites used to measure carbon fluxes have been implemented, including four towers in Canadian cities (Christen et al., 2009).

In order to measure representative carbon fluxes at the neighbourhood scale, instruments must be mounted 2-3 times the average building and vegetation height to ensure air flow is not influenced by individual buildings or trees and is representative of a large area (i.e. an entire neighbourhood). Additionally, the surface in the primary upwind direction should show uniform building, vegetation, and road characteristics (e.g. density, geometry, cover). This was the motivation to erect UBC's urban climate research tower in the Vancouver-Sunset neighbourhood in 1978, following an extensive analysis of urban form and topography. The Vancouver-Sunset neighbourhood was identified as an extraordinarily flat, and

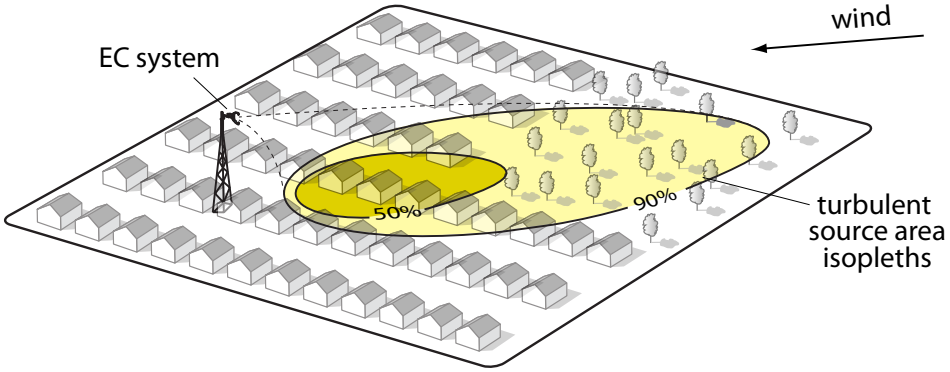

Figure 2.7.2: Conceptual diagram of a flux source area model. The source area is oriented along the direction of the mean wind and the isopleths are the contributions of the surface to the measured flux signal.

homogeneously developed area.

The surface from which EC instrumentation measures carbon exchange (or other trace-gases) is called the flux source area and its orientation and extent are primarily controlled by wind direction and atmospheric stability (e.g. Schmid, 1994). Source areas constantly change and reshape with changing wind direction and atmospheric conditions. Source areas at any time are oriented along the axis of the mean wind direction. Source area models have been developed to delimit the surface area contributing to flux measurements. Figure 2.7.2 shows how model results are visualized as surface isopleths. Isopleths are showing the probability of the surface of origin of the measured signal for the given situation.

2.7.3. Carbon Flux Tower 'Vancouver-Sunset'

Site and instrumentation - The EC system used in this study is located in the centre of the chosen study area on a tower 28.8 m above the local ground surface (494290, 5452601, UTM-10). The tower is located within the Mainwaring Power Substation of BC hydro, and is operated by UBC Geography / the UBC Soil Water Air Laboratory.

Data used in this study was sampled from May 2008 to April 2010 as part of research in the network 'Environmental Prediction in Canadian Cities' funded by the Canadian Foundation for Climate and Atmospheric Sciences (CFCAS). Previous work on the urban carbon cycle at this research site includes carbon-dioxide concentration (Reid and Steyn, 1997) and flux measurements in 2001 (Walsh, 2005).

The instrumentation consists of a sonic anemometer (CSAT 3-d sonic anemometer, Campbell Scientific, Logan, UT, USA) and an open-path infrared-gas analyzer (Li-7500, Li-Cor Inc., Lincoln, NE, USA) (Figure 2.7.3). Three dimensional wind velocities and CO_2 concentrations are sampled at 20 Hz and are collected on a data logger (CR3000, Campbell Scientific, Logan, UT, USA).

Data processing – Vertical fluxes of CO_2 were calculated as the covariance of fluctuations from the mean of vertical wind velocities and CO_2 concentrations. 30-minute averaging periods were chosen to capture the circulation periods of large eddies and fulfil requirements for signal

Table 2.7.1: Monthly summary of data coverage for carbon fluxes measured at the tower from May 1, 2008 – April 30, 2010.

Month	Total Hours Observed (n)	Data Coverage (%)
January	1680	56.5
February	1983	73.8
March	2163	72.7
April	2130	74.0
May	2284	76.7
June	1980	68.8
July	2612	87.8
August	2184	73.4
September	2340	81.2
October	2114	71.0
November	1668	57.9
December	1390	46.7
Total	**24528**	**70.0**

stationarity. First, the coordinate system of the wind velocity components is rotated two times so that it is aligned with the mean wind direction and the mean vertical wind is zero. Then, 30-minute covariances of fluctuations of vertical wind and CO_2 concentrations are calculated and corrections are applied to account for changes in air density (Webb, et al. 1980) and spatial separation between gas-analyzer and anemometer (Moore, 1986). Fluxes undergo several quality control checks, with all details given in Crawford et al. (2010). Using this procedure, 30-minute CO_2 fluxes were calculated for the full 2-year cycle (May 2008 – April 2010). Data coverage for the 2-year period is 70.0% (Table 2.7.1). Of the missing data, 26.6% is due to weather (i.e. rain, snow, or dew on the instruments) or failure to meet quality control standards, and 3.4% is from EC system failure.

Source areas - The long-term source area of the EC system is shown in Figure 2.7.6. This map was calculated using a 2-dimensional gradient diffusion and crosswind dispersion model (Kormann and Meixner 2001) that was run for all 30 min periods between May 1, 2008 and April 30, 2010 at a 2m grid resolution over a domain of 2000 by 2000m. Following the procedure described in Chen et al. (2009), the long-term integrated source area

Figure 2.7.3: Photo of the EC instrumentation on top of the carbon flux tower taken with a fisheye lens. The sonic anemometer is on the left, the gas analyzer on the right. Both instruments are mounted 28.8 m above the local surface (Photo by R. Ketler, UBC).

was calculated as the average of all individual (changing) 30-min source areas during that period. Figure 2.7.6 shows that 50% of the measured flux signal is from within approximately 400 m of the tower. The source area includes the intersection of Knight Street and 49th Avenue.

Calculation of annual total flux - For annual flux densities, 30-minute fluxes were integrated and spatially sorted to account for different emission characteristics across the source area. Each valid 30-min measurement is sorted by (i) month of the year, by (ii) hour of the day, and by (iii) wind direction (vector average) into one of four sectors (NE (0-90º), SE (90º-180º), SW (180º-270º), and NW (270º-360º). For each month and each wind sector, a typical diurnal course of the flux is then calculated by averaging all situations when wind was from a given sector and within a selected hour. Hours without any occurrence of the wind direction from that sector were linearly interpolated for up to 3 hours. The average diurnal course of that month was then integrated over a full day to retrieve a daily carbon flux density (g C m^{-2} day^{-1}) for each wind sector and each month. For the annual flux density, monthly values from the given sector were integrated and weighted by the number of days in the given month. This procedure was separately applied for weekdays and weekends. Flux densities integrated for the entire neighbourhood were calculated as the average flux from each of the four wind sectors.

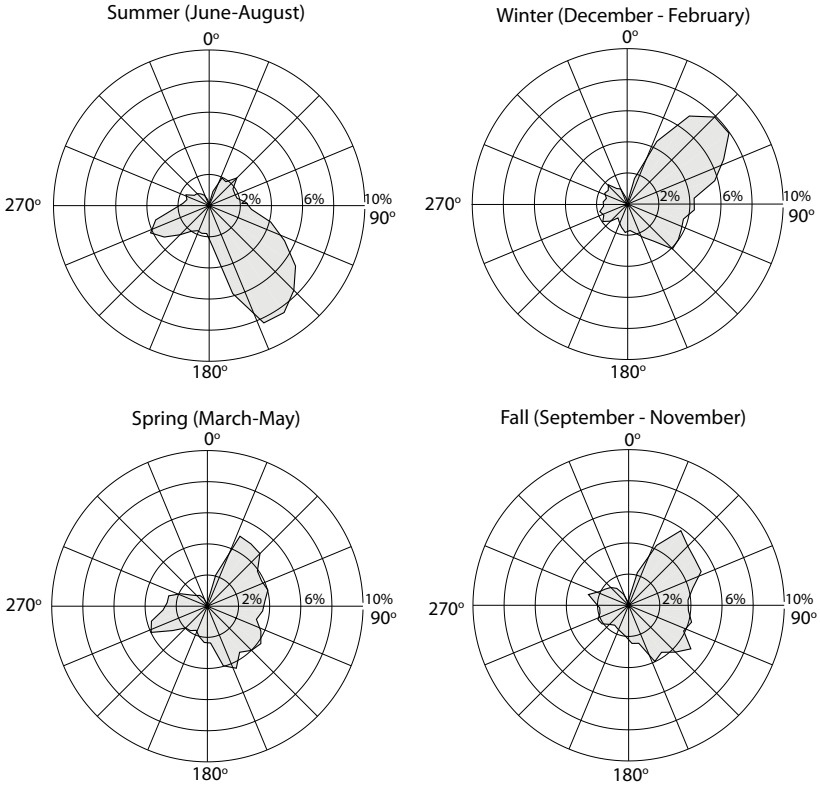

Figure 2.7.4: Seasonal distributions of wind directions measured at the carbon flux for May 2008 – April 2010. Data are 5-minute vector means binned into 10º segments.

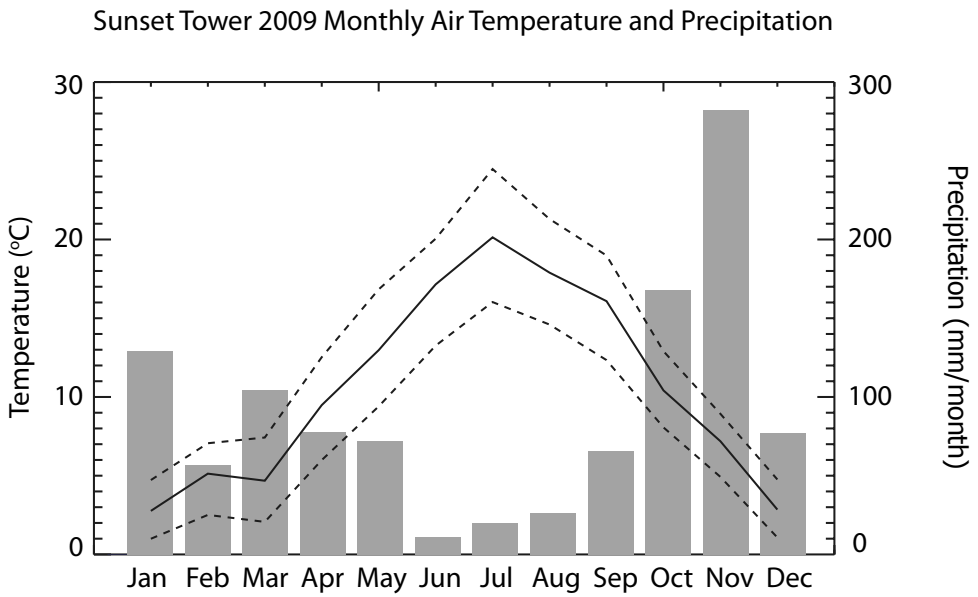

Figure 2.7.5: Observed mean air temperatures (solid line is mean air temperature, dashed lines are mean daily maximum and minimum air temperature) at the carbon flux tower during 2009. Precipitation data (bars) were measured during 2009 at Vancouver International Airport, located approximately 10 km south west of the study area.

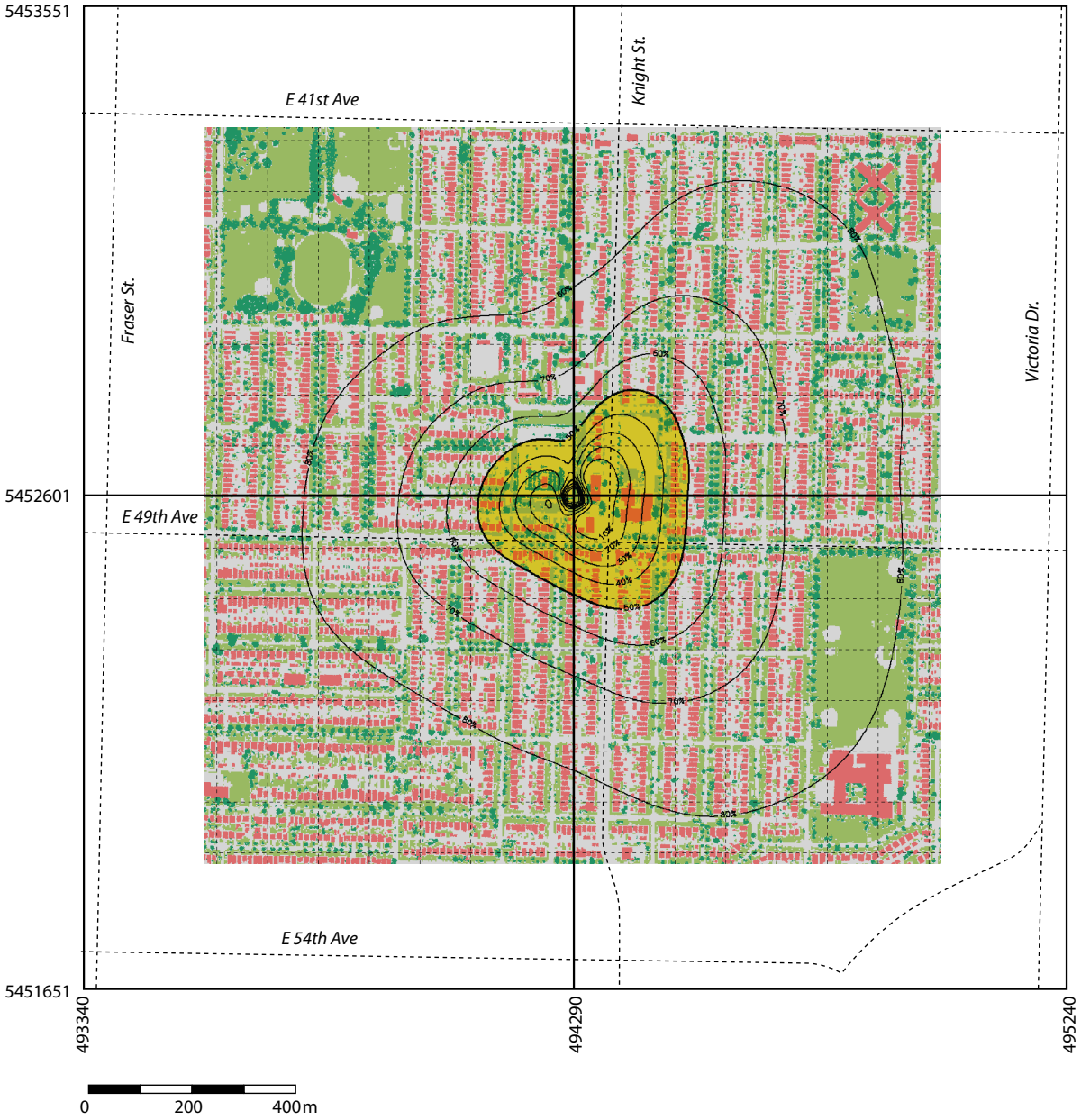

Figure 2.7.6: Map of the long-term integrated flux source area for the carbon flux tower between May 1, 2008 and April 30, 2009 superimposed over the LiDAR / Quickbird derived land-cover map (subset of study area).

References:

Baccini, P., Brunner P. H. (1991). *Metabolism of the anthroposphere*. Springer, Berlin.

Baldocchi, D. (2008). Breathing of the terrestrial biosphere: lessons learned from a global network of carbon dioxide flux measurement systems. *Australian Journal of Botany, 56*, 1-26.

Bayer, T. (2009). Automated building simplification using a recursive approach. In *Cartography in Central and Eastern Europe* (Eds. G. Gartner., & F. Ortag.) Springer: Berlin, 121-146.

Buringh, P. (1984). Organic Carbon in Soils of the World. In *The Role of Terrestrial Vegetation in the Global Carbon Cycle: Measurement by Remote Sensing* (Eds. G. M. Woodwell, 1984 SCOPE). Published by John Wiley & Sons Ltd.

Cairns, M.A., Brown, S., Helmer, E.H., & Baumgardner, G.A., 1997. Root biomass allocation in the world's upland forests. *Oecologia 111*, 1–11.

Chen, B., Black, T.A., Coops, N.C., Hilker, T. Trofymow, J.A., & Morgenstern, K. (2009). Assessing tower flux footprint climatology and scaling between remotely sensed and eddy covariance measurements. *Boundary-Layer Meteorol, 130*(2), 137-167.

Christen, A., Coops, N., Crawford, B., Liss, K., Oke, T. R., & Tooke, R. (2009). *The role of soils and lawns in urban-atmosphere exchange of carbon dioxide.* 7th International Conference on Urban Climate, Yokahama, Japan, June 29 - July 3, 2009.

Christen, A., Crawford, B., Liss K., Siemens, C. (2010). Soil properties at the Vancouver EPiCC experimental sites. *EPiCC Technical Report No. 2, 28pp*. Retreived on June 20, 2010 from http://www.geog.ubc.ca/~epicc/reports/Vancouver-EPiCC-Tech-Report-2.pdf

Christen, A., Grimmond, C. S. B., Roth, M., & Pardyjak, E. (2009). The IAUC Urban Flux Network - An international network of micrometeorological flux towers in urban ecosystems. *Eos Trans. American Geophysical Union, 90*(52), Fall Meet. Suppl., Abstract B31C-06

Churkina, G., Brown, D. G., & Keoleian, G. (2009). Carbon stored in human settlements: the conterminous United States. *Global Change Biology, 16*(1), 135-143

Codoban, N., & Kennedy, A. C. (2008). Metabolism of neighbourhoods. *Journal of Urban Planning, D-Asce, 134*(1), 21-31.

Natural Resources Canada (2009). C*ommunities | Urban Archetypes Project*. Retreived in June 20, 2010 from http://canmetenergy-canmetenergie.nrcan-rncan.gc.ca/eng/buildings_communities/communities/urban_archetypes_project.html

City of Vancouver, Traffic and intersection counts as referenced in VanMap. City of Vancouver web-based mapping system (2010). Retreived on June 20, 2010 from http://vancouver.ca/vanmap

Crawford, B. Christen, A., Ketler, R. (2010). *EPiCC Technical Report 1: Processing and quality control procedures of turbulent flux measurements during the Vancouver EPiCC experiment*. Retreived on June 20, 2010 from http://www.geog.ubc.ca/~epicc/reports/Vancouver-EPiCC-Tech-Report-1.pdf

ecoENERGY, Natural Resources Canada (2007). 2005 Canadian Vehicle Survey Summary Report.
Ministry of Community Services, Province of British Columbia (2008), Greenhouse Gas Emission Assessment Guide For British Columbia Local Governments.

Goodwin, N.R., Coops, N.C., Tooke, T.R., Christen, A., and Voogt, J.A. (2009). Characterising urban surface cover and structure with airborne LiDAR technology. *Canadian Journal of Remote Sensing 35*, 297-309.

Grimmond, C.S.B., King, T.S., Cropley, F.D., Nowak, D.J., & Souch, C (2002). Local-scale fluxes of carbon dioxide in urban environments: methodological challenges and results from Chicago. *Environmental Pollution, 116*, S243-S254.

Haltrecht, D., & Fraser, K. (1997). Validation of HOT2000 using HERS BESTEST. *IBPSA,* Natural Resources Canada's CanmetENERGY. Retreived on June 20, 2010 from http://www.ibpsa.org/proceedings/BS1997/BS97_P009.pdf

Heiple, S., & Sailor, D. (2008). Using building energy simulation and geospatial modeling techniques to determine high-resolution building sector energy consumption profiles. *Energy and Buildings, 40*(8), 1426-1436.

Keoleian, G. A., Blanchard, S., & Reppe, P. (2000). Life-cycle energy, costs, and strategies for improving a single-family house. *Journal of Industrial Ecology, 4*, 135–156.

Kormann, R., & Meixner, f. X. (2001). An analytical footprint model for non-neutral stratification. *Boundary-Layer Meteorology 99*, 207-224.

Liss, K., Crawford, B., Jassal, R., Siemens, C., & Christen A. (2009). Soil respiration in suburban lawns and its response to varying management and irrigation regimes. P*roc. of the AMS Eighth Conference on the Urban Environment*, Phoenix, AZ, January 11-15, 2009.

Liss, K., Tooke, R., Coops, N., & Christen, A., (2010). Vegetation Characteristics at the Vancouver EPiCC experimental sites. *EPiCC Technical Report No. 3, 38 pp.* Retreived on June 20, 2010 from http://www.geog.ubc.ca/~epicc/reports/Vancouver-EPiCC-Tech-Report-3.pdf

Ministry of Transportation, Province of British Columbia and Greater Vancouver Transportation Authority (TransLink) (no date), Greater Vancouver Trip Diary Survey, 2004

Moore, C.J. (1986). Frequency response corrections for eddy correlation systems. *Boundary-Layer Meteorology, 37*, 17-35.

Moriwaki, R., & Kandaz, M. (2004). Seasonal and diurnal fluxes of radiation, heat, water vapor, and carbon dioxide over a suburban area. *Journal of Applied Meteorology, 43*, 1700-1710.

Nowak, D. J. (1996). Estimating leaf area and leaf biomass of open-grown deciduous urban trees. *Forest Sciences, 42*(4), pp. 504-507

Ogren, E., & Evans, J. R. (1993). Photosynthetic light-response curves: The influence of CO2 partial pressure and leaf inversion. *Planta, 189*, 182-190.

Reid, K. H., & Steyn, D. G. (1997). Diurnal variations of boundary-layer carbon dioxide in a coastal city - Observations and comparison with model results. *Atmospheric Environment, 31*(18), 3101-3114.

Prairie, Y. T., & Duarte C. M. (2006). Direct and indirect metabolic CO2 release by humanity. *Biogeosciences Discussion, 3,* 1781-1789.

Province of British Columbia (2008). B*C GHG Emissions Assessment Guide*. Retreived on June 20, 2010 from http://www.townsfortomorrow.gov.bc.ca/docs/ghg_assessment_guidebook_feb_2008.pdf

Sambridge, M., Braun, J., & McQueen, H. (1995). Geophysical parametrization and interpolation of irregular data using natural neighbours. *Geophysical Journal International 122*, 837-857.

Schmid, H. P. (1994). Source Areas for Scalars and Scalar Fluxes. *Boundary-Layer Meteorology, 67*, 293–318.

Tropea, C., Yarin A. L., & Foss J. F. (2007). *Springer Handbook of Experimental Fluid Mechanics*. Springer, Berlin, 1557 p.

Sibson, R. (1981). A brief description of natural neighbourhood interpolation. In *Interpreting Multivariate Data* (Ed. Barnett, V.). Wiley: Chichester, 21–53.

Statistics Canada (2004). *Food statistics' Catalogue No. 21–020-XIE, Vol., 4, No. 1*. Agriculture Division, Ottawa.

Tooke, R., Coops, N.C., Goodwin, N.R., & Voogt J.A. (2009). The influence of Vegetation Characteristics on Spectral Mixture Analysis in an Urban Environment. R*emote Sensing of Environment, 113*, 398-407

Walsh, C.J. (2005). Fluxes of radiation, energy, and carbon dioxide over a suburban area of Vancouver. *BC. M.Sc. Thesis, Department of Geography, University of British Columbia*.

Webb, E.K., Pearman, G. I., & Leuning , R. (1980). Correction of flux measurement for density effects due to heat and water vapour transfer. *Quarterly Journal of the Royal Meteorological Society, 106*, 85-100.

3.1 Carbon Emissions from Buildings

This section describes modelled results of energy and carbon emissions attributable to the building urban metabolism component.

3.1.1 Carbon emissions from buildings

The energy intensity of residential sub-types ranged from 517-1017 MJ m^{-2} of finished floor area. These values compare relatively well with canmetENERGY urban archetypes project, although energy totals for single family dwellings post 1965 were slightly larger than expected (modelled = 596-804 MJ $m^{-2,}$ canmetENERGY urban archetypes = 434-812 MJ m^{-2}). This is in part due to the increased occupancy modelled in each sub-type when compared to the urban archetypes study.

The total modelled carbon flux attributable to buildings was 2.58 kg C m^{-2} (see section 2.3). Locally emitted carbon made up the majority of this total (2.46 kg C m^{-2}) due to the large number of detached homes heated by natural gas. Table 3.1.1 lists the fluxes for the entire study area and the different sectors. Building carbon emissions are estimated to total approximately 40% of all modelled LOCAL emissions (46% of all local fossil fuel emissions).

Table 3.1.1 Modelled building carbon emissions per area

	All Sectors (kg C m^{-2} $year^{-1}$)	NE (kg C m^{-2} $year^{-1}$)	SE (kg C m^{-2} $year^{-1}$)	SW (kg C m^{-2} $year^{-1}$)	NW (kg C m^{-2} $year^{-1}$)
Local	2.46	2.56	2.40	2.77	2.14
External	0.11	0.11	0.11	0.11	0.10
Total	**2.58**	**2.67**	**2.52**	**2.89**	**2.24**

Table 3.1.2 Modelled building carbon emissions per capita

	All Sectors	NE	SE	SW	NW
Total Population	23,168	6,430	5,493	6,925	4,319
Total (kg C cap^{-1} $year^{-1}$)	385	359	396	362	445

3.1.2 Land use and modelled building carbon emissions

Table 3.1.3 summarizes building carbon fluxes according to land use. The largest emissions were found in the SW sector which contains a small amount of green space and a larger built fraction of 0.214 (Table 3.1.3). Emissions from non-residential buildings were significantly less than residential emissions and relatively constant among sectors due to commercial strips found along Fraser street and Victoria drive. The proportion of emissions from commercial buildings attributable to local sources was 89% due to the larger electricity share compared to SFD.

As expected energy and carbon emissions intensity decreased with typology intensity. The highest emissions were found in detached dwellings followed by attached and stacked dwelling types (Table 3.1.5). It is clear a large proportion of emissions reduction potential exists in retrofitting older detached dwellings, where air leakage, poor insulation and inefficient heating systems all contribute to large carbon intensities. This is highlighted by a new construction rate of approximately 1.04% $year^{-1}$ (calculated from BC-Assessment data) and the fact new construction is typically built to national performance standards. For an extended survey on energy reduction potential in existing building stocks see Harvey, 2009.

Table 3.1.3: Fraction built area (plan area occupied by buildings) of study area quadrants.

	All Sectors	NE	SE	SW	NW
Built Fraction (%)	19.2	19.5	19.0	21.4	17.0

Table 3.1.4: Modelled building carbon emissions for Residential and 'Other' land use in study area quadrants.

	All Sectors (kg C m^{-2} $year^{-1}$)	NE (kg C m^{-2} $year^{-1}$)	SE (kg C m^{-2} $year^{-1}$)	SW (kg C m^{-2} $year^{-1}$)	NW (kg C m^{-2} $year^{-1}$)
Residential Local	2.15	2.28	1.98	2.58	1.75
Residential External	0.07	0.08	0.06	0.09	0.06
Other Local	0.32	0.27	0.42	0.20	0.39
Other External	0.04	0.03	0.05	0.02	0.05

3.1.3 Carbon Storage in Buildings

Organic carbon is stored in buildings in substantial amounts, and it is not relevant in terms of emissions since it is not released unless the building is removed or catches on fire. The amount of carbon stored in buildings at Sunset was approximately three times combined storage in vegetation and soils. This carbon is incorporated in the building's structure, but also in furniture and books (Churkina, 2010). The carbon pool in buildings is estimated to be 13.06 kg C m^{-2}, which includes residential and non-residential building structures and furniture.

Table 3.1.5: Modelled building carbon emissions by sub-type

	Fraction of Built Volume	Energy Intensity (MJ m^{-2} floor area $year^{-1}$)	Carbon Intensity (kg C m^{-3} $year^{-1}$)
SFD (pre1965)	21.0	1017	2.95
SFD (1965-1990)	34.0	804	2.43
SFD (post 1990)	21.1	596	1.69
Duplex	1.5	598	1.61
Row	0.2	580	1.55
Apartment	4.6	517	1.03
Mixed-use	3.2	739	1.48
Extended Care	0.2	1367	2.73
Warehouse	0.1	232	0.46
Civic	6.8	870	1.73
Commercial	2.2	904	1.80
Office	1.1	665	1.33
Retail	4.1	905	1.80

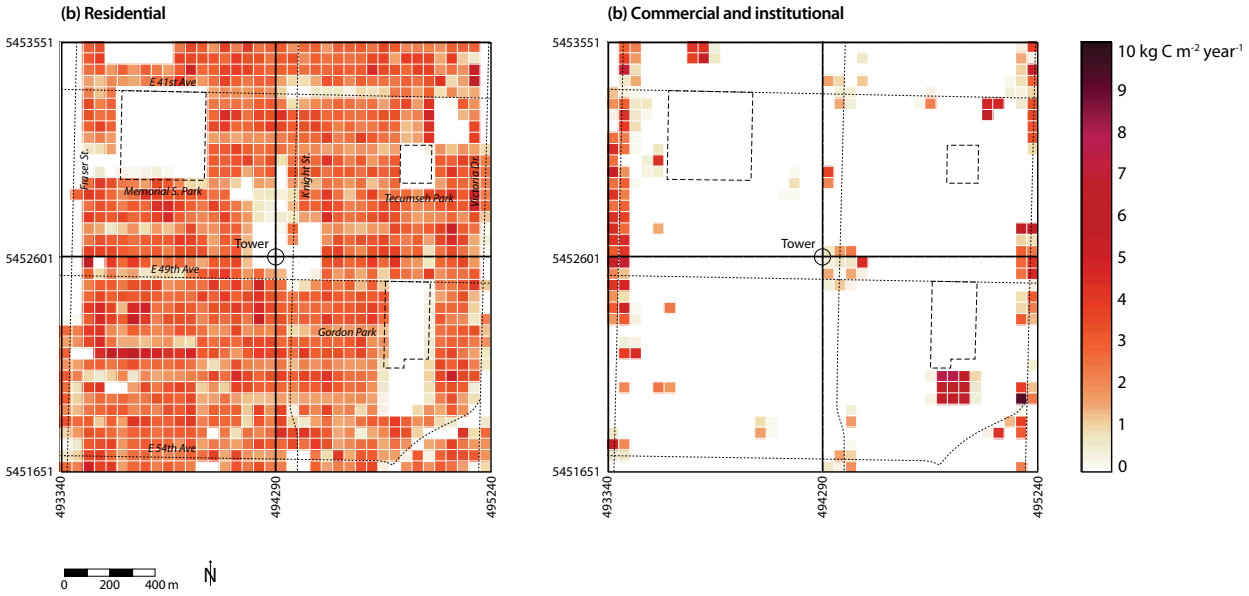

Figure 3.1.1: (a) Modelled local residential carbon emissions (b) Modelled local commercial carbon emissions

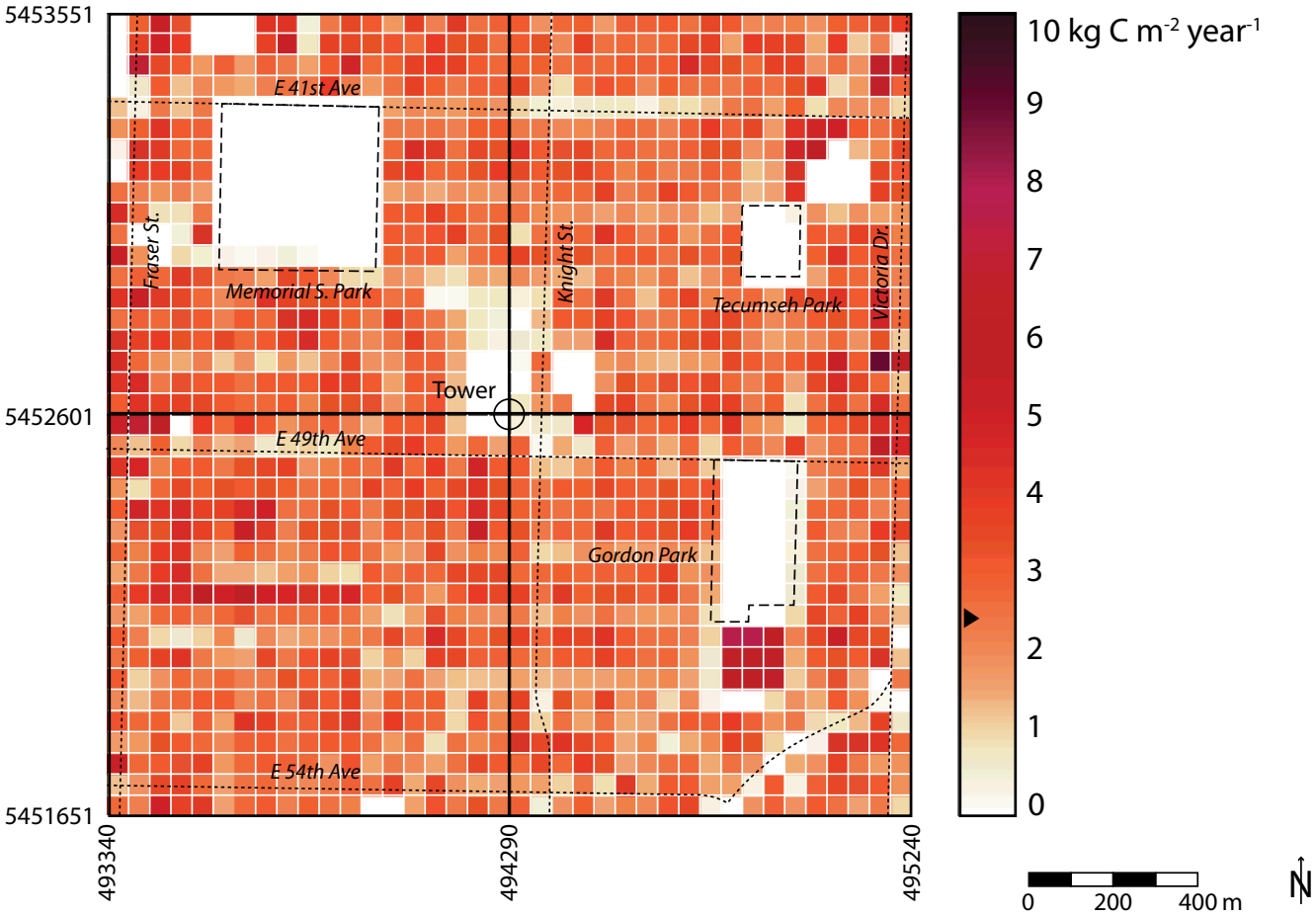

Figure 3.1.2:Modelled total carbon emissions attributable to buildings

3.2 Carbon Emissions from Transportation

This section describes results from calculations of carbon emissions attributable to the transportation urban metabolism component.

3.2.1 Carbon Emissions from Transportation

Methods described in Section 2.4 yield estimated annual carbon emissions attributable to transportation sources of 11.04 tC or 3.06 kg C m^{-2} or 477.37 kg C cap^{-1} within the study area. These emissions derive from the following types of travel and vehicles.

Spatially these emissions distribute along arterial and local roads as summarized in Table 3.2.2 and illustrated in Figure 3.2.1. Most emissions concentrate along Knight Street, the highest volume arterial with the greatest share of heavy freight trips. In descending order (greatest to lowest carbon emissions concentration):

As arterial roads and associated traffic volumes and carbon emissions are distributed asymmetrically in study area quadrants (two arterials in the NW quadrant; three arterials one of which is Knight Street in the NE; three arterials, one of which is East 49th Avenue, in the SW and 4 arterials two of which are Knight Street and East 49th Avenue in the SE) — See Table 3.2.3. In addition as the two highest volume arterial roads are in the SE quadrant within 130m of the carbon flux tower at the centre of the study area, they appear to create an over representation of measured carbon emissions in that quadrant.

Table 3.2.1: Annual carbon emissions attributable to vehicles by type

	Total: t C $year^{-1}$	**Per area: kg C m^{-2} $year^{-1}$**	**Per Capita: kg C m^{-2} $year^{-1}$**
All Vehicles		3.06kg	477.37kg
All Light Vehicles	9,052t / 82%		
Non-local Light Vehicles	7,826t / 71%		
Local Light Vehicles	1,226t / 11%		53.0kg
Transit Vehicles	445t / 4%		19.33kg
All Freight Vehicles	1,547t / 14%		

Table 3.2.3: Annual carbon emissions distributed by quadrant.

	All Sectors	NE	SE	SW	NW
All Transportation Emissions per Area / Sector (t C year^{-1})	**10,604**	3,041	3,899	2,157	1,507
All Traffic Transportation (Local + Through) Emissions per Unit Ground Area (kg C m^{-2} year^{-1})	**2.93**	3.37	4.32	2.39	1.67
Local (kg C m^{-2} year^{-1})	**0.31**	0.36	0.47	0.28	0.20
Through (kg C m^{-2} year^{-1})	**2.62**	3.01	3.85	2.11	1.47

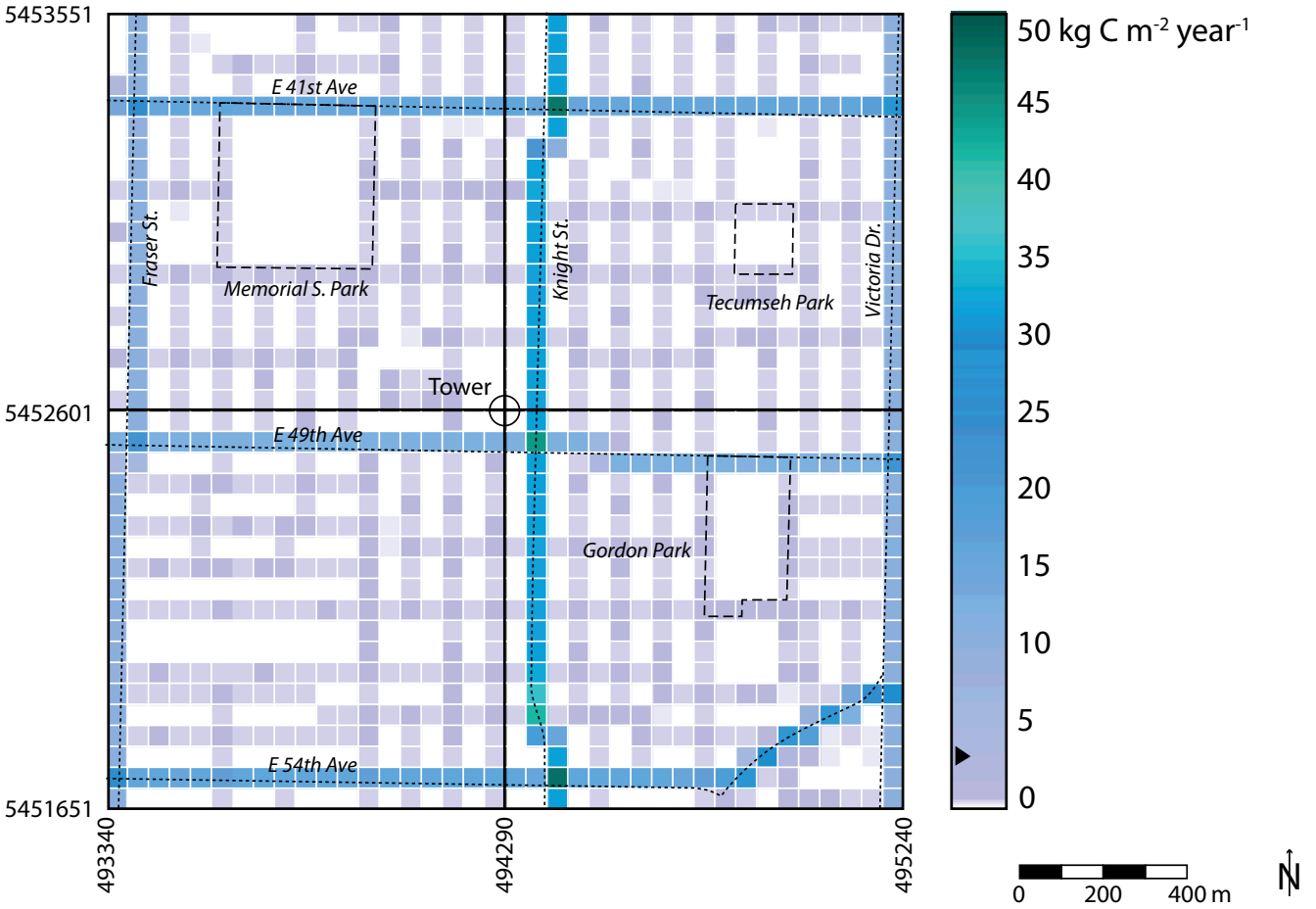

Figure 3.2.1: Annual carbon emissions attributable to transportation 50m rasters

3.3 Carbon Emissions from the Human Metabolism, Food and Waste

This section describes results from calculations of carbon emissions attributable to the human metabolism.

3.3.1 Carbon storage in the human body

Carbon storage in the human body was calculated based on Section 2.5.2 as an average of 9 kg C cap^{-1}. Table 3.3.1 lists the carbon storage in the human body per ground area. It is clear when comparing carbon stored in the human body to carbon stored in buildings, soils and vegetation, that the human body is a negligible small pool. Carbon stored in pets and animals is expected to be even smaller, and is therefore not considered in this study.

However, it is interesting to note that the human body is also the most active carbon pool in the urban ecosystem in terms of throughput. With an average carbon input / output of 106 kg C cap^{-1} $year^{-1}$, the statistical turnover rate of carbon in the human body is only 31 days.

3.3.2 Emissions by human respiration

The carbon emission through human respiration was calculated based on Section 2.5.3. Table 3.5.2 lists calculated values for the entire study area and the different sectors. The average carbon flux density in the study area was estimated 0.49 kg C $year^{-1}$ m^{-2}. This is in a similar magnitude as flux densities reported by Matese et al. (2009) for the city centre of Firenze, Italy that were 0.35 kg C m^{-2} $year^{-1}$. With the high population density in this neighbourhood, human respiration is responsible for about 8% of the carbon dioxide emissions in

Table 3.3.1: Population, population density and calculated carbon storage in the human body for the study area.

	All Sectors	NE	SE	SW	NW
Total Population in Area / Sector	23168	6430	5493	6925	4319
Population Density (Inh. ha^{-1})	64.2	71.3	60.9	76.7	47.9
Total Carbon Stored in the Human Body (t)	209	58	49	62	39
Carbon stored in the Human Body / Unit Ground Area (kg C m^{-2})	**0.058**	**0.064**	**0.055**	**0.069**	**0.043**

Table 3.3.2. Calculated respiratory release of carbon totals and per unit ground area

	All Sectors	NE	SE	SW	NW
Total Carbon Released in Area / Sector (t C $year^{-1}$)	1767	491	419	528	330
Carbon Released by Human Respiration per Unit Ground Area (kg C m^{-2} $year^{-1}$)	0.49	0.54	0.46	0.59	0.37

the neighbourhood (see Section 3.5). This makes human respiration from an ecological viewpoint a relevant process. In comparison, Moriwaki and Kanda (2004) found for a densely populated Japanese residential neighbourhood that 38% of the total carbon emissions in summer and 17% of that in winter were caused by human respiration. However, human respiration should not be overstated in emission reduction strategies, since it cannot be changed and as it is renewable carbon that is emitted.

3.3.3 Lateral fluxes of carbon in food and waste

Lateral fluxes (imports / exports) in this component were calculated based on the per capita fluxes discussed in Section 2.5.4 and 2.5.5 and are listed in Table 3.3.3. Those lateral fluxes are not emitted to the atmosphere although production and distribution of food as well as waste decomposition / management will cause carbon emissions outside the neighbourhood (not included in this study).

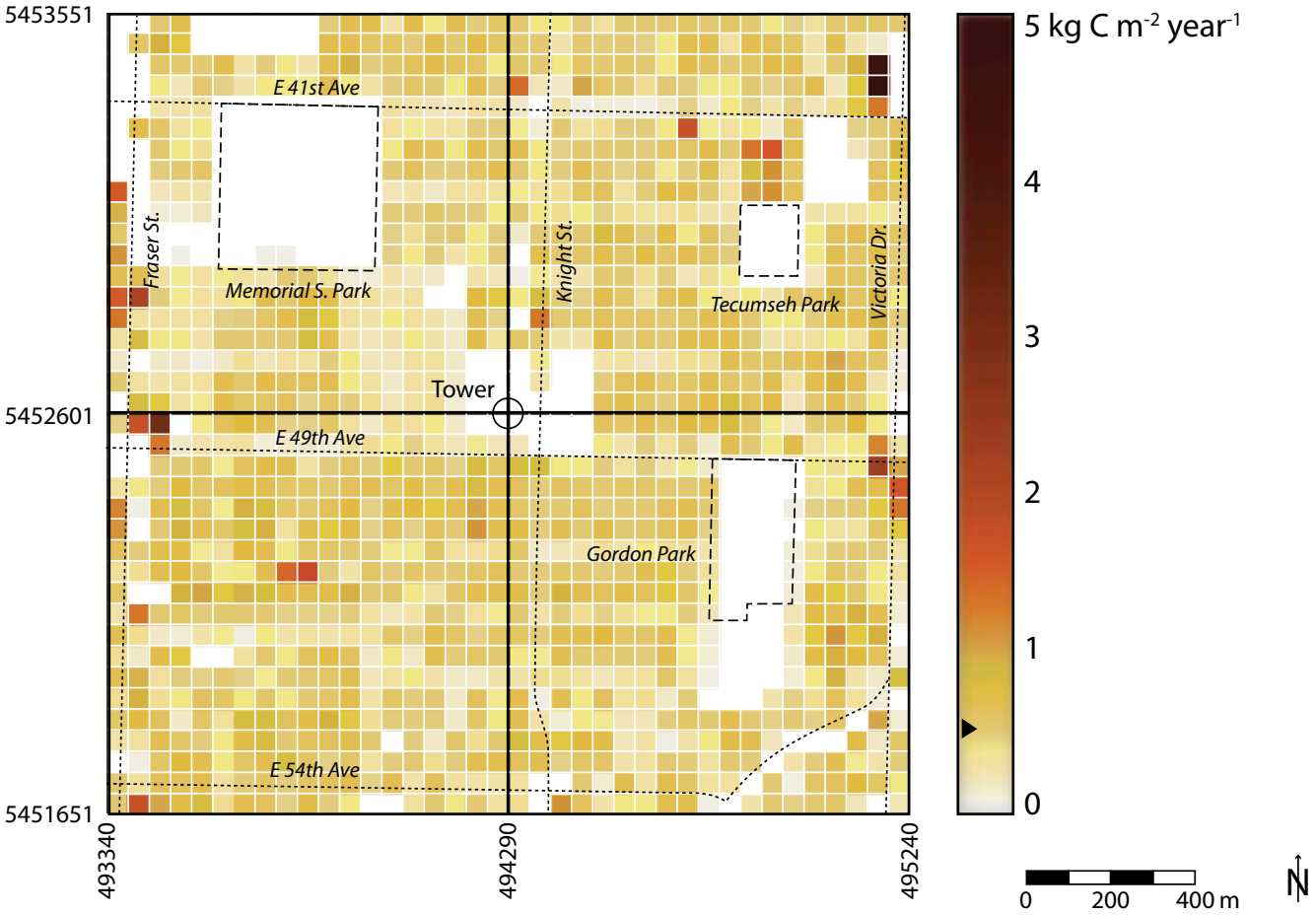

Figure 3.3.1: Calculated respiratory release of carbon based on a 50m raster.

Table 3.3.3. Calculated lateral fluxes of carbon related to carbon contained in food and waste.

	All Sectors	NE	SE	SW	NW
Carbon Imported through Food per Unit Ground Area (kg C m^{-2} $year^{-1}$)	0.97	1.08	0.92	1.16	0.73
Carbon Consumed by Humans per Unit Ground Area (kg C m^{-2} $year^{-1}$)	0.68	0.76	0.65	0.81	0.51
Carbon Exported by Food Waste kg C m^{-2} $year^{-1}$)	0.29	0.32	0.28	0.35	0.22
Carbon Exported by Human Waste kg C m^{-2} $year^{-1}$)	0.19	0.21	0.18	0.23	0.14

3.4 Carbon Emissions from and Uptake by Soils and Vegetation

This section reports calculated carbon storage and emissions from urban soils and vegetation and uptake by vegetation in the study area. It reports net emissions and carbon sequestration by urban vegetation.

3.4.1 Carbon Storage in Soils and Vegetation

For one square meter pervious surface the measured carbon content in the soil was C_s = 9.65 kg C m^{-2} (see Section 2.6.1). This is within the expected range of 3.5-14 kg C m^{-2} reported for urban soils in Pouyat et al. (2002) based on data from five different cities in the US. If C_s is multiplied by the vegetated pervious surface fraction (35.7%, see Table 3.4.1 and Figure 3.2.1), we estimate the neighbourhood-wide average carbon storage in soils $C_{s,n}$ = 3.45 kg C m^{-2}.

Table 3.4.1. Surface area covered by ground vegetation (lawns) and tall vegetations (trees > 2m). Land-cover was calculated on a 1 x 1 m raster using LiDAR and optical remote sensing data (Section 2.2)

The carbon storage in vegetation biomass in the study area was calculated separately for lawns (0.13 kg C m^{-2}) and trees (1.42 kg C m^{-2}). The sum of both is listed as $C_{v,n}$ in Table 3.4.2. The NW sector shows highest $C_{v,n}$ values, as it includes Memorial South Park with 30 m tall deciduous trees that contribute substantially to the neighbourhood's above-ground biomass (Figure 3.4.1).

The detailed allocation of carbon stored in different vegetation parts is listed in Table 3.4.3 based on methods described in Section 2.6.1. The calculated carbon stored in vegetation biomass in the Sunset study area is only half the average value reported for carbon storage in urban trees of US North-Western cities (3.2 kg m^{-2}), for which an average of 32.7% tree cover is reported (Nowak and Carne, 2002). This is realistic, as the study area shows only 11.3% tree cover, and a relatively low to medium-sized street tree population compared to other Vancouver neighbourhoods.

Table 3.4.1: Surface area covered by ground vegetation (lawns) and tall vegetations (trees > 2m). Land-cover was calculated on a 1 x 1 m raster using LiDAR and optical remote sensing data (Section 2.2)

	All Sectors	NE	SE	SW	NW
Surface Cover Fraction of Ground Vegetation (Lawns)	24.4%	20.4%	26.0%	21.7%	29.4%
Surface Cover Fraction of Trees	11.3%	11.2%	9.7%	10.4%	13.4%
Total Vegetated Surface Cover	**35.7%**	**31.6%**	**35.7%**	**32.0%**	**43.2%**

3.4.2 Laterally exported carbon through maintenance biomass removal

The annual lateral export (flux) of carbon F_{exp} is calculated to be 0.07 g C m^{-2} $year^{-1}$. This number is the sum of carbon exported by tree removal / maintenance / prunning (0.01 g C m^{-2} $year^{-1}$), removal of lawn clippings (0.02 g C m^{-2} $year^{-1}$ assuming that 35% of all properties export clippings), and by autumnal removal of leaves / litter (0.04 g C m^{-2} $year^{-1}$, assuming two thirds of all leaves are removed). Unaccounted are the export and import due to gardening activities (e.g. mulching, topsoil). Carbon exported laterally can be released (decomposed) outside the system (composting) or sequestered in landfills.

Table 3.4.2:. Measured and/or estimated carbon pools in soils and vegetation biomass in the Vancouver-Sunset neighbourhood for all four sectors separately and the full study area.

	All Sectors (kg C m^{-2})	**NE (kg C m^{-2})**	**SE (kg C m^{-2})**	**SW (kg C m^{-2})**	**NW (kg C m^{-2})**
Carbon Stored in Soils ($C_{s,n}$)	3.43	3.04	3.44	3.08	4.17
Carbon Stored in Vegetation ($C_{v,n}$)	1.55	1.36	1.28	1.21	2.35
Total	**4.98**	**4.40**	**4.72**	**4.29**	**6.52**

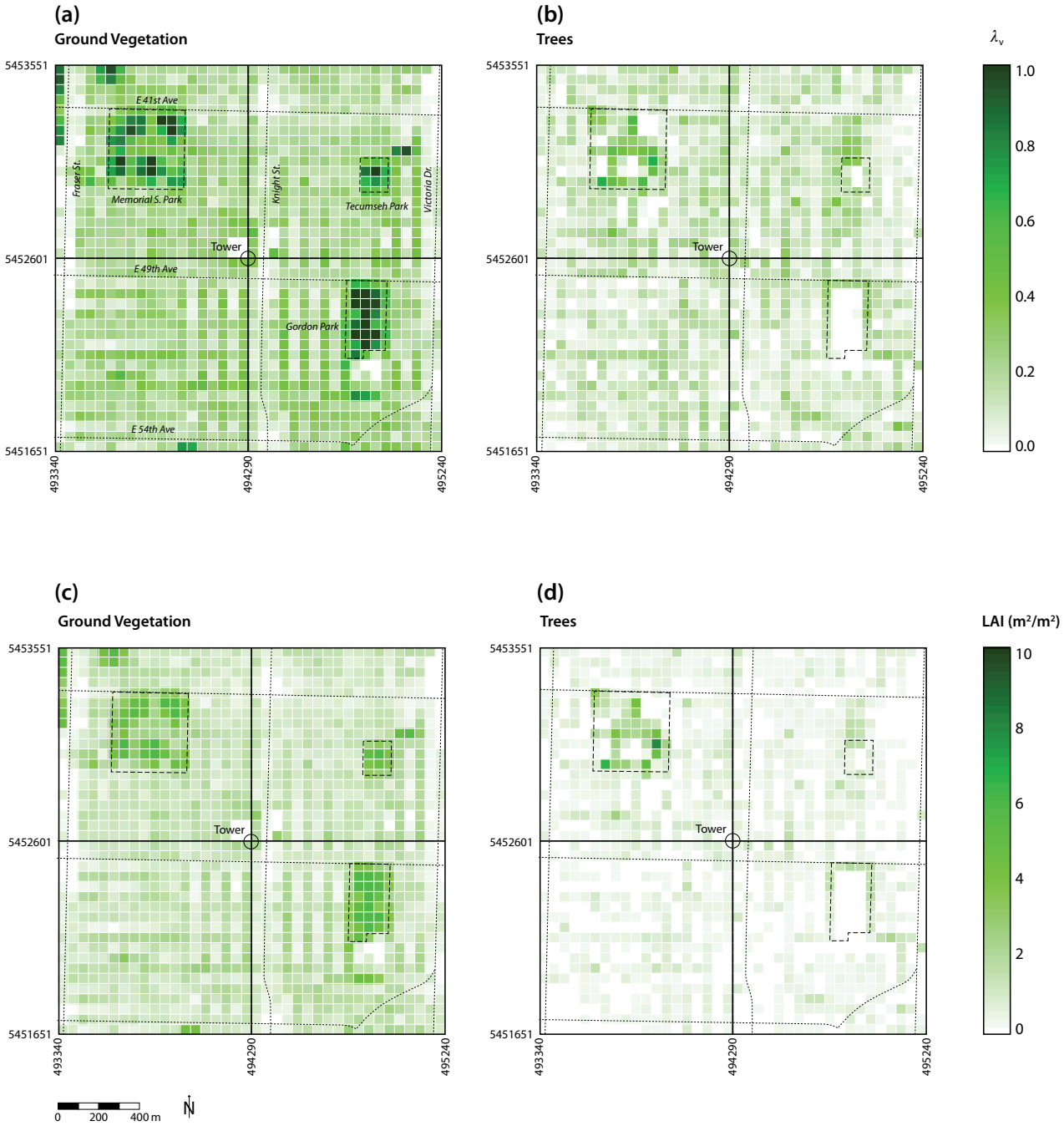

Figure 3.4.1: Maps of surface area covered by (a) ground vegetation (lawns) and (b) tall vegetations (trees > 2m), (c) leaf area index of lawns, and (d) leaf area index of trees based on remote sensing data.

3.4.3 Carbon Emissions

Carbon emissions by respiration were separately calculated for the process of autotrophic and heterotrophic soil respiration *($R_{soil+lawn}$)*, and autotrophic above-ground leaf and bole respiration of trees (R_{tree}). The detailed methodology is described in Section 2.6.2. Respiration from bushes and other low ornamental plants were not considered.

The neighbourhood-wide emission due to soil and lawn respiration were calculated as 0.33 g C m^{-2} $year^{-1}$ (Table 3.4.4). This value includes autotrophic respiration of lawns and tree roots. Values are higher for the SE and NW sectors which contain extensive sport-fields and park areas (Memorial South Park) (Figure 3.4.2a).

Table 3.4.3: Estimated carbon pools in different parts of the urban vegetation in the Vancouver-Sunset neighbourhood for the full study area.

Carbon Pool	Carbon Storage (kg C m^{-2})
Above-ground Tree (Woody) Biomass	1.03
Below-ground Tree (Root) Biomass	0.32
Leaf Biomass (Broadleaf Trees)	0.06
Needle Biomass (Coniferous Trees)	0.01
Total in Tree Biomass	1.42
Lawn Biomass	0.3
All Vegetation Components	**1.55**

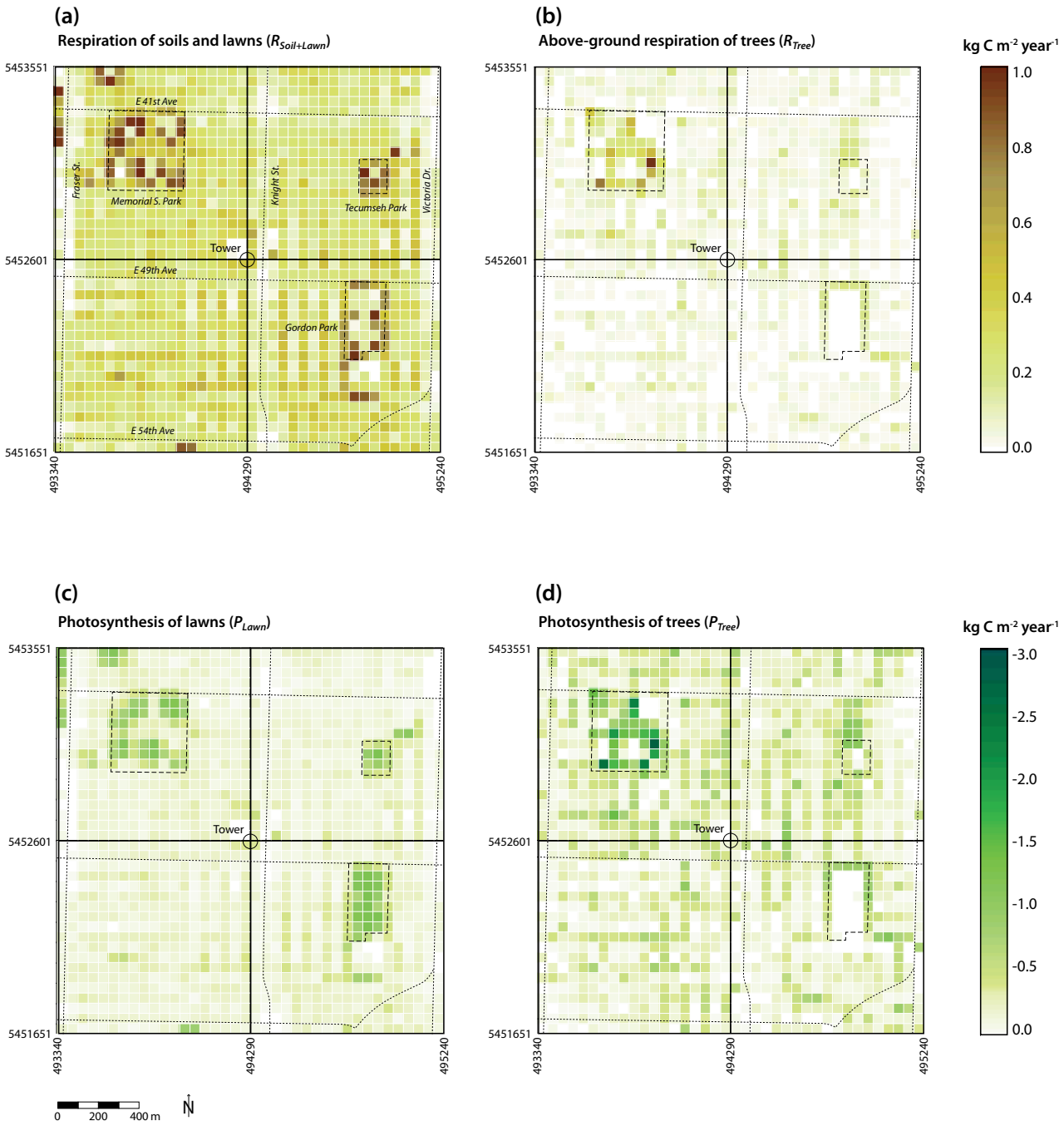

Figure 3.4.2: Maps of modelled (a) soil and lawn respiration, (b) above ground respiration, (c) photosynthesis by lawns and (d) photosynthesis of trees on the 50 x 50 m raster.

The calculation is based on closed-chamber measurements in the study area, which indicate that emissions peak during summer and fall months, and are strongly controlled by temperature and irrigation. Extensive and regular lawn irrigation was shown to control annual soil respiration by a factor two. Lawn respiration ranged between 0.81 kg C m^{-2} (lawn) $year^{-1}$ for properties with no irrigation and 1.79 kg C m^{-2} (lawn) $year^{-1}$ for properties with regular and extensive lawn sprinkling in the city of Vancouver (Liss et al., 2009). However, it is important to note that although lawn sprinkling reduction / regulations would reduce carbon emissions through $R_{soil+lawn}$, such restriction would also reduce carbon sequestration by lawn photosynthesis (see section 3.4.4).

Autotropic above-ground respiration was modelled based on leaf area. Emissions are smaller (0.05 kg C m^{-2} $year^{-1}$) compared to below-ground and lawn respiration (Table 3.4.4 and Figure 3.4.2b).

3.4.4 Carbon Uptake

Carbon uptake by photosynthesis was calculated separately for lawns *(P_{lawn})* and included private properties, sport fields, public parks, and trees *(P_{tree})*. P_{tree} incorporates street and private trees. The detailed methodology is described in Section 2.6.3. Photosynthesis of small bushes. garden plots, and ornamental plants was not separately considered but modelled similar to lawns. Lawns are the predominant vegetated ground cover.

Lawns cover 24.4% of the study plan area whereas trees only 11.2% (Table 3.4.2). Photosynthesis of lawns was calculated -0.48 kg C m^{-2} $year^{-1}$ and photosynthesis of trees was -0.28 kg C m^{-2} $year^{-1}$ (Table 3.4.5). The NW sector with Memorial South Park shows highest uptake by photosynthesis. For example, the average P_{lawn} + P_{tree} of Memorial Park is modelled -1.45 kg C m^{-2} $year^{-1}$ due to tall and mature freestanding trees and extensive, irrigated lawn surfaces (Figure 3.4.2c and d).

It should be noted that the regular clipping of lawns increases the growth rate, and therefore significantly increases lawn photosynthesis compared to photosynthesis of trees, but radiation at ground level is reduced by shading (building, trees), so lawns do not necessarily result in more efficient carbon sequestration. On average, carbon is cycled through lawn (plant) biomass in only 226 days, whereas carbon taken up by trees resides in tree biomass on average for 5 years.

Table 3.4.4:. Modelled respiration separately for soils / lawns and above-ground vegetation of trees.

	All Sectors (kg C m^{-2} $year^{-1}$)	**NE (kg C m^{-2} $year^{-1}$)**	**SE (kg C m^{-2} $year^{-1}$)**	**SW (kg C m^{-2} $year^{-1}$)**	**NW (kg C m^{-2} $year^{-1}$)**
Soil and Lawn Respiration ($R_{soil+lawn}$)	0.28	0.24	0.30	0.25	0.34
Autotrophic Above Ground Respiration of Trees (R_{tree})	0.05	0.04	0.04	0.03	0.08
Total ($R_{soil+lawn}$ + R_{tree})	**0.33**	**0.28**	**0.34**	**0.28**	**0.42**

3.4.5 Net emissions by the urban biosphere

The total net emissions between urban soils, vegetation and the atmosphere, F_{net} (net ecosystem exchange) was calculated by adding all components in direct exchange with the atmosphere, i.e.

$$F_{net} = R_{soil+lawn} + R_{tree} + P_{lawn} + P_{tree}$$

Table 3.4.6 lists the net emissions for the study area and all four sectors, and the negative values indicate that there is a net uptake of carbon in the order of -0.16 kg C m^{-2} $year^{-1}$. Figure 3.4.3 shows the 50 x 50 m raster map of calculated net emissions, which can reach values up to -0.51 kg C m^{-2} $year^{-1}$ in areas of Memorial South Park.

3.4.6 Carbon Sequestration by the Urban Biosphere

Carbon sequestration in the study area by trees, lawns and soils was calculated by

$$Sequestration = F_{net} - F_{exp}$$

The urban ecosystem pool is expected to accumulate carbon (sequester carbon) at 0.09 kg C m^{-2} $year^{-1}$ which is the difference of the estimated F_{net} = -0.16 kg C m^{-2} $year^{-1}$ net uptake (Table 3.4.5) and 0.07 kg C m^{-2} $year^{-1}$ lateral export F_{exp} (Section 3.4.2).

This corresponds to an accumulation rate of currently 1.8% per year of the total carbon stored in the soil and vegetation pool. The carbon sequestered is expected to accumulate dominantly in tree biomass and soils. Figure 3.4.4 visualizes the vegetation growth in the area over the last 30 years. It shows photos taken at exactly the same location with obvious changes in tree volume from the 1980s to 2009. Also soils are expected to accumulate carbon over time. One of the few studies that measured organic carbon in urban soils after urbanization showed that urban gardening and land-use increased and accumulated carbon in soil after an initial decrease due to development (Golubiewski, 2006).

Table 3.4.5: Modelled photosynthesis separately lawns and trees.

	All Sectors (kg C m^{-2} $year^{-1}$)	NE (kg C m^{-2} $year^{-1}$)	SE (kg C m^{-2} $year^{-1}$)	SW (kg C m^{-2} $year^{-1}$)	NW (kg C m^{-2} $year^{-1}$)
Lawn (P_{lawn})	-0.21	-0.17	-0.24	-0.18	-0.26
Tree (P_{tree})	-0.28	-0.27	-0.22	-0.22	-0.39
Total (P_{lawn} + P_{tree})	**-0.49**	**-0.44**	**-0.46**	**-0.40**	**-0.65**

Table 3.4.6: Modelled net emissions from vegetation and soils

	All Sectors (kg C m^{-2} $year^{-1}$)	NE (kg C m^{-2} $year^{-1}$)	SE (kg C m^{-2} $year^{-1}$)	SW (kg C m^{-2} $year^{-1}$)	NW (kg C m^{-2} $year^{-1}$)
Total	**-0.28**	**-0.27**	**-0.23**	**-0.23**	**-0.37**

In summary, the urban biosphere sequesters carbon at 0.09 kg C m^{-2} $year^{-1}$. This value is compared to measured values over grassland and forests in the Vancouver area in Table 3.4.7. It shows that because only 36% of the urban surface is vegetated, sequestration is significantly less to that of unmanaged grassland or even a mature forest. The urban vegetation sequesters 1.4% of the local emissions in this neighbourhood (1.7% of fossil fuel emissions).

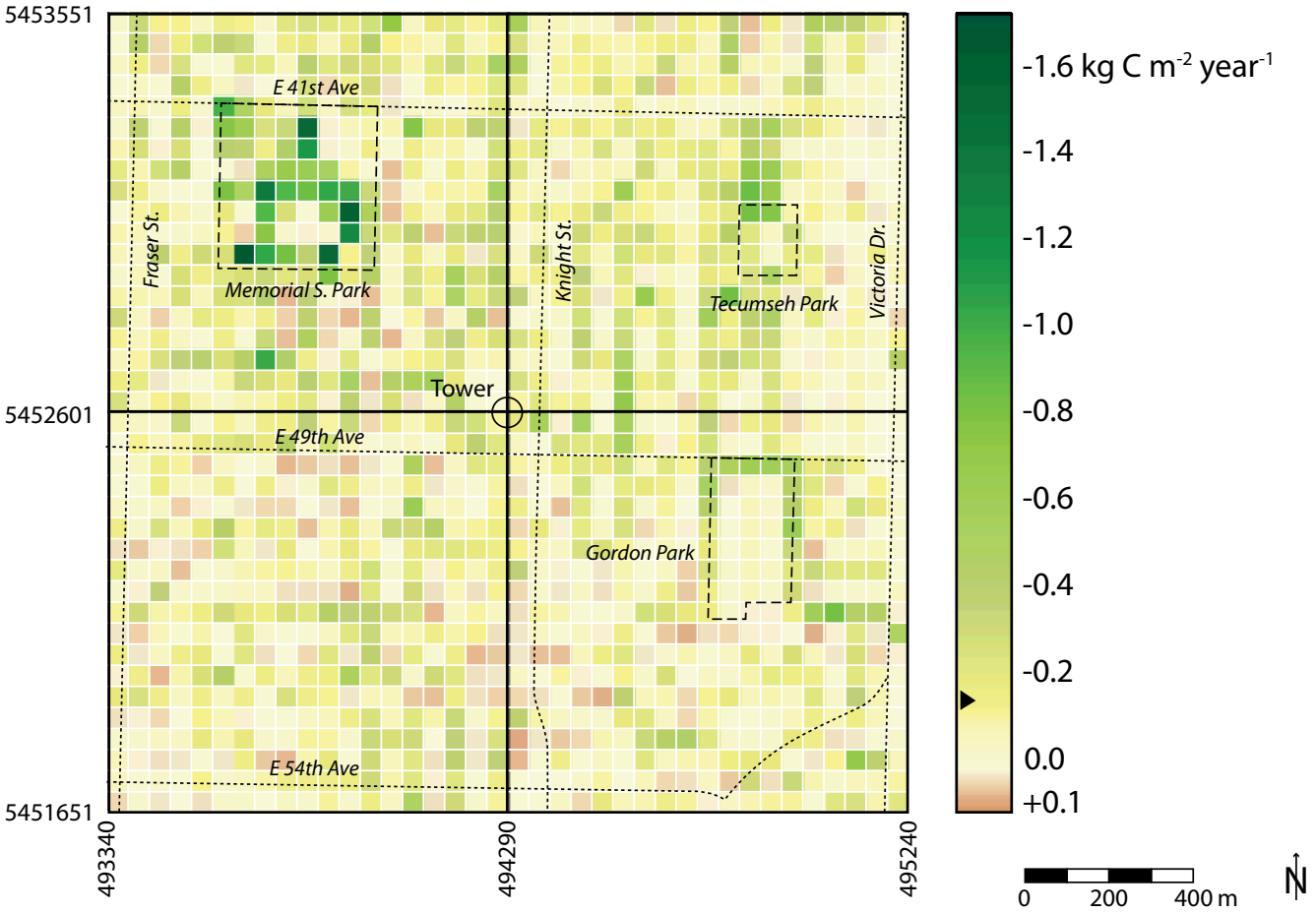

Figure 3.4.3:. Map of modelled net emissions (negative values mean uptake) on a 50 by 50 m raster for the study area.

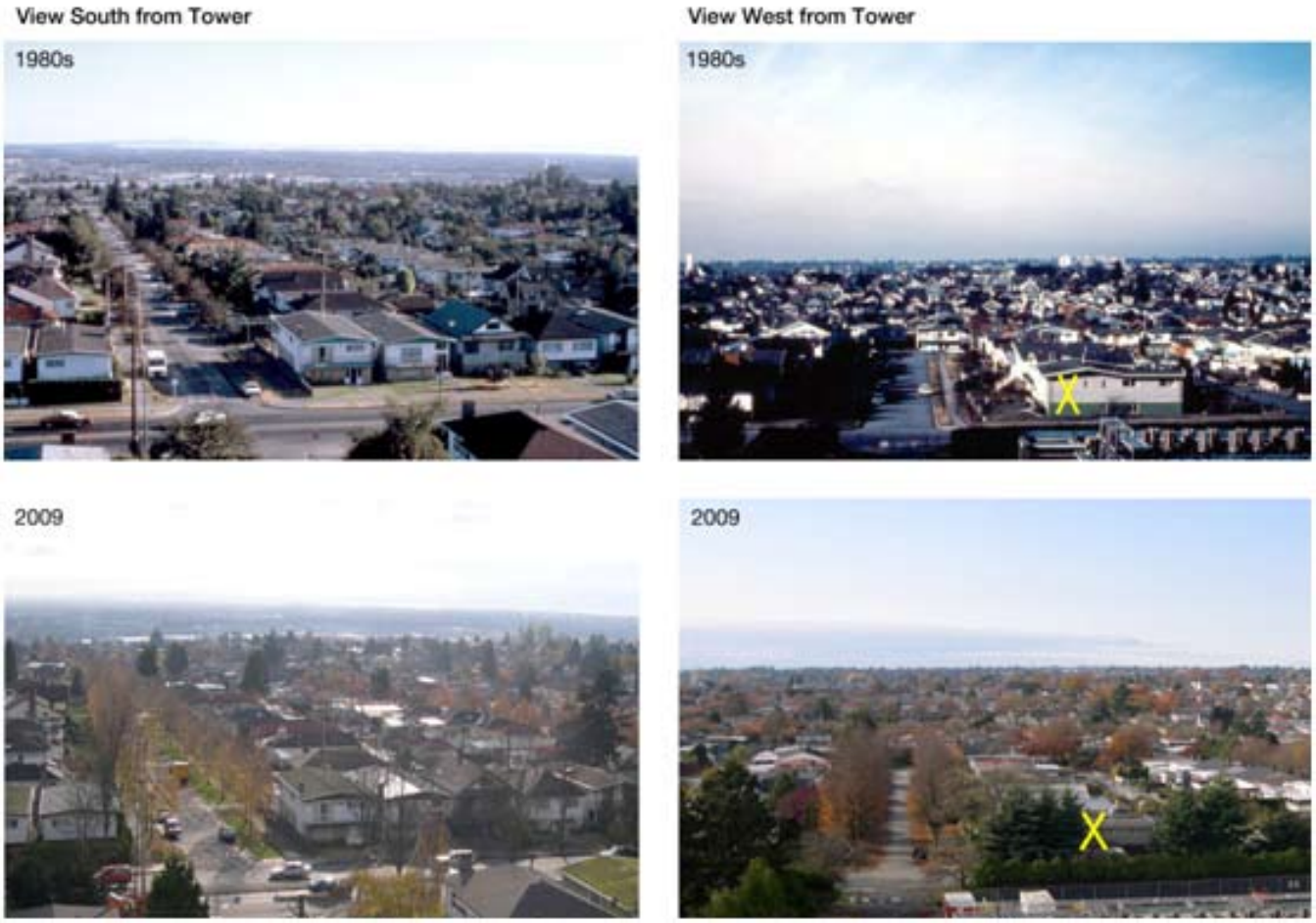

Figure 3.4.4: Vegetation growth between the 1980s and 2009 (Source: UBC Geography photo archive).

Table 3.4.7: Comparison of annual carbon sequestration by urban vegetation in the study area to annual carbon sequestration by other ecosystems (grassland, forest) in the Vancouver area.

Site	Land Use	Annual Carbon Sequestration (kg C m^{-2} $year^{-1}$)	Source
Vancouver-sunset, BC	Urban	-0.09	This Study (Modelled)
Westham Island, Delta, BC	Unmanaged Grassland	-0.25	EPiCC Network, 2008 (Measured, Unpublished)
Campbell River, BC	Mature West coast Forest (60 Years Old)	-0.36	Canadian Carbon Program (Measured, Krishnan et al., 2009)

3.5 Integrated Modelled Carbon Cycle

This section discusses the integrated emissions, which were calculated by adding all four components (buildings, transportation, human metabolism, and vegetation/soils) in the study area. We compare the magnitude of the different components and link them to the local carbon cycle at the neighbourhood-scale by constructing a full mass balance including lateral fluxes and pools of carbon.

3.5.1 Integrated Per-area Carbon Emissions

The different local emission components (buildings, transportation, human metabolism, and vegetation/soils) are shown for each of the four quadrants in Table 3.5.1 and Figure 3.5.1. The SE sector shows highest integral emissions, which is explained by the higher fraction of arterial roads, and hence increased transportation emissions (see Section 3.2). Inversely, the NW sector has lowest emissions because only two arterial road segments are included (41st Ave. and Fraser St.) and building / population density is slightly lower due to Memorial South Park.

Out of all carbon emissions (renewable and fossil fuel), 2.47 kg C m^{-2} $year^{-1}$ (40%) are originating from buildings, 2.93 kg C m^{-2} $year^{-1}$ (47%) from transportation, 0.33 kg C m^{-2} $year^{-1}$ (5%) from human respiration and 0.48 kg C m^{-2} $year^{-1}$ (8%) from respiration of soil and vegetation. Those are offset by an annual uptake of -0.49 kg C m^{-2} $year^{-1}$ (-9% of emissions) though photosynthesis of urban vegetation (lawns and trees).

Out of the local fossil fuel emissions in the study area, 46% originate from the building sector, whereas 54% is from the transportation sector. 51% of all local fossil fuel emissions are of local origin, 49% are from through traffic.

It is worth stating that numbers listed in Table 3.5.1 include only local emissions due to local activities and local emissions due to external activities (see Figure 1.3.2). When incorporating external emissions due to local activities (electricity consumption, food production, waste), emissions will be higher (as discussed in Section 3.1).

Table 3.5.1: Comparison of the carbon emissions and uptake from all different components and integrated emissions (total) for the complete study area and the different sectors.

	All Sector (kg C m^{-2} $year^{-1}$)	NE (kg C m^{-2} $year^{-1}$)	SE (kg C m^{-2} $year^{-1}$)	SW (kg C m^{-2} $year^{-1}$)	NW (kg C m^{-2} $year^{-1}$)
	Emissions				
Buildings	2.47	2.56	2.41	2.78	2.13
Transportation	2.93	3.37	4.31	2.39	1.67
Human Metabolism, Food & Waste	0.49	0.54	0.46	0.59	0.37
Vegetation & Soils	0.33	0.28	0.34	0.29	0.42
	Uptake				
Vegetation & Soils	-0.49	-0.44	-0.46	-0.40	-0.65
	TOTAL				
	5.74	**6.31**	**7.07**	**5.64**	**3.93**

However as those emissions are not happening on the neighbourhood scale, and not measured on the tower, they have not been included in the maps.

On a spatial scale, for each raster element, all four components were summed and the integral emissions (or uptake) map is shown in Figure 3-5-2. It is evident from the map that arterial roads are emission 'hot spots', where, on a relatively small area, significant emissions are found. Other components (buildings, human metabolism, vegetation) are relatively uniformly distributed within the study area, with the exception of parks show dominating carbon uptake.

3.5.2 Integrated Per-capita Carbon Emissions

Per capita emissions from all sectors (buildings, transportation, human metabolism, vegetation / soil) are shown in Table 3.5.2. Those numbers have to be interpreted carefully, as total local emissions are not necessarily reflecting residential activities only and include through traffic and commercial activities. Further, they do not include activities of local residents outside the neighbourhood (see Sections 1.2 and 1.3 for a detailed discussion of the problem).

3.5.3 Neighbourhood Carbon Cycle

Figure 3.5.4 illustrates the integral carbon cycling (fluxes and pools) in the neighbourhood for a mass balance. Numbers denote carbon fluxes in kg C m^{-2} $year^{-1}$ or carbon pools in kg C m^{-2} (in italics). Fluxes leaving the neighbourhood system on top are local carbon emissions into the atmosphere minus uptake of atmospheric carbon (5.73 kg C m^{-2} $year^{-1}$, see Section 3.5.1). Those fluxes are detectable at the carbon flux tower (Section 3.6) as indicated by

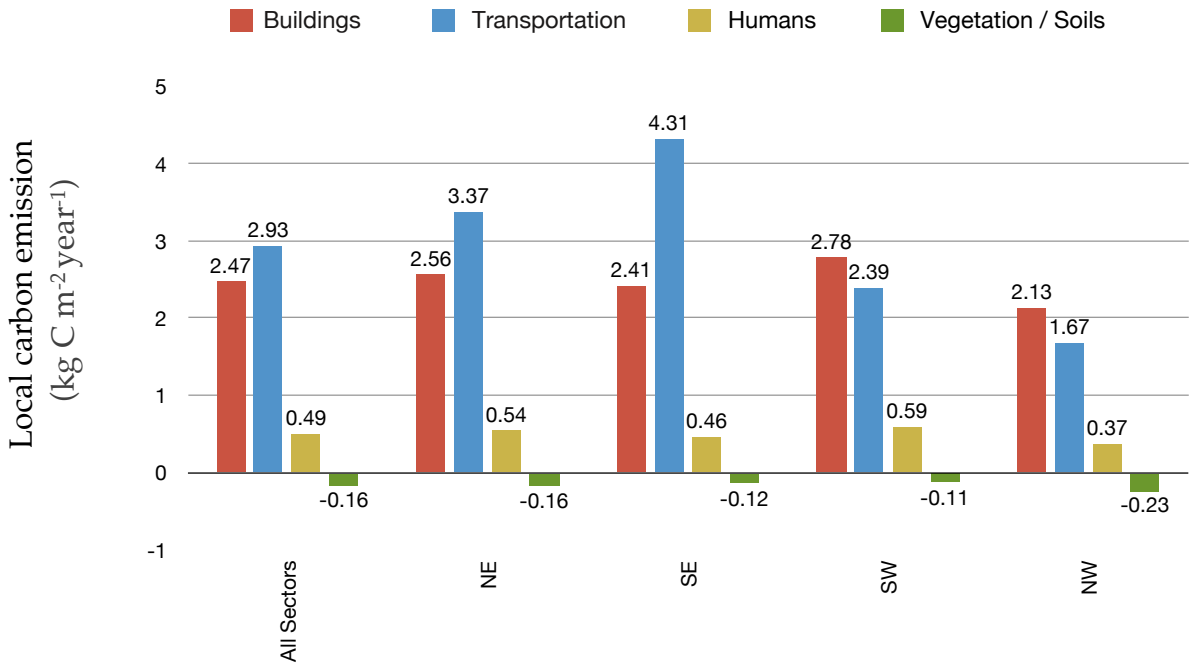

Figure 3.5.1: Comparison of the different emission components in the whole study area and for the different sectors. Vegetation shows the net-effect incorporating both, uptake and emissions.

the line 'tower measurements'. Fluxes entering the neighbourhood system on the left hand side of the diagram are lateral imports of carbon (6.69 kg C m^{-2} $year^{-1}$), and fluxes leaving the neighbourhood on the right hand side are lateral exports (0.87 kg C m^{-2} $year^{-1}$). Red and blue arrows are fossil fuel carbon while green, yellow are mostly renewable carbon. Grey arrows denote both, fossil fuel and renewable carbon.

Of all carbon that is imported laterally, 2.47 kg C m^{-2} $year^{-1}$ (37%) are imported in form of natural gas, 2.93 kg C m^{-2} $year^{-1}$ (44%) in form of gasoline or diesel (mostly through vehicles driving into the 'system'), 0.97 kg C m^{-2} $year^{-1}$ (15%) in form of food, and 0.22 kg C m^{-2} $year^{-1}$ (3%) in form of construction material, paper and plastic. Of all carbon entering the system, 83% is from fossil fuel sources, and 17% is renewable carbon.

Of all carbon that is exported laterally, 0.07 kg C m^{-2} $year^{-1}$ (8%) are exported in form of garden waste, 0.19 kg C m^{-2} $year^{-1}$ (22%) in form of human waste, 0.29 kg C m^{-2} $year^{-1}$ (33%) in form of food waste, and 0.32 kg C m^{-2} $year^{-1}$ (33%) in form of other waste (e.g. woodm plastic, paper). Most carbon leaving the system laterally is renewable carbon.

The system's mass balance of carbon (in kg C m^{-2} $year^{-1}$) can then be written as import minus exports (atmospheric net emissions plus lateral export):

$$6.69 - (5.73 + 0.87) = +0.09$$

Hence, the urban ecosystem in expected to accumulate +0.09 kg C m^{-2} $year^{-1}$ in tree and soil biomass. Table 3.5.3 shows the different carbon pools of (renewable) carbon in the study neighbourhood, the sequestration and calculated average turnover rates.

Table 3.5.2: Comparison of per-capita carbon emissions for the complete study area and the different sectors.

	All Sectors (kg C m^{-2} $year^{-1}$)	**NE (kg C m^{-2} $year^{-1}$)**	**SE (kg C m^{-2} $year^{-1}$)**	**SW (kg C m^{-2} $year^{-1}$)**	**NW (kg C m^{-2} $year^{-1}$)**
All Local Emissions	893	886	1162	735	821
Excluding through Traffic	485	462	527	459	510
Excluding Through Traffic but Including Building Related External Emissions	502	477	545	473	531

Table 3.5.3: Comparison of the different carbon pools of renewable carbon in the study neighbourhood and their sequestration and calculated average turnover rates.

	Human Body	**Lawn Biomass**	**Tree Biomass**	**Soils**	**Building Structures**
Total Carbon Stored in Pool (kg C m^{-2})	0.06	0.13	1.42	3.43	13.06
Current Sequestration Rate (kg C m^{-2} $year^{-1}$)	~0	~0	-0.09		~0
Turnover Rate	30 days	120 days	5 years	8 years	90 years

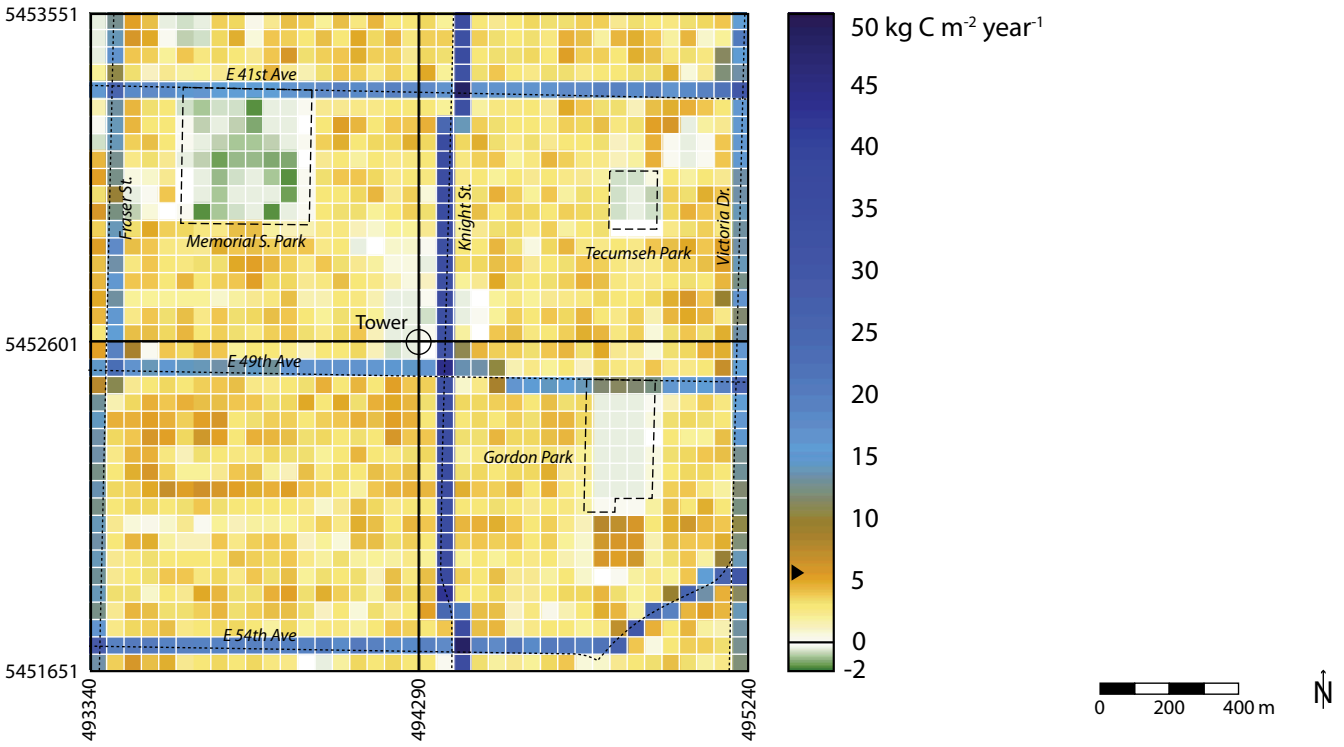

Figure 3.5.2: Map of integrated carbon emissions in the study area with 50 x 50 m resolution.

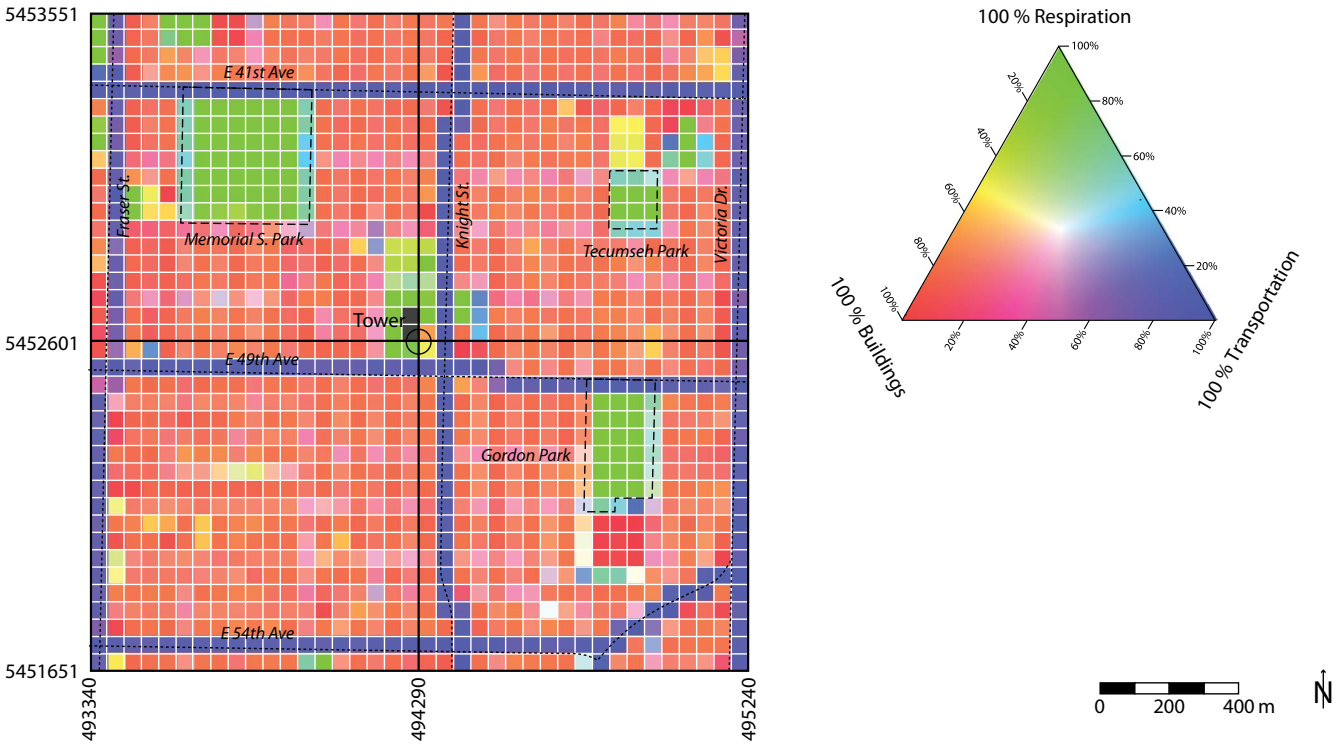

Figure 3.5.3: RGB composite map of relative contributions of local emission sources – buildings (red), transportation (blue) and respiration (green) to the total emissions from each raster cell. Raster cells drawn in black are cells with zero emissions.

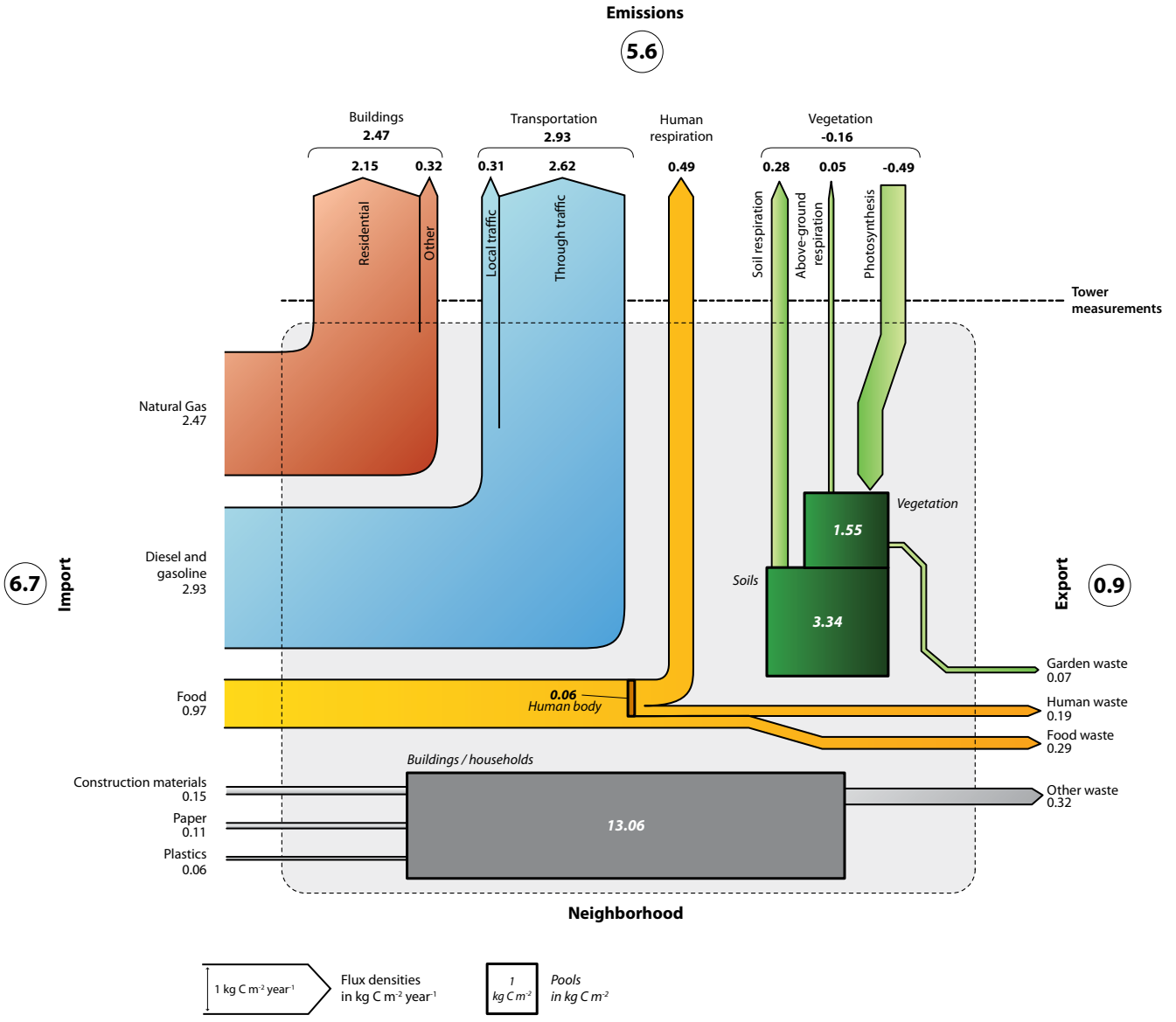

Figure 3.5.4: Integral modelled carbon cycle (fluxes and pools) in the study neighbourhood. Numbers denote carbon fluxes in kg C m^{-2} $year^{-1}$ or carbon pools in kg C m^{-2}. Fluxes leaving the neighbourhood system on top are local carbon emissions into the atmosphere and uptake of atmospheric carbon. Fluxes entering the neighbourhood system on the left hand side of the diagram are lateral imports of carbon, and fluxes leaving the neighbourhood on the right hand side are lateral exports.

3.6 Comparison of Current Model with Direct Carbon Flux Measurements and Consumption Inventoriess

This section presents the results from two years of direct flux measurement on the carbon flux tower. Spatial and temporal patterns in the measured emissions are discussed. Measurements are then compared to model results.

3.6.1 Direct carbon flux measurements – temporal and spatial dynamics

Monthly carbon (CO_2) fluxes were calculated from the continuous flux measurements on the carbon flux tower over two years from May 1, 2008 – April 30, 2010 according to the procedure described in Section 2.7.3.

Figure 3.6.1 and Table 3.6.1 summarize monthly average fluxes in g C m^{-2} day^{-1} for the average of both years. Largest emissions were recorded in the winter months when space-heating requirements are highest and CO_2 uptake from vegetation is minimal (maximum in December with 22.1 g C m^{-2} day^{-1}). During summer, increased CO_2 sequestration from vegetation is expected, as well as reduced motorized traffic load and no space heating, hence lowering overall measured emissions. The monthly minimum recorded was16.0 g C m^{-2} day^{-1} in August during school holidays. The annual average determined was 18.4 g C m^{-2} day^{-1} which corresponds to 6.71 kg C m^{-2} $year^{-1}$.

Measured fluxes were separated into four wind sectors (Table 3.6.1). Emissions over the SE sector are highest with an annual total of 13.16 kg C m^{-2} $year^{-1}$. This is attributable to emissions along two arterial roads (49th Ave. / Knight St.) that intersect just 130 m upwind of the instruments to the SE. Lowest emissions are measured over the NW sector where no arterial roads are encountered up to a 750m distance from the tower (2.81 kg C m^{-2} $year^{-1}$). It is also interesting to note that emissions measured over the NE sector (6.57 kg C m^{-2} $year^{-1}$) are higher than those from the SW sector (4.31 kg C m^{-2} $year^{-1}$), although both sectors contain a similar arrangement with one major arterial road. A comparable distribution of emissions was

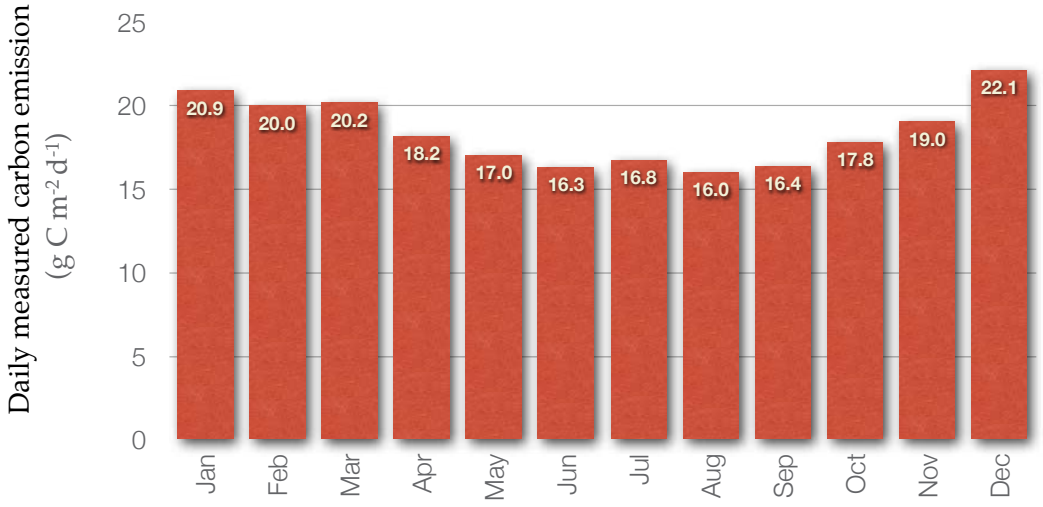

Figure 3.6.1: Monthly average emissions (g C m^{-2} day^{-1}) measured on the carbon flux tower for all wind directions (equally weighted).

Table 3.6.1: Monthly average emissions measured on the carbon flux tower. 'All Wind Sectors' results are equally weighted averages from the four wind sectors. Numbers highlighted in green are minima, highlighted in red are maxima.

Month	All Wind Sectors ($g\ C\ m^{-2}\ day^{-1}$)	NE (0-90⁰) ($g\ C\ m^{-2}\ day^{-1}$)	SE (90-180⁰) ($g\ C\ m^{-2}\ day^{-1}$)	SW (180-270⁰) ($g\ C\ m^{-2}\ day^{-1}$)	NW (270-360⁰) ($g\ C\ m^{-2}\ day^{-1}$)
January	20.90	18.81	37.41	14.58	12.78
February	20.00	20.32	36.42	13.78	9.48
March	20.18	19.67	37.13	14.47	9.44
April	18.19	16.50	38.37	11.20	6.67
May	17.01	18.37	35.52	9.50	4.65
June	16.30	16.81	36.66	7.66	4.07
July	16.76	16.98	35.76	10.05	4.25
August	16.00	14.03	36.27	9.42	4.28
September	16.36	16.48	33.94	9.87	5.14
October	17.83	18.38	34.42	11.55	6.96
November	19.04	19.03	34.05	13.21	9.89
December	22.14	20.68	36.86	16.35	14.70
Total ($kg\ C\ m^{-2}\ year^{-1}$)	**6.71**	**6.57**	**13.16**	**4.31**	**2.81**

Table 3.6.2: Measured weekday and weekend emissions from the SE sector by month.

Month	Weekdays ($g\ C\ m^{-2}\ day^{-1}$)	Weekends ($g\ C\ m^{-2}\ day^{-1}$)	Difference Weekdays-Weekend ($g\ C\ m^{-2}\ day^{-1}$)	Difference Weekday -Weekend (%)
January	39.60	33.61	5.99	15%
February	40.11	31.90	8.21	20%
March	39.17	28.57	10.6	27%
April	40.05	29.76	10.29	26%
May	38.20	28.26	9.94	26%
June	39.52	27.50	12.02	30%
July	38.69	27.23	11.46	30%
August	39.21	29.04	10.17	26%
September	35.79	26.20	9.59	27%
October	36.98	28.63	8.35	23%
November	38.49	26.35	12.14	32%
December	37.76	36.02	1.74	5%
Total	**38.63**	**29.42**	**9.21**	**24%**

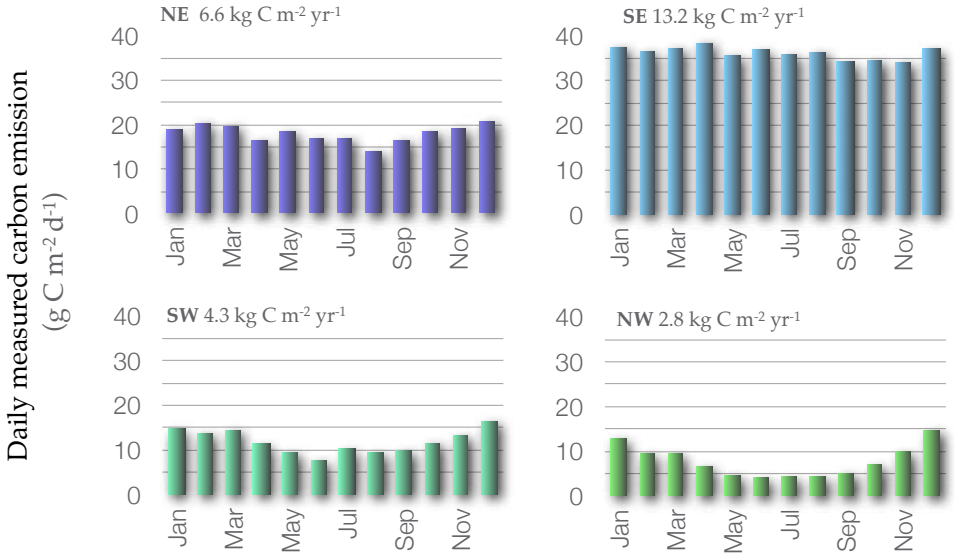

Figure 3.6.2: Visualization of the monthly average emissions (in g C m^{-2} yr^{-1}) measured from the carbon flux tower for each wind sector separately.

measured by Walsh (2005), who compiled carbon flux measurements on the same tower for the year 2001 using independent instrumentation and data processing procedures. She reported highest emissions from SE (9.64 kg C m^{-2} $year^{-1}$) and lowest emissions from NW (2.42 kg C m^{-2} $year^{-1}$).

When stratifying emission measurements into weekends and weekdays (Section 2.7.3), emissions were found always to be lower on weekends for all wind sectors and months, with greatest differences observed for the SE sector (23.8 % weekend reduction, see Tables 3.6.2 and 3.6.4).
Figure 3.6.3 illustrates the potential of using carbon flux measurements to help in understanding and quantifying the urban metabolism even over a daily cycle. Shown are hourly values for four selected months (March, June, September and December) and for all four sectors in mg C m^{-2} s^{-1}. Measured carbon emissions show significant differences between nighttime and daytime. Emissions in all sectors converge to low background values during early morning hours, when traffic is minimal, but show considerable variation during daytime. Interesting is that select hours in the NW sector around noon in June indicate negative values, i.e. demonstrate that uptake of carbon by photosynthesis is the dominant effect in this special case.

3.6.2 Modelled Values vs. Carbon Flux Measurements.

Tables 3.6.3 to 3.6.5 compare carbon fluxes measured on the tower to model results from Section 3.1 to 3.5. The model results used for the comparison are aggregated in two different ways. In a simple approach (*'Radius aggregation'*) all grid cells of the 50m raster that fall within a 400 m radius around the tower are considered and averaged (equally weighted). Those values are then compared to the tower measurements. A 400 m radius was chosen because this corresponds the 50% source area (i.e. more than half of the signal measured at the tower comes from this area, and

the remainder comes from a larger upwind area).

In a more sophisticated aggregation approach, called '*Source-area aggregation*', model values are weighted by the turbulent source area using a detailed backward dispresion model, which is described in Section 2.7.3. Source areas were calculted for each 30 min step, and summed using the same process by which fluxes were aggregated (i.e. for each hour of the day and each month of the year). In this approach, modelled emissions on the 50 x 50 m grid were weighted by the spatial source -area distribution. A small fraction of the flux (12%) is predicted to originate outside the 1900 x 1900 study area. This fraction was assumed to represent the average emission within the entire study area, assuming that the urban form continues in a similar pattern outisde the study area.

For the average of all emissions within a 400-m-radius buffer around the tower, the model results agree very well with the measurements, i.e. 6.71 kg C m^{-2} $year^{-1}$ measured vs. 6.25 kg C m^{-2} $year^{-1}$ modelled. The model slightly underestimates actual emissions by 0.25 kg C m^{-2} $year^{-1}$ (or 4%). With the actual errors associated with the uncertainty of the 400 m buffer source area, this is a surprisingly successful result. The model results are split up into different components in Table 3.6.4.

The different wind sectors within the 400-m-radius buffer show higher differences, in particular the SE-sector, where measurements are significantly higher (13.16 kg C m^{-2} $year^{-1}$) than modelled values

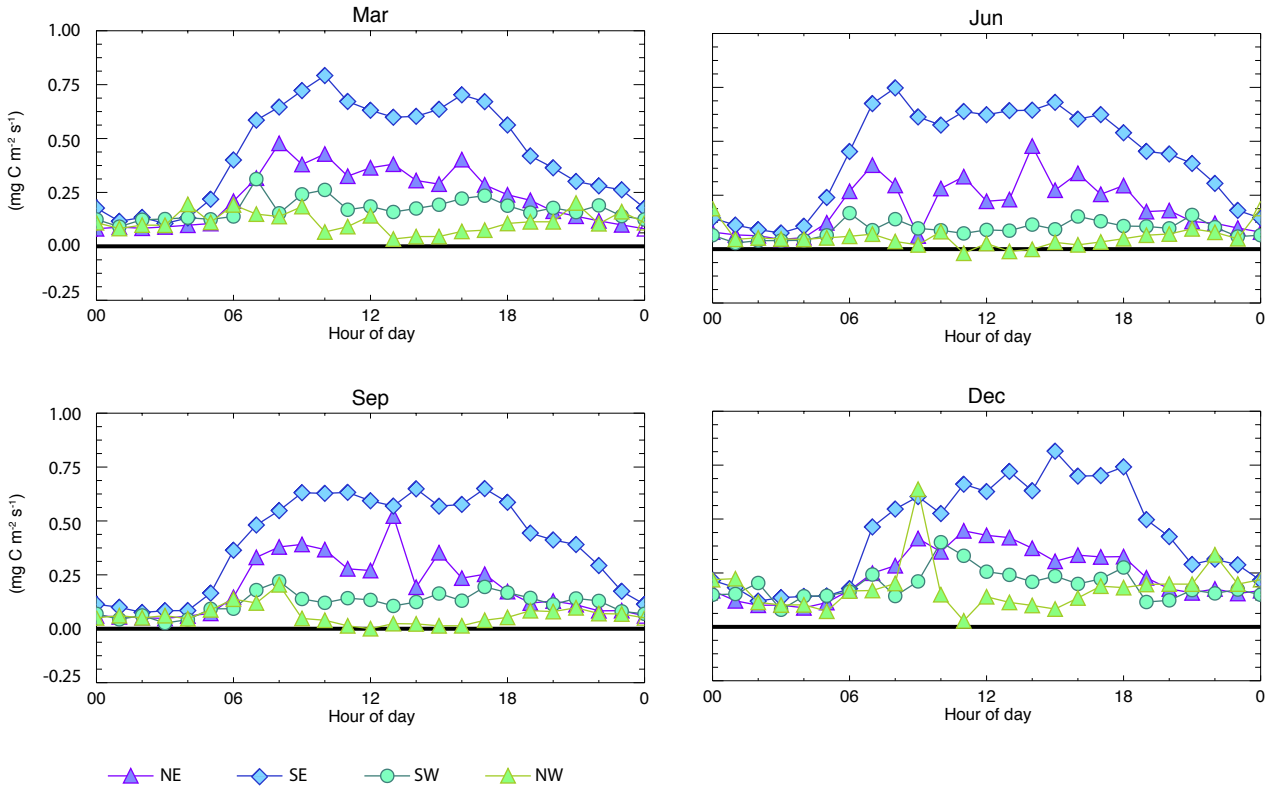

Figure 3.6.3: Daily courses of measured emissions on the carbon flux tower.

(10.17 kg C m^{-2} $year^{-1}$). This might be an over-proportional contribution of traffic-related emissions from the near-field (intersection 49th Ave. / Knight St. with traffic lights) where both idling and moving vehicles are injecting carbon, but which is not accounted for in the model. In turn, in the two sectors that show arterial road segments without intersections (NE and SW), the model overestimates emissions. Improving the transportation model and incorporating speed of vehicles in each cell could resolve some of those inaccuracies.

3.6.3 Source-area Aggregation

The source area aggregation is more meaningful than the 400-m-radius buffer method because a significant portion of the measured emissions originate beyond the 400 m boundary. The source areas are based on standard dispersion theory (see Figure 3.6.4) and blend-off to represent the diminishing contributions of far-field areas rather than abruptly and unreaslistically cut-off at 400 m. The source-area aggregated model results are 7.46 kg C m^{-2} $year^{-1}$ (11% higher than the measured 6.71 kg C m^{-2} $year^{-1}$). Figure 3.6.1a illustrates that the source area model combined with the emission model suggests that approximately 70% of all fluxes that were measured at the tower (5.22 kg C m^{-2} $year^{-1}$) originate from transportation (restricted to a narrow part of Knight and 49th Avenue). 27% (2.05 kg C m^{-2} $year^{-1}$) originate from buildings, 5% from human respiration and -2% (-0.17 kg C m^{-2} $year^{-1}$) is offset by vegetation. Although in the entire study area, emissions from buildings and transportation are of approximately equal strength

Table 3.6.3: Comparison of modelled and measured carbon emissions for a 400-m-radius buffer around the tower

	All Sector	NE	SE	SW	NW
Carbon flux Density Measured (kg C m^{-2} $year^{-1}$)	6.71	6.57	13.16	4.31	2.81
Carbon Flux Density Modelled (kg C m^{-2} $year^{-1}$) and aggregated for a 400-m-radius buffer	6.46	7.62	10.17	5.81	2.27
Difference modelled (kg C m^{-2} $year^{-1}$)	0.25	1.05	2.99	1.50	0.54
Difference Percentage	4%	16%	23%	35%	19%

Table 3.6.4: Modelled carbon emissions for a 400m buffer around the tower. The total is compared in Table 3.6.3 against tower flux data.

	All Sectors (kg C m^{-2} $year^{-1}$)	NE (kg C m^{-2} $year^{-1}$)	SE (kg C m^{-2} $year^{-1}$)	SW (kg C m^{-2} $year^{-1}$)	NW (kg C m^{-2} $year^{-1}$)
Buildings	2.40	2.06	2.67	3.03	1.82
Transportation	3.76	5.29	7.13	2.31	0.35
Human Metabolism, Food & Waste	0.47	0.45	0.51	0.61	0.29
Vegetation & Soils	-0.16	-0.18	-0.14	-0.15	-0.19
TOTAL	**6.46**	**7.62**	**10.17**	**5.81**	**2.27**

(40% and 47% of all emissions respectively), the specific location of the tower close to an intersection makes the signal from transportation in the tower signal more relevant. Interestingly, the sector where transportation is small (NW) shows the best agreement between tower and model (2.81 kg C m^{-2} $year^{-1}$ measured vs. 2.87 kg C m^{-2} $year^{-1}$ modelled).

In summary, agreement between measured and model fluxes (in both aggregation approaches) is a very positive outcome and the use of direct carbon flux measurements is shown to be a promising method to validate fine-scale emission inventories / models. Tower measurements can be also used to identify model components that require improvement, in this case the transportation model.

Figure 3.6.4: (a) Long-term integrated turbulent source area and (b) relative CO_2 flux contribution (Product of Figure 3.6.2 and 3.6.4a).

Earlier, annual measured weekend in net emissions were demonstrated to be 24% less than weekday emissions in the SE area (Table 3.6.2). Next, we determine the weekend-weekday difference for the transportation emissions component only. Table 3.6.6 compares the observed emission reduction weekday – weekend in three of four sectors to the modelled transportation sector emissions. The relative emission reduction on weekends (measured, but expressed as fraction of the modelled carbon flux from the transportation sector) is estimated 42%. This suggests that weekend traffic emits 42% less than weekday traffic in the study area.

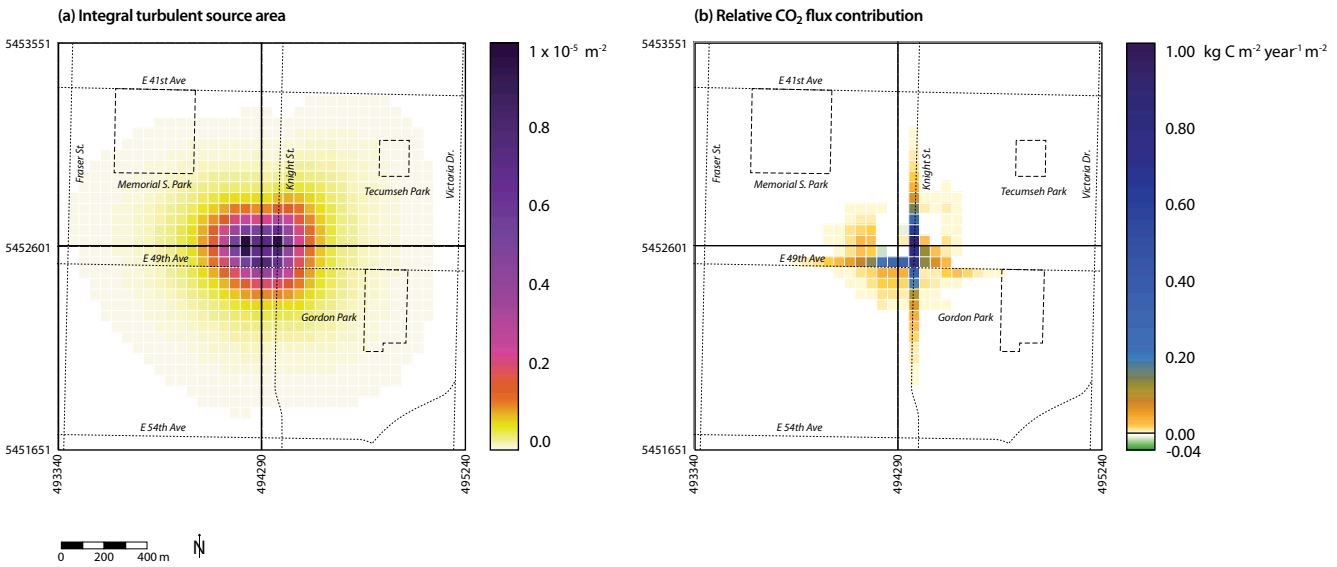

Figure 3.6.4: (a) Long-term integrated turbulent source areas and (b) relative CO2 flux contribution (Product of Figure 3.6.2 and 3.6.4a).

Table 3.6.5: Comparison of modelled and measured carbon emissions weighted by the long-term turbulent source area of the tower.

	All sectors
Carbon Flux Density Measured (kg C m^{-2} day^{-1})	6.71
Carbon Flux Density Modelled (kg C m^{-2} day^{-1}) and Aggregated by the Long-term Source Area	7.46
Difference Measured - Modelled (kg C m^{-2} day^{-1})	**0.75**
Difference (%)	**11**

Table 3.6.6: Comparison of measured carbon emission reduction on weekends to the modelled transportation sector emissions for a 400-m-radius buffer around the tower. Not enough measurements on weekends with wind from NW were available to estimate the reduction in the NW sector.

	Sectors NE, SE, & SW	**NE**	**SE**	**SW**	**NW**
Modelled Flux Density from Transportation (g C m^{-2} day^{-1})	13.15	14.1	19.1	6.2	1.1
Measured Difference Between Weekday-Weekend (g C m^{-2} day^{-1})	5.71	7.31	9.79	5.59	n/a
Percentage of Measured Weekend Reduction to Total Modelled Transportation Flux (%)	**42%**	**38%**	**48%**	**40%**	**n/a**

References:

Churkina, G. (2010). Carbon stored in human settlements: the conterminous United States. *Global Change Biology, 16*(1), 135-143.

Harvey, L. (2009). Reducing energy use in the building sector: measures, costs, and examples. *Energy Efficiency, 2* (2), 139-163.

Golubiewski, N. E. (2006). Urbanization increases grassland carbon pools: Effects of landscaping in Colorado's front range. *Ecological Applications, 16*(2), 555-571.

Krishnan, P., Black, T. A., Jassal, R.S., Chen, B., & Nesic, Z. (2009). Interannual variability of the carbon balance of three different-aged Douglas -fir stands in the Pacific Northwest. *Journal of Geographysical Research* (114), G04011.

Liss, K., Crawford, B., Jassal, R., Siemens, C., & Christen, A. (2009). Soil respiration in suburban lawns and its response to varying management and irrigation regimes. *Proc. of the AMS Eighth Conference on the Urban Environment*, Phoenix, AZ, January 11-15, 2009.

Moriwaki, R., & Kanda, M. (2004). Seasonal and diurnal fluxes of radiation, heat, water vapor, and carbon dioxide over a suburban area. *Journal of Applied Meteorology 43*, 1700-1710.

Matese A., Gioli B., Vaccari F. P., Zaldei A., Miglietta F. (2009). Carbon Dioxide Emissions of the City Center of Firenze, Italy: Measurement, Evaluation, and Source Partitioning. *Journal of Applied Meteorology and Climatology, 48*(9), 1940-1947

Natural Resources Canada (2009). C*ommunities | Urban Archetypes Project*. Retreived in June 20, 2010 from http://canmetenergy-canmetenergie.nrcan-rncan.gc.ca/eng/buildings_communities/communities/urban_archetypes_project.html

Nowak, D. J., & Crane, D. E., (2002). Carbon storage and sequestration by urban trees in the USA. *Environmental Pollution, 116*, 381-389.

Pouyat, R., Groffman, P., Yesilonis, I., L., & Hernandez, L. (2002). Soil carbon pools and fluxes in urban ecosystems. *Environmental Pollution, 116*, S107-S118

Walsh, C. J. (2005). Fluxes of radiation, energy, and carbon dioxide over a suburban area of Vancouver, BC. *M.Sc. Thesis, Department of Geography, University of British Columbia.*

4.1 Carbon Emissions Scenarios

Four carbon reduction scenarios are extrapolated from measured results reported at the May 27 workshop. Their purpose is to be heuristic and illustrative — to demonstrate the potential and limitations attributable to uniformly applied change in the study area and estimate the associated carbon reduction potential. To simplify and validate these illustrations with data collected, we consider only a narrow definition of local emissions — those attributable to local sources emitted in the study area. No attempt is made to estimate non-local origin emissions of local origin emissions outside the study area.

To streamline modeling, each scenario is built and modeled incrementally — subsequent scenarios build off the results of prior scenarios. We will not iterate or model from base assumptions. Results are reported at total carbon per year and total carbon per capita year in the study area. This latter category is crucial as population and jobs must increase and compact in the study area to realize improvement in both building and transportation sectors. An illustration of scenario decisions and numbers reported can be seen in figure 4.1.1.

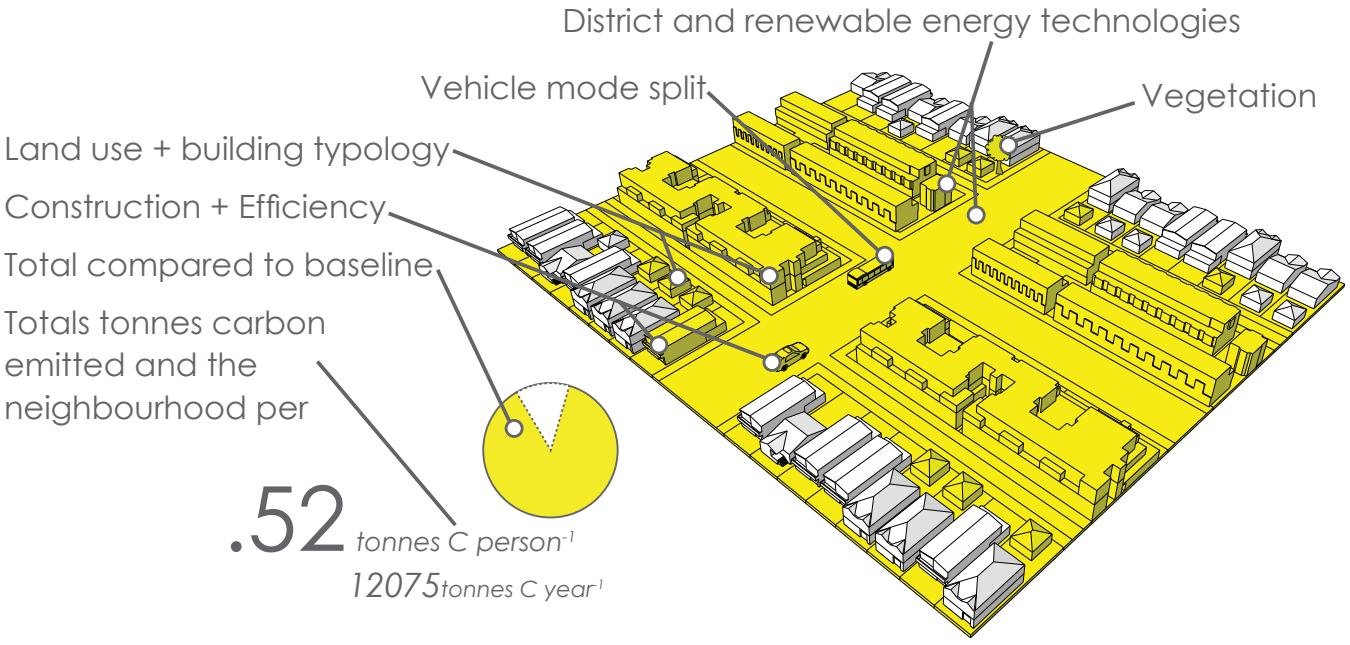

Figure 4.1.1: Schematic of carbon reduction scenario decisions

Baseline

.52 *tonnes C person*$^{-1}$

12119 tonnes C year^{-1}

64 people hectare $^{-1}$

14 jobs hectare $^{-1}$

Scenario 1: Modified Baseline

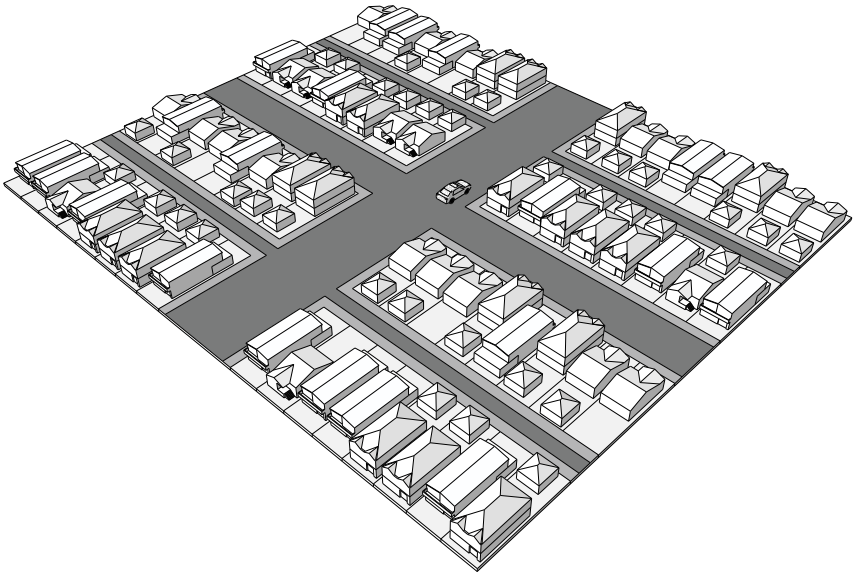

Buildings	
Local Carbon	8715
External Carbon	420
Total tonnes Carbon	**9135**
Transportation	
Total tonnes Carbon	**1542**
Human metabolism	
Total tonnes Carbon	**1767**
Vegetation and Soils	
Total tonnes Carbon	**-325**

Table 4.1.1 Modelled carbon emissions SC3 (i.e. t C year^{-1})

4.1.1 Scenario 1: Modified Baseline

The first scenario interpolates local origin / local emission results from those previously reported. Only transportation emissions are modified from the baseline reported in previous sections. The changes to transportation illustrate only transit and local origin light vehicle trips. The modified baseline provides the framework for subsequent scenarios to be measured against.

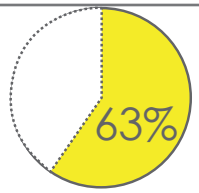

.33 tonnes C person^{-1}

7624 tonnes C year^{-1}

64 people hectare $^{-1}$

14 jobs hectare $^{-1}$

Scenario 2: Optimize Sunset

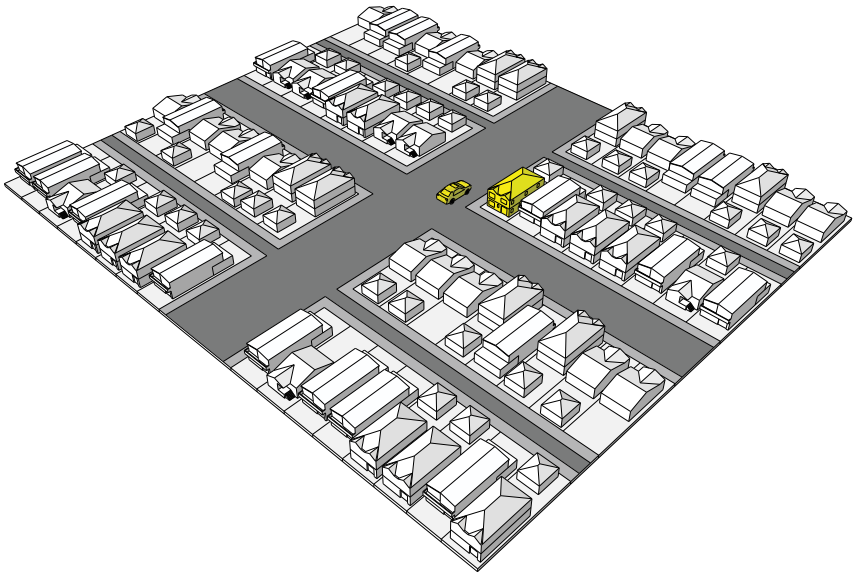

Buildings	
Local Carbon	4826
External Carbon	312
Total tonnes Carbon	**5138**
Transportation	
Total tonnes Carbon	**1044**
Human metabolism	
Total tonnes Carbon	**1767**
Vegetation and Soils	
Total tonnes Carbon	**-325**

Table 4.1.2 Modelled carbon emissions SC3 (i.e. t C year^{-1})

4.1.2 Scenario 2: Optimize Sunset

The second scenario 'Optomize Sunset' illustrates best possible energy performance from current policy and regulatory standards — without spatial change to the study area. This scenario illustrates the effect of elevating all existing buildings to best practice envelope and space conditioning systems standards and elevating the engine fuel efficiency of the local origin passenger and transit vehicle fleet to best 2008 practice.

In order to estimate the potential for carbon reduction through building retrofits, a collection of upgrades were developed for each archetype. These collections were sensitive to building construction, age and land use. Once an upgrade package was developed for each archetype, simulations were run in HOT2000 for ground oriented residential typologies and NRCan Screening tool for all other typologies. The upgrades that were assumed possible are extensive and therefore may at times not make economic sense. However, the purpose of the 'Optimize Sunset' scenario is to illustrate the potential for retrofitting the existing building stock without changing urban form or land use mix. The upgrades follow prescriptive retrofits outlined in CMHC (2007), Detail Practice (2008), Building Insight (2008) and the R-200 standard.

Scenario highlights in addition to those reported in MODIFIED BASELINE:

Change to Building sector

Efficiency:

- Envelope construction: Extensive retrofit of existing buildings following the R-2000 and Greening the BC building code standards. Upgrades were vintage sensitive and improved upon assumed CMHC Building code standards (CMHC, 2005). Included in many of the upgrades were wall, roof, and foundation insulation along with improved air change values (assumed to be more difficult in older dwellings) and CSA energySTAR windows.
- Space conditioning and Domestic Hot Water (system and efficiency): Systems in older dwelling were replaced with newer, more efficient models and hot water tanks was insulated.

Demand:

- Lighting and appliances: Decreased lighting load based on predicted CFL share found in Survey for Household Energy use, 2007.

Source:

- Fuel share: No change

Typology:

- Population: No change
- Jobs: No change
- Archetypes: No change

Change to Transportation sector

Efficiency:

- Average transit and light passenger vehicle fuel efficiency increased

Demand:

- No change

Source:

- No change

Change to Vegetation and Soils

- Green roofs: No change
- Ground vegetation: No change
- Trees: No change

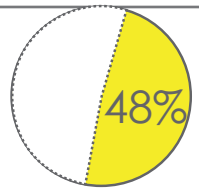

.26 *tonnes C person*$^{-1}$

11309 tonnes C year^{-1}

123 people hectare $^{-1}$

34 jobs hectare $^{-1}$

Scenario 3: Transit Oriented Sunset

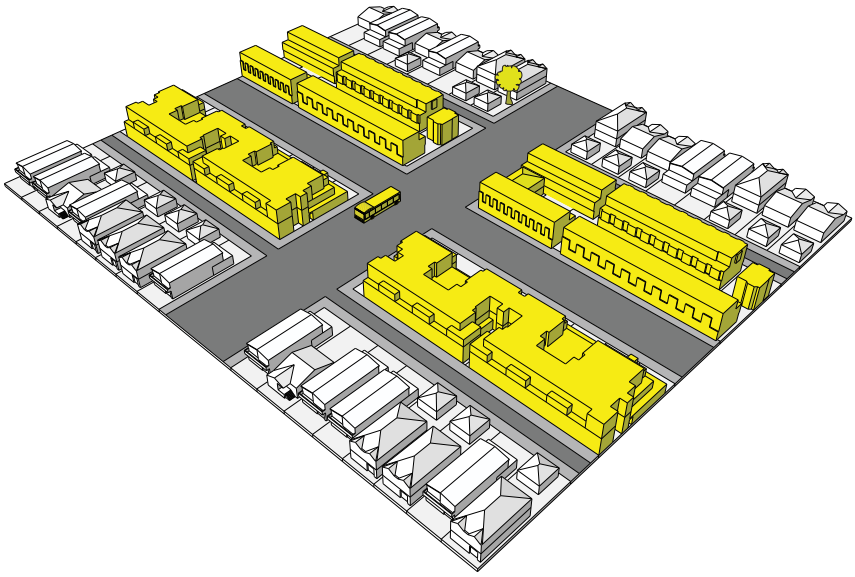

Buildings	
Local Carbon	5903
External Carbon	572
Total tonnes Carbon	**6475**
Transportation	
Total tonnes Carbon	**1928**
Human metabolism	
Total tonnes Carbon	**3386**
Vegetation and Soils	
Total tonnes Carbon	**-480**

Table 4.1.3 Modelled carbon emissions SC3

4.1.3 Scenario 3: Transit Oriented Sunset

The third scenario illustrates the opportunity of future 'Smart Growth' and transit-oriented growth in the study area. Population and job growth are based on a pro-rata share of the anticipated Metro future growth estimated in the Sustainability By Design project (SxD). The growth pattern of this scenario concentrates along corridors and in nodes in compact energy efficient building types. Energy intensity and the subsequent carbon emissions for new development are borrowed from Scenario 2. The net loss of ground vegetation due to greater development density has been offset by more intensive green roof and tree planting. Infill suites and lane houses take place in single family areas outside of the development corridor and no net change to impervious ground cover is assumed. Transportation is based on favorable transit-oriented and walkable neighbourhood mode splits (again SxD provides guidance here) and a technology based engine fuel efficiency performance improvement — the California 2020 standard, for example.

Scenario highlights in addition to those reported in MODIFIED BASELINE:

Change to Building sector

Efficiency:

- Envelope construction: Same standard applied as in Scenario2: Optimize Sunset.
- Space conditioning and Domestic Hot Water (system and efficiency): Same standard applied as in Scenario2: Optimize Sunset.

Demand:

- Lighting and appliances: Same standard applied as in Scenario2: Optimize Sunset.

Source:

- Fuel share: No change

Typology:

- Population: The number of people was increased by a factor of 1.9 following the sustainable by design predictions for the neighborhood (find source...).
- Jobs: The number of jobs was increases by a factor of two following the sustainable by design guidelines for the neighbourhood (find source...). Baseline employment was assumed to follow 13.7 jobs hectare-1 suggested by SXD.
- Archetypes: The population and job growth was accommodated for in new four storey mixed use buildings (40%), row houses (35%), and mid rise residential (25%). The new development was restricted to parcels bordering transit corridors (Fraser, Knight, Victoria, E. 41st, E. 49th, and E. 57th). Additional population was accommodated for by laneway housing infill in existing single family residential areas.

Change to Transportation sector

Efficiency:

- Average transit and light passenger vehicle fuel efficiency increased

Demand:

- Mode split adjusted to reflect a doubling of transit and pedestrians / cycling share (site Calgary source...) and subsequent reduction in private automobiles (approximately 1/3 share each).

Source:

- No change

Change to Vegetation and Soils

- Green roofs: 5% of buildings assumed to be built with green roofs.
- Ground vegetation: Ground vegetation decreased as a result of new development (decrease from 24.2% plan area down to 22.2%). Areas covered by semi-permeable driveways was increased from 0% to 2% of plan area.
- Trees: An increase in areas covered by trees was assumed (increase from 10.6% to 15%).

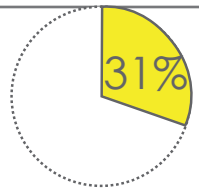

.16 *tonnes C person*$^{-1}$

7076 tonnes C year^{-1}

123 people hectare $^{-1}$

34 jobs hectare $^{-1}$

Scenario 4: Low Carbon Sunset

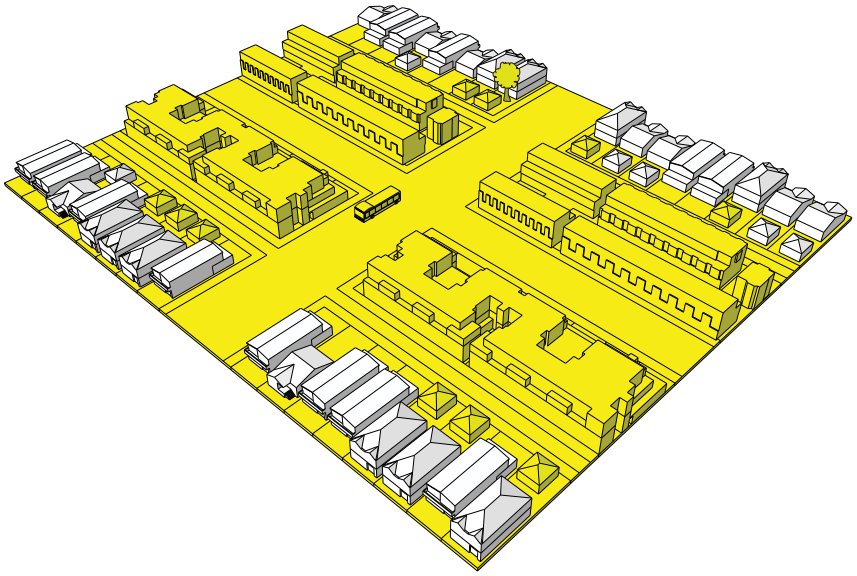

Buildings	
Local Carbon	2789
External Carbon	572
Total tonnes Carbon	**3361**
Transportation	
Total tonnes Carbon	**964**
Human metabolism	
Total tonnes Carbon	**3386**
Vegetation and Soils	
Total tonnes Carbon	**-635**

Table 4.1.4 Modelled carbon emissions SC3

4.1.4 Scenario 4: Low Carbon Sunset

The fourth scenario LOW CARBON SUNSET adds the best known technical innovations and improvements to the population and job intensification, spatial pattern and building types of TOD SUNSET. For example, this scenario includes carbon neutral transit, aggressive adoption of electrically powered private vehicles, and district energy systems. All new development along the corridors (i.e 100% saturation of district energy, similar to that assumed by Miller and Cavens, 2008) found in the TOD Sunset scenario is connected to a district energy system, such as a biomass plant or solar hot water distribution system. The district energy is assumed to accommodate all new space heating and domestic hot water loads through carbon neutral means (e.g. BC Assessment guides suggested GHG factors).

Scenario highlights in addition to those reported in MODIFIED BASELINE:

Change to Building sector

Efficiency:

- Envelope construction: Same standard applied as in Scenario2: Optimize Sunset.
- Space conditioning and Domestic Hot Water (system and efficiency): Same standard applied as in Scenario2: Optimize Sunset.

Demand:

- Lighting and appliances: Same standard applied as in Scenario2: Optimize Sunset.

Source:

- Fuel share: It is assumed possible to provide 100% of space heating and domestic hot water loads by district energy biomass, sewer heat recovery or solar thermal in the new development along the corridor (Miller and Cavens, 2008).

Typology:

- Population: Same as in Scenario 3: Transit Oriented Sunset.
- Jobs: Same as in Scenario 3: Transit Oriented Sunset.
- Archetypes: Same as in Scenario 3: Transit Oriented Sunset.

Change to Transportation sector

Efficiency:

- Same as in Scenario 3: Transit Oriented Sunset.

Demand:

- Same as in Scenario 3: Transit Oriented Sunset.

Source:

- All transit is assumed to be carbon neutral (electric powered for example).
- Light passenger vehicle fleet is assumed to be 50% electric powered.

Change to Vegetation and Soils

- Green roofs: 20% of buildings assumed to be built with green roofs.
- Ground vegetation: Ground vegetation decreased as a result of new development (decrease from 24.2% plan area down to 22.2%). Areas covered by semi-permeable driveways was increased from 0% to 5% of plan area.
- Trees: An increase in areas covered by trees was assumed (increase from 10.6% to 20%).

Table 4.1.5 Scenario attributes summary table

	Scenario	Mod. Baseline	Opt. Sunset	TOD Sunset	Low Carbon
Building	**Energy efficiency**				
	Envelope standard	/	R-2000 + BCBC	R-2000 + BCBC	R-2000 + BCBC
	Space conditioning + DHW standard	/	R-2000 + BCBC	R-2000 + BCBC	R-2000 + BCBC
	Energy demand				
	Lighting and appliance upgrade	/	lighting load	Lighting load	Lighting load
	Residential floor area (m^2)	923512	923512	1660787	1660787
	Other floor area (m^2)	198708	198708	366162	366162
	Energy source				
	District Energy System	/	/	/	Yes
	Local tonnes carbon (NG)	8715	4826	5903	2789
	External tonnes carbon (Elec)	420	312	572	572
	Building Emissions (tonnes)	**9135**	**5138**	**6475**	**3361**
Transportation	**Energy efficiency**				
	Private vehicles (L/100km)	12.0 (G)	8.6 (G)	6.7 (G)	3.4 (G)
	Transit (L/100km)	39.0 (D)	28.0 (D)	21.7 (D)	10.9 (D)
	Energy demand				
	Total private automobile trips / day	42050	38922	51666	51666
	Total transit trips / day	7506	8688	51666	51666
	Total cycling or pedestrian trips / day	8201	8688	51666	51666
	Energy source				
	Gasoline (G) litres (L)	1749697	1160681	1198536	600164
	Diesel (D) litres (L)	518779	372457	1512547	756274
	Carbon-neutral Fuel	0	0	0	50%
	Transportation Emissions	**1542**	**1044**	**1928**	**964**
Human	Population	23,135	23,135	44352	44352
	People $hectare^{-1}$	64	64	123	123
	Jobs	4938	4903	12363	12363
	Jobs $hectare^{-1}$	14	14	34	34
	Human Metabolism Emissions	**1769**	**1769**	**3386**	**3386**
Vegetation	Plan area covered by buildings	21.0%	21.0%	25.3%	25.3%
	Plan area covered by ground vegetation	24.2%	24.2%	22.2%	22.2%
	Plan area covered by trees	10.6%	10.6%	15.0%	20.0%
	Plan area with semi-permeable driveways	0.0%	0.0%	2.0%	5.0%
	Fraction of building plan area with green roofs	0.0%	0.0%	5.0%	20.0%
	Vegetation + Soils Emissions	**-325**	**-325**	**-480**	**-635**

4.2 Scenario Discussion

With British Columbia's Bill 27 carbon emissions reduction targets of 33% reduction from 2007 levels by 2020 and 80% by 2050 as context, the four scenarios offer one illustration of the potential building and urban form implications of those targets, albeit a spatially constrained and primarily local (with the exception of off-site hydroelectricity emissions) one. Not considered, for example, are the significant fuel energy implications of travel to and from the study area that are influenced by regional land use, employment and transportation policy and infrastructure or fundamental change in human behaviour with respect to travel choices and energy use. Neither were food- nor waste-related energy and carbon fully considered in the baseline.

Using the Modified Baseline scenario as a proxy for 2007 local origin emissions, on a per capita basis, the 2020 (33%) goal could be slightly exceeded (37% less than 2007 baseline) by the technology-based, fuel efficiency improvements of the Optimize Sunset scenario. In this scenario, the greatest reduction (56% of sector baseline) is attributable to whole neighbourhood upgrades to best practice envelope and space conditioning standards in the building sector and a lesser, but still significant reduction (67% of sector baseline) attributable to whole neighbourhood upgrades of all passenger and transit vehicles to best practice fuel efficiency standards in the transportation sector.

Reductions greater than those achieved in the Optimize Sunset scenario would not be achievable without change to the form and structure of the study area and / or introduction of high performance energy supply and conservation technologies not yet commercially viable or available at this time. TOD Sunset Scenario, for example, uses urban form strategies — higher density and greater land use mix — to reduce passenger vehicle trip demand in the transportation sector and thermal energy demand in the building sector. To achieve that densification this scenario approximately doubles the population and jobs in the study area and, in so doing, increases total energy consumption and carbon emissions in the study area. However, because population and job growth concentrates in more efficient buildings in close proximity to transit routes, building energy efficiencies and economies along increased transit ridership reduces per capita carbon emissions to 52% less than the 2007 baseline — about halfway between the 2020 and 2050 targets.

The Low Carbon Scenario illustrates that approximately 17% of the remaining 28% per capita carbon emissions gap could come from advance energy source and conservation technologies such as high performance fuel efficient infrastructure, buildings and vehicles and low carbon fuels in combination with the urban form based strategies of TOD Sunset Scenario. Widely applied vegetation changes, such as the greening of roof surfaces, while desirable from stormwater and hydrologic points of view, yield very minor direct improvement to study area carbon sequestration. However, other indirect effects of urban vegetation such as reduction in space conditioning loads attributable to shading and sheltering would likely yield energy demand reduction benefits not measurable within the scope of this study. The

remaining 11% gap to an 80% carbon emissions reduction has not been accounted but potentially achieveable with greater urban form or behaviour change or higher performance technologies than those anticipated and illustrated by these scenarios.

References:

Builder Insight (2008). *Greening the BC Building Code : First Steps.* Retrieved on June, 2010 from: http://www.hpo.bc.ca/PDF/BuilderInsight/BI5.pdf

Canadian Home Builders' Association (2010). *R-2000 Building Performance Based Standard*. Retreived on June, 2010 from: http://r2000.chba.ca/What_is_R2000/R2000_standard.php

Canadian Mortgage and Housing Corporation CMHC (2007). Canadian Wood Frame Housing Construction. *CMHC, 1967*, revised 2007.

Miller, N., Cavens, D. (2008). City of North Vancouver 100 Year Sustainability Vision: GHG Measurement and Mapping. *Prepared for the Ministry of Environment CEEI Working group.*

Province of British Columbia (2008). B*C GHG Emissions Assessment Guide*. Retreived on June 20, 2010 from http://www.townsfortomorrow.gov.bc.ca/docs/ghg_assessment_guidebook_feb_2008.pdf

Richarz, C., Schulz, C., Zeitler, F., (2007). Energy-Efficiency Upgrades. *Detail Practice books.* Birkhauser

Principal funding for this project has been provided by CanmetENERGY, Natural Resources Canada, Ottawa. Jessica Webster, project manager.

The Canadian Foundation for Climate and Atmospheric Sciences (CFCAS) funded the acquisition and processing of the LiDAR data as well as the two-year measurements on the carbon flux tower. This was funded as part of the CFCAS network "Environmental Prediction in Canadian Cities (EPiCC)". Selected research infrastructure on the tower was supported by NSERC RTI (Christen, #344541-0) and CFI / BCKDF (Christen). We acknowledge the support of BC Hydro, the City of Vancouver, Environment Canada and Terasen Gas for providing additional data and to BC Hydro for their in-kind support (tower access) in the Mainwaring substation.

We further acknowledge the significant technical support of staff at the University of British Columbia including (in alphabetical order): Jonathan Bau, Kate Liss, Rick Ketler, Zoran Nesic, Julie Ranada, Chad Siemens.

Andreas Christen, Assistant Professor of Geography (Principal Investigator) with Nicholas Coops, Professor of Forestry and Canada Research Chair in Remote Sensing and Ronald Kellett, Professor of Landscape Architecture (Co-Investigators) at the University of British Columbia.

Contributing project team members, researchers, co-authors and illustrators include Ben Crawford, Eli Heyman and Michael van der Laan, Geography, Rory Tooke, Forestry and Inna Olchovski, Landscape Architecture.